2011

Combustion Phasing and Engine Performance of an HCCI Engine Utilizing Simulated Biomass Gas

Dale Haggith
University of Windsor

Combustion Phasing and Engine Performance of an HCCI Engine Utilizing Simulated Biomass Gas

By

Dale Edward Haggith

A Thesis
Submitted to the Faculty of Graduate Studies
through Mechanical, Automotive and Materials Engineering
in Partial Fulfillment of the Requirements for
the Degree of Master of Science at the
University of Windsor

Windsor, Ontario, Canada

2011

Combustion Phasing and Engine Performance of an HCCI Engine Utilizing Simulated Biomass Gas

by

Dale Haggith

APPROVED BY:

_____

Dr. E. Tam, Outside Department Reader
Civil and Environmental Engineering

_____

Dr. J. Johrendt, Department Reader
Mechanical, Automotive, and Materials Engineering

_____

Dr. A. Sobiesiak, Advisor
Mechanical, Automotive, and Materials Engineering

_____

Dr. R. Barron, Chair of Defence
Mechanical, Automotive, and Materials Engineering

20 September 2011

DECLARATION OF ORIGINALITY

I hereby certify that I am the sole author of this thesis and that no part of this thesis has been published or submitted for publication.

I certify that, to the best of my knowledge, my thesis does not infringe upon anyone's copyright nor violate any proprietary rights and that any ideas, techniques, quotations, or any other material from the work of other people included in my thesis, published or otherwise, are fully acknowledged in accordance with the standard referencing practices. Furthermore, to the extent that I have included copyrighted material that surpasses the bounds of fair dealing within the meaning of the Canada Copyright Act, I certify that I have obtained a written permission from the copyright owner(s) to include such material(s) in my thesis and have included copies of such copyright clearances to my appendix.

I declare that this is a true copy of my thesis, including any final revisions, as approved by my thesis committee and the Graduate Studies office, and that this thesis has not been submitted for a higher degree to any other University or Institution.

ABSTRACT

In this work the viability of a simulated biomass gas which resembles in its composition so called producer gas is investigated as a fuel for HCCI engines. There were several fuel compositions used in this study; the main difference in fuel mixture compositions was the change of the H_2 to CO ratio. Indicated performance of the HCCI engine was evaluated based on in-cylinder and cycle-resolved pressure measurements. The performance and phasing analysis consisted of peak in-cylinder pressures, pressure rise rates, indicated mean effective pressure (IMEP), indicated efficiency, start of combustion timing, and combustion duration. Combustion phasing and performance of the engine was found to be significantly affected by variations in both intake charge temperature and equivalence ratio. The effects of engine speed are more unclear; however, there are some effects at different engine speeds which are speculated to be attributed to air/fuel mixing and possible charge stratification.

.

DEDICATION

The work conducted in this study would not have been made possible without the love and support from my grandparents Ed and Shirley Lindsay. I could not fathom where or who I would be without their constant presence providing guidance and positive reinforcement throughout the course of my entire life. My Father Donald Haggith and Mother Deborah Colbert were also very supportive and inquisitive throughout the pursuit of my education which I appreciate endlessly. I would also like to dedicate this work to my supervisor and mentor Dr. Andrzej Sobiesiak who believed in my abilities very early in my university education. He believed, supported and guided me throughout the course of both my undergraduate and M.A.S.c. degrees which I cannot thank him enough for.

ACKNOWLEDGEMENTS

When I set out in the field of combustion research several graduate students aided me with their knowledge and friendship; Prakash Gnanam, Micheal Johnson and Nima Gharib were great colleagues to have worked with. The research itself on biogas HCCI combustion was initiated at the University of Windsor by a post doctoral fellow Dr. Grzegorz Przybyla and I would like to thank him for introducing such an interesting topic.

I would like to thank Dr. Johrendt and Dr. Tam for participating on my Thesis Committee. I would to thank Bruce Gadal and Waseem Habash and their staff at St. Clair College for their support and co-operation; St Clair College is where the experimental setup for this work is currently located and where the experiments in this study were conducted.

TABLE OF CONTENTS

LIST OF TABLES

LIST OF FIGURES

ABBREVIATIONS

HCCI	homogeneous charge compression ignition
NOx	nitrious oxides
PM	particulate matter
SI	spark ignition
CI	compression ignition
CR	compression ratio
SOC	start of combustion
EGR	exhaust gas recirculation
TDC	top dead center
CO	carbon monoxide
H_2	hydrogen
CH_4	methane
CO_2	carbon dioxide
N_2	nitrogen
CV	calorific value
K	Kelvin degrees
°C	degrees Celsius
RPM	revolutions per minute
λ	excess air ratio
COV	coefficient of variation
IMEP	indicated mean effective pressure
BMEP	brake mean effective pressure
ppm	parts per million
NVO	negative valve overlap
Φ	equivalence ratio

ULSD	ultra low sulphur diesel
LTHR	low temperature heat release
HTHR	high temperature heat release
CAD	crank angle degrees
PRF	primary reference fuel
ICE	internal combustion engine
NG	natural gas
RG	reformer gas
T_{in}	intake charge temperature
O_2	oxygen
ISFC	indicated specific fuel consumption
LCV	lower calorific value
DI	direct injection
UHC	unburnt hydrocarbons
LPG	liquid petroleum gas
THC	total hydrocarbons
MRG	methanol reformed gas
DME	dimethyl ether
AC	alternating current
VSD	variable speed drive
ECU	electronic control unit
CAS	combustion analysis system
DAQ	data acquisition
HRR	heat release rate
HR	heat release
AFR	air-to-fuel ratio
$dP/d\theta$	pressure rise rate

CHAPTER I

INTRODUCTION

1.1 HCCI Basics

HCCI combustion mode for engine technology has been a growing area of interest for over a decade. As the name indicates in HCCI engines a homogeneous charge (fuel/air mixture) is created then the mixture is compressed. Ignition of the mixture is due to the auto-ignition properties of the fuel used and the temperature conditions in-cylinder derived from the compression process. HCCI engines are desirable for their improved thermal efficiency, ability to accommodate a variety of fuels and reduced NOx & PM (particulate matter) emissions [1]. The HCCI concept contains aspects from both conventional types of internal combustion engines; SI (Spark Ignition) & CI (Compression Ignition).

In a conventional SI engine a homogeneous charge is created consisting of some hydrocarbon fuel and an oxidizing agent (air). This mixture is then brought into the cylinder, compressed (CR ~8-11) and ignited (via a spark plug) [2]; the spark timing controls the pressure conditions generated from the expansion of combustion products. Once the spark plug fires a flame front propagates through the combustion chamber from the point of origin to the cylinder walls. The mixture of fuel/air for SI combustion needs to be at approximately the stoichiometric ratio of fuel and air ϕ=1 throughout the entire combustion chamber (meaning theoretical amount of air to oxidize all of the fuel with no excess oxygen; equivalence ratio (Φ) is the comparison of theoretical AFR (air-to-fuel ratio) and actual AFR). In CI engines only air is brought into the cylinder and compressed (CR ~12-24) [3]. The fuel is injected directly into the combustion chamber; it then starts atomizing (fuel breaks into tiny individual droplets), vaporizing, mixing and reacting with air. The fuel injection timing controls the on-set of and pressure – crank angle history of CI combustion; once the fuel droplets start to vaporize and mix with air within the flammability limits of the fuel the mixture region around each droplet will auto-ignite due to fuel properties. The way which the fuel mixes and burns in CI combustion allows the "global" equivalence ratio to be lean (ϕ=0.8) but locally at the flame location the mixture is still approximately stoichiometric or rich (ϕ=1-1.8) [3].

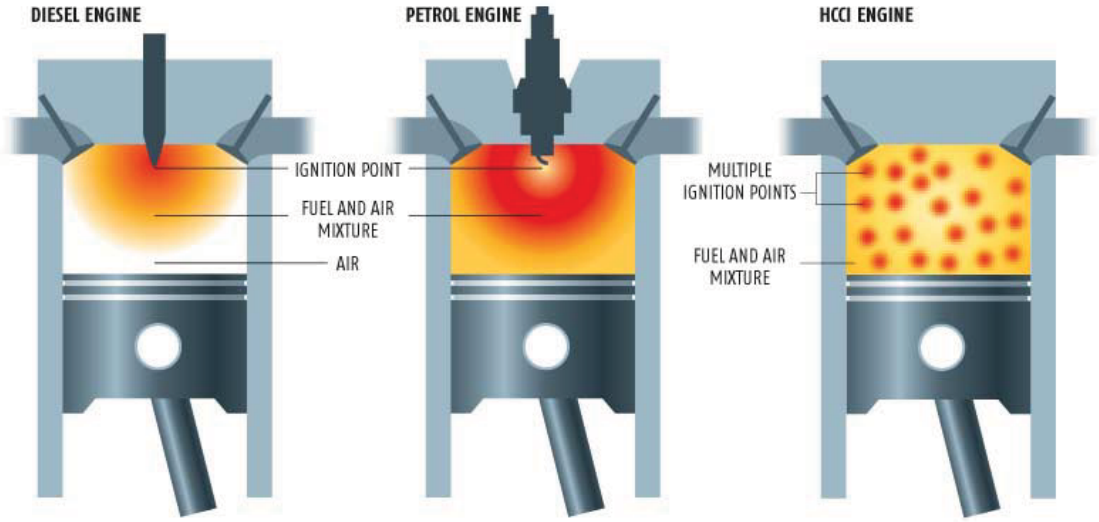

Figure 1.1: CI, SI & HCCI Pictorial Comparison [4]

The combination of the two conventional methods for combustion to form this alternative HCCI combustion mode has its advantages and drawbacks as shown in Figure 1.1. The phasing of the combustion event encompasses both the on-set timing and duration of heat release; it is somewhat problematic and complex as there is not direct control of the start of combustion (SOC) (in SI is spark timing and in CI is fuel injection timing). Some methods for control of HCCI combustion phasing are: variation of the intake charge temperature [5], modification of the compression ratio [6], intake charge boosting [1] and the introduction of EGR [7, 8]. In HCCI engines the energy release occurs simultaneously throughout the combustion chamber due to the auto-ignition at multiple locations of the homogeneous charge. For this reason the period of heat release is generally short and located close to TDC; this can cause extremely high in-cylinder pressures with richer mixtures which could lead to knock and eventual engine damage.

1.2 Biogas Introduction

The concept of gasification from solid feedstock is not a new idea/process and can be accomplished through different methods (most commonly fixed bed and fluidised bed gasifiers) which will be discussed in more detail in Chapter 2 of this study. Biomass gas is composed of gaseous products generated from a partial oxidization reaction of a biomass substrate; it is accompanied by other substances such as tar which are by-

products of the process [9]. In the case of the work conducted here the compositions used are derived from possible variances in gaseous mixture components found through the process of gasification of wood products. The gasification of wood products is considered because waste wood or by-product wood waste could be a viable renewable source of supply for the biogas production process which does not impact the supply of food.

The components found in the gaseous mixture derived from wood are CO, H_2, CH_4, CO_2 and N_2 [10], taking into consideration that any water vapour formed during the partial oxidation transformation is filtered out. If just the components identified above are considered only CO, H_2 and CH_4 could contribute to the release of energy by further oxidation reactions and therefore a focus will be brought to the variances found with these mixture components. The percentage of CH_4 is small (3-5%) and therefore almost all of the energy released is derived from the H_2 and CO constituents [10]. The total gravimetric contribution which the reactive components have within such mixtures is small, mostly being dominated by N_2, and therefore a reduction in the calorific value (CV) of the fuel mixture occurs.

According to [11] there is limited current data concerning the combustion characteristics of biomass gas containing H_2 and CO as the majority reactive components with regards to properties such as flammability limits, flame speeds and ignition characteristics; excluding 100%H_2. With limited information and data concerning the combustion properties of these biogas mixtures a study such as this work could help provide insight into the viable range of biogas fuels.

1.3 Objective

The goal of this work is to experimentally investigate the viability of biomass gas as a fuel for HCCI engine combustion.

1.4 Scope

In this study, performance and combustion phasing of a HCCI engine will be quantified utilizing premixed compositions of biomass gas with a varied CO/H_2 ratio. Several known HCCI engine operating parameters which affect the phasing of

combustion and inherently the performance will be manipulated (intake charge temperature, equivalence ratio, engine speed). Through the experiments conducted here a preliminary engine operation "map" can be determined and potentially applied to HCCI engines in a variety of applications (stationary power generation as main focus).

CHAPTER II

REVIEW OF LITERATURE

2.1 HCCI Fundamental Research

As identified in Chapter 1 there is no direct control over the SOC or the rate at which the combustion event occurs in HCCI combustion. There are however, methods that have been researched which are implemented as indirect control of the combustion processes by setting the conditions under which combustion is initiated and carried out. Increased/optimized performance and extension of the HCCI operating range is the objective of modifying the combustion event and therefore with operating condition modification inherent control over the phasing and duration of the combustion event is indicated.

2.1.1 Variations in Intake Charge Temperature

One of the most studied methods for combustion control is intake charge preheating. Through preheating of the fresh fuel/air mixture it is shown that the SOC timing can be altered and the rate at which heat is released can be changed based on the level of preheating [5].

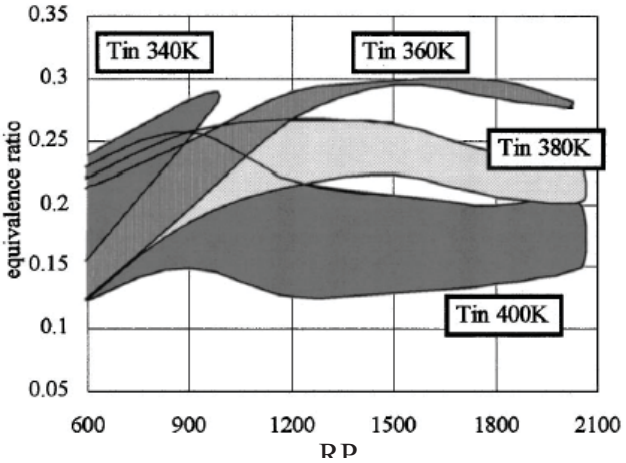

Figure 2.1: Operational Range with various intake air temperature (CR=16.55) [12]

In the work of [12] various intake charge temperatures (67˚C, 87˚C, 107˚C, & 127˚C) were investigated at a constant compression ratio of 16.6 with respect to

equivalence ratio and engine speed using n-butane as fuel. Figure 2.1 shows that as the intake charge temperature increases the operational range shifts to higher engine speeds, however a reduction in the equivalence ratio is required therefore affectively decreasing the amount of chemical energy which was released. In the work conducted for [13] an HCCI engine was operated with a fixed compression ratio of 16.5 and fixed engine speed of 1500 RPM fuelled with ethanol. The results are reported with respect to λ (the excess air ratio $\{1/\lambda = \Phi\}$) instead of equivalence ratio. In this study it was determined that at lower intake temperatures a richer mixture ($\Phi = 0.5$ or $\lambda = 2$) could be ignited without causing engine knock, as the intake temperature was increased at the same rich equivalence ratio knock was encountered. However it was found that the lean operational range (up to $\Phi = 0.18$ or $\lambda = 5.5$) could be extended with increases in intake temperature. In the work of [14] it is shown that for a constant compression ratio of 16 and engine speed of 1500 RPM, as the intake temperature increases from 40˚C to 110˚C the resultant BMEP decreased drastically from 4.0 bar to 0.5 bar. These results are attributed to phasing of the combustion event. By increasing the intake temperature the auto-ignition temperature for the fuel/air mixture is reached earlier during the compression stroke at constant compression ratio. With too advanced combustion (BTDC) the expanding combustion products do work on the piston while the compression stroke is still completing (negative work). The resultant negative work done on the piston reduces the amount of positive net work out from the system which was shown in [14] as the reduction in BMEP.

2.1.2 Effects of Intake Charge Boosting

Intake charge boosting is primarily used with the expectation of expanding the operational range. In the work of [15] a Volvo TD100 Diesel engine was converted for HCCI operation with the capability of variable compression ratios, intake air preheating, air/fuel equivalence ratio and intake boost pressure. It was found that the level of intake charge preheating needed to accomplish ultra lean HCCI combustion could be drastically reduced almost to the point of elimination with increasing inlet pressure (boost). The idea of charge dilution from excess air inducted from boost (creation of extrememly lean

charge) aids in the problematic nature of the speed of the combustion caused by the chemical reaction rates. The performance of the engine in terms of IMEP [15] was greatly improved up to 14 bar from more conventional HCCI technology which can attain up to 5 bar. Similar results of significant increases in IMEP values due to intake boost were found in [16]. In [16] a maximum IMEP was recorded at 16.34 bar with no knock/pressure ringing at 3.25 bar intake pressure. Unlike the study done in [15], in [16] EGR was added to the incoming charge; it was found with increasing boost at a constant equivalence ratio (if no EGR is added at a constant intake temperature with boost pressures above 1.8 bar) a reduction in equivalence ratio is required to maintain low levels or avoid pressure ringing/knock.

2.1.3 Variable Compression Ratio Application

Another method to modify the temperature conditions of the fuel/air charge in the cylinder is through modification of the compression ratio; it has been reported that HCCI combustion is strongly influenced by compression ratio changes [5].

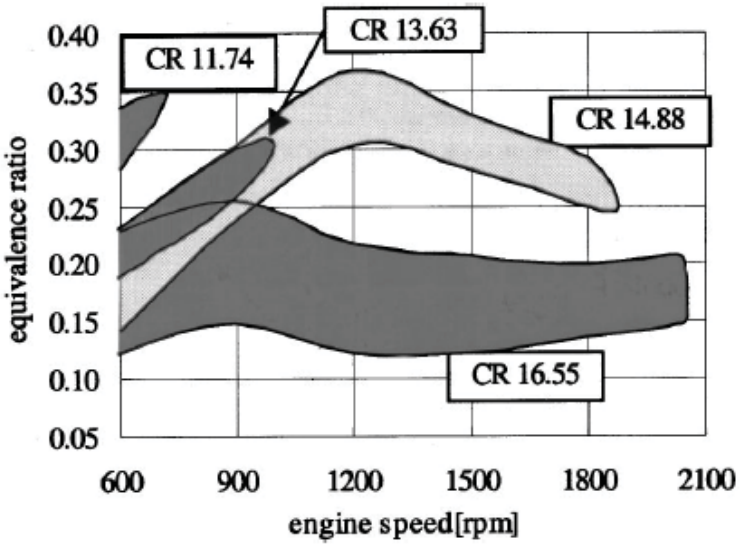

Figure 2.2: Operational Range with various compression ratio (Tin=400 K) [12]

In [12] several different compression ratios were utilized to determine the effect compression heating has on combustion. In Fig. 2.2 the operation range of the HCCI engine is depicted at a constant intake temperature in terms of equivalence ratio and

engine speed. It is shown that the largest compression ratio maintains the largest operating range for combustion in terms of both equivalence ratio and engine speed. When operating at higher compression ratios the maximum equivalence ratio is limited effectively restricting gains in performance.

The effect which increased compression ratios have on reducing required intake charge temperatures was further investigated in the work conducted in [17]. Here compression ratios ranging from 12:1 to 18:1 were used at various intake charge temperatures over a range of air-to-fuel ratios for stable to moderate combustion. The air-fuel ratio (AFR) represents the comparison of mass of air to mass of fuel which is present in the delivered charge; this ratio will vary based on the fuel used but can be approximated at 14.5 for most liquid fuels. If the AFR_{actual} increases the mixture becomes leaner; HCCI engines operate with increased AFR_{actual} or decreased equivalence ratios (~1/3). Therefore, one can expect AFR_{actual} in the range of ~25 to 60. In Figure 2.3 it is shown that if the compression ratio is increased the temperature created from compression is sufficient for ignition; the maximum IMEP obtained (5.4 bar) corresponds to the highest compression ratio used at the lowest (close to ambient) intake temperature.

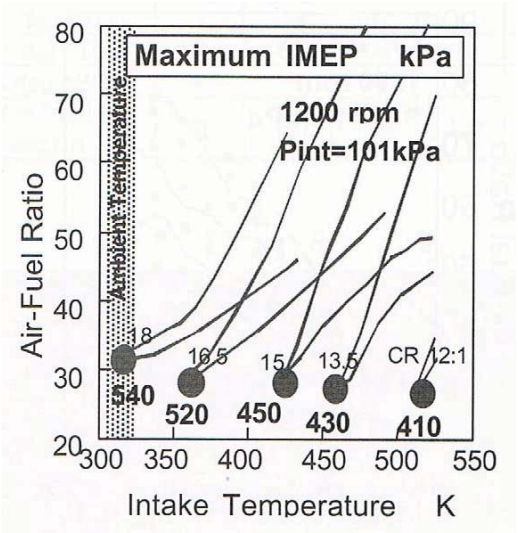

Figure 2.3: Effect of Compression Ratio on Stable and Moderate Combustion Region and on Maximum IMEP (1200rpm) [17]

2.1.4 EGR as a Combustion Controller

Since HCCI combustion can be summarised as a chemical kinetic process which relies on in-cylinder temperature, pressure and composition of the charge another interesting approach to combustion control through the addition of EGR is currently under investigation by many researchers. Through the research conducted on classification of effects EGR has on HCCI combustion there are three main topics: dilution effect (presence of inert gases in EGR), thermal effect (heat transfer, quality of EGR mixture, temperature, heat capacity), and chemical effects [18]. The focus of the work in [18] is directed toward understanding the chemical effects EGR has on combustion through the chemical species CO, NO, & CH_2O (formaldehyde) which are common reactive species found in HCCI exhaust. It was found in this work that the chemical effect of CO found in EGR was varied. For instances where 170ppm and lower levels were added to the intake no effect was induced. When a level of between 170-1000ppm was added SOC was delayed and at levels up to 10000ppm the chemical energy supplied by the oxidization of the CO plays an important role and increases the peak pressures. In terms of NO addition it can both promote and inhibit ignition delay; with a small amount of 45ppm can affect both the heat release phasing and the total amount of heat released. CH_2O (Formaldehyde) is shown to delay auto-ignition and negatively affect the heat release process. The researchers of [19] investigate both experimentally and numerically the effects which EGR has on the onset of combustion. In [19] it was found that the SOC could be retarded due to a thermodynamic cooling effect attributed to a high heat capacity of CO_2 and H_2O. Similar results to those found in [18] were also reported here where there was either an enhancement or suppression of SOC based on partially oxidized components such as CO or NO found in EGR. Another method to implement combustion products within the fresh charge is referred to as NVO (Negative Valve Overlap) [20]. Through either variable valve timing or preset valve timing the exhaust valve is closed before it reaches TDC on the exhaust stroke (with the intake valve remaining closed until sometime after TDC) combustion products from the previous cycle are trapped in the cylinder [21]. With DI technology a small fraction of fuel is injected into the compressed combustion product and air mixture to induce fuel

reformation. In both [20] and [21] the goal of trapping the hot combustion residuals in-cylinder is to accomplish "reformation" of the injected fuel through partial oxidation reactions. These reactions create new molecules such as H_2 which are thought to aid in the battle of combustion control for HCCI technology.

2.1.5 Engine Speed Implications

The last major factor which contributes to problems with combustion control is engine speed; as engine speed changes the available time for the combustion event changes. As was shown in [12] the operating range can be influenced by not only modifications to parameters such as intake temperature or compression ratio but also by the engine speed. With higher engine speeds there is less time for the mixture to self-ignite and completely burn. As the engine speed increases the SOC needs to be advanced in order to have enough time to release all of the energy from the oxidization of the fuel; the ignition delay time remains constant due to chemical kinetics. Experiments were carried out in [22] isolating engine speed by holding the intake temperature (45˚C), coolant temperature (90˚C) and compression ratio (CR = 15.3) constant while varying the engine speed from 600rpm to 900rpm. At higher engine speeds, low heat transfer to the wall occurs due to reduced cycle evolution times. Through the experiments conducted in [22] it was determined that the timing/phasing with regards to low temperature reactions which occur regarding a dual stage fuel (iso-butane used here) in terms of crank angle remains constant. A dual stage fuel has a high cetane number meaning it auto-ignites readily when mixed with air and has a dual stage burn; this dual stage heat release consists of a low temperature heat release (LTHR) or cool flame and a main burn stage or high temperature heat release (HTHR); shown in Fig. 2.4. This results because the various chemical reactions are governed by temperature conditions. The work of [22] goes on to state that the time delay between the low temperature reactions and main combustion event is reduced as engine speed is increased which is attributed to a reduction in heat transfer to the wall. A stronger focus was brought to the effects which equivalence ratio has in conjunction with engine speed for the investigation conducted in [24].

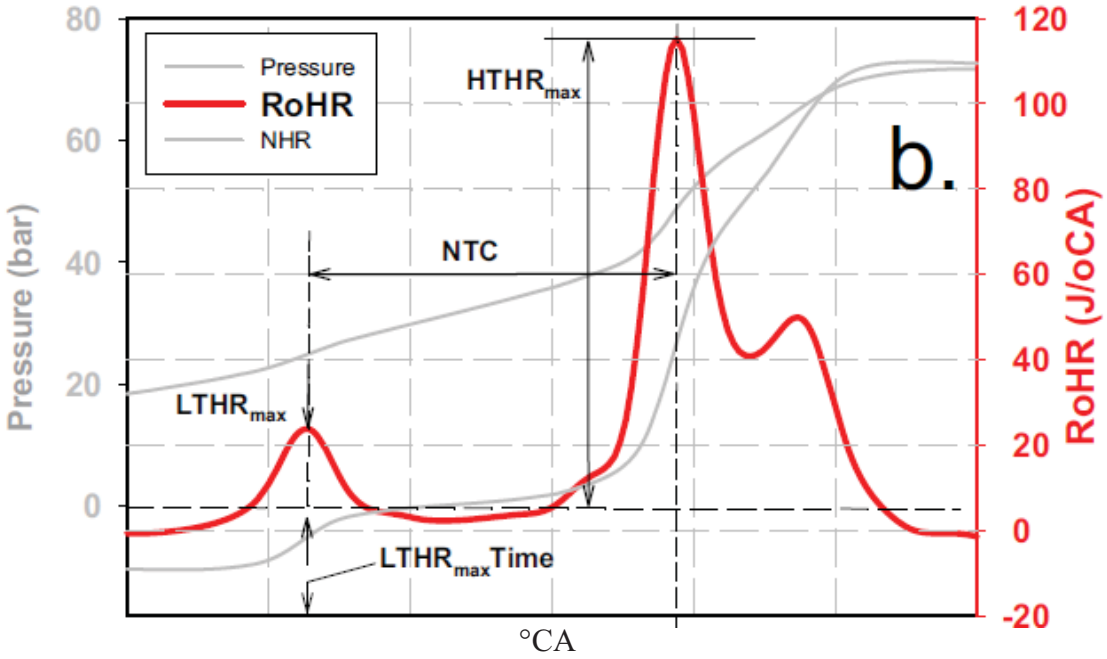

Figure 2.4: Heat release parameters definitions net rate of heat release (RoHR) [23]

It was found that for richer mixtures (up to $\phi = 0.4$) the timing was advanced due to compression heating effects but as the charge was leaned out this effect was not sufficient to compensate for a reduction in actual time of the cycle and combustion was inherently retarded. In contradiction to [22], [24] found that the low-temperature reaction phasing was advanced as engine speed increased. The use of standard ultra-low sulphur diesel (ULSD) in HCCI combustion for the purposes of investigating the effect of engine speed was carried out in [23]. In [23] the operating conditions were: compression ratio to 11, with initial temperature of the fuel/air mixture at 68˚C and boosting the intake pressure to 1.55 bar using no EGR at an equivalence ratio of 0.26. In Figure 2.5 the effect of engine speed on on-set of LTHR is quantified. As the engine speed is increased the amount of energy released over a certain amount of time (ms) is generally constant. However, it is clearly shown that as engine speed increases the amount of energy released with respect to crank angle decreases. This LTHR provides both energy to aid in the initialization of the main combustion event and intermediate radical chemical species which lead to HTHR reactions for the main combustion event [23]. Since the LTHR is negatively affected by increases in engine speed the main combustion event is also then retarded as a result.

The fuel used for the work conducted in this thesis does not generate the dual stage heat release and therefore engine speed effects correlating to high cetane fuels may not translate into results found with the biomass gas fuels used here.

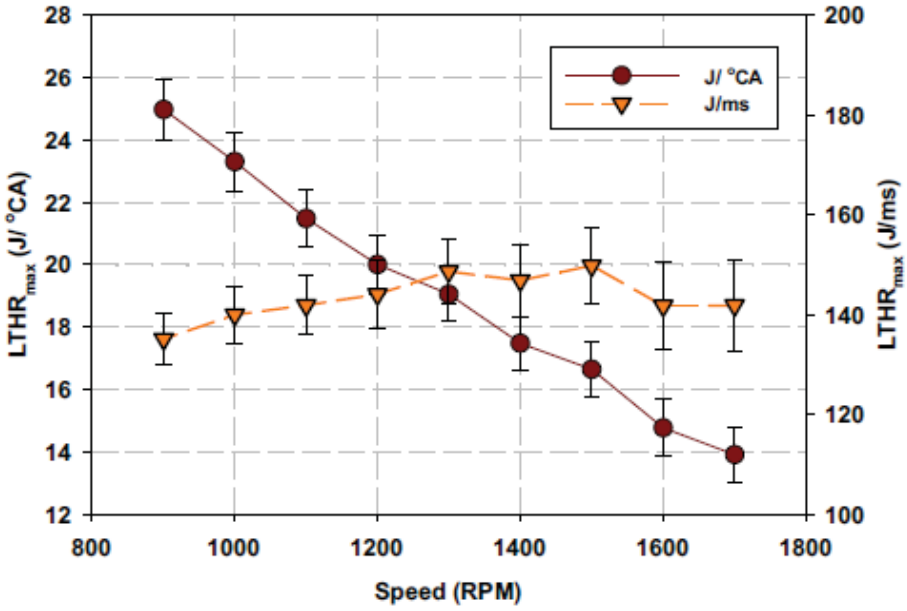

Figure 2.5: Effect of engine speed on maximum rate of low temperature heat release ($LTHR_{max}$) for crank angle (CAD) and time (ms) basis, ULSD fuel, CR=11.0, T_{mix}=68°C, MAP=1.55kPa, 0% EGR, AFR=57 [23]

2.2 HCCI Fuels and Fuelling Strategies

HCCI combustion has been investigated using conventional petroleum products such as gasoline and diesel [16, 17, 25, and 27], direct comparison of performance and emissions with conventional combustion modes (SI and CI) is of relative ease. As an inevitable rise in energy demand/usage increases with population and industry growth a focus is being brought to renewable/alternative sources of energy [26]. Researchers of HCCI have utilized the ability for combustion of alternative sources. The concept of variations in fuelling/fuels will be discussed in this section.

2.2.1 Fuel Classification & Application

There is a fundamental difference between types of fuels based on the process used to ignite them and the nature of subsequent combustion process. If a fuel is referenced by its octane number, which is an indication of the fuel's ability to resist auto ignition, the fuel is generally meant for use in a SI engine as the ignition is induced by the spark release [3]. If a fuel is referenced identifying its cetane number, which is an indication of the fuel's readiness to auto-ignite, the fuel is generally used in CI combustion and SOC is controlled by temperature and pressure conditions at the injection timing of the fuel [3]. Due to the method for combustion in HCCI where a premixed charge is auto-ignited a variety of fuels can be utilized as long as in-cylinder conditions are created where auto-ignition will occur [28]. The researchers of [28] used PRFs (Primary Reference Fuels) and conventional commercial fuels to demonstrate the ability of HCCI to accommodate both high octane and high cetane fuels through the modification of parameters which effect in-cylinder conditions, mainly compression ratio. It was shown through the work of [28] that combustion of almost any liquid fuel could be achieved. Pure n-heptane with an octane number of zero was combusted at a compression ratio of 11 and no intake air preheating. Under the same inlet conditions iso-octane with an octane number of 100 was combusted at a compression ratio of 21.5. As expected more energy was required to ignite higher octane fuels and in this work the added initial energy was induced through a higher compression ratio. One group of researchers [29] chose to investigate high octane fuels (with octane numbers over 90) to determine not only the operating conditions but also what small changes in octane rating and chemical composition of the fuels would effect HCCI combustion. It is shown that for multiple fuels having almost identical octane numbers (~94) and under the same operating conditions combustion could be obtained with one fuel and not another. With varied composition (hydrocarbon chain length, internal molecule structure, and bond energies) there are different chemical kinetic paths even though similar octane ratings are present. Each fuel composition is strongly dependent on the operating conditions (intake temperature, engine speed, compression ratio, EGR rate, etc). With the understanding of differences due to chemical kinetics based on fuel compositions therefore rendering

conventional octane ratings of fuels inaccurate for HCCI engines the researchers in [30] experimentally investigated then developed a new fuel index based on HCCI combustion. This index is limited to the fuels experimentally tested in the study and cannot be extrapolated to predict behaviours of new types of fuels such as the gaseous fuel used in this thesis. However, the index developed incorporates motor octane number (MON), heat release data, and molecule properties (paraffin %, olefin %, and aromatic %). By taking the chemical properties into account this new index will better reflect the auto-ignition process which occurs in HCCI engines.

2.2.2 Natural Gas as an Alternative

Liquid fuels are not the only hydrocarbons investigated with regards to HCCI engines. Natural gas has long been researched as an ICE fuel and thought of as a good alternative to liquid petroleum products. One issue with the term natural gas is that the gas itself is a mixture of various chemical components such as methane, ethane, propane, & butane and the fraction in which these components are present in the mixture varies [31]. The main constituent in natural gas is methane (CH_4) which has the property of a high auto-ignition temperature [32] which leads to a high octane rating of natural gas. Although natural gas contains large fractions of CH_4 which is not an ideal fuel for HCCI it is the higher hydrocarbon components which make natural gas a suitable candidate for HCCI combustion. The researchers of the simulation work in [31] showed that there is a strong dependence of mixture properties for HCCI combustion and that a relatively small replacement of CH_4 with higher hydrocarbons (which react first) changes the chemical kinetics allowing for a fairly significant reduction in required intake charge temperature (~40K). In the work of [32] it was found that stable combustion could be achieved using a fixed composition of natural gas (methane 88%, ethane 6%, propane 4%, and butane 2%, by volume). Various operating conditions such as intake temperature, internal EGR using NVO, boosting, engine speed, and cooled external EGR to understand the effects these parameters have on NG HCCI combustion. It was found in [32] that turbocharging using decreasing amounts of internal EGR was an effective method for operating region expansion. The external EGR in conjunction with turbocharging also led to an increase

in the operating region of by limiting the chemical kinetics from the cool exhaust products. It was also noted that the thermal efficiency increased as engine speed increased which was contributed to lower heat transfer to the walls, however the higher engine speed conditions did negatively affect the operating region for HCCI combustion.

2.2.3 Fuel Reformation

Another fuelling concept which is being developed for HCCI combustion involved introducing reformer gas with the fresh air/fuel charge. This reformer gas is a mixture of gaseous components with the composition primarily dominated by H_2 and CO also containing larger fractions of H_2O, CO_2, and N_2; it is produced through the partial oxidation of virtually any hydrocarbon fuel [33]. The idea of using reformer gas as a secondary fuel for ignition control utilizing high octane PFRs was the basis for the experimental work conducted in [33]. In this work the RG was a simulated mixture consisting of 75% H_2 and 25% CO by volume and delivered from storage tanks. Through Figure 2.6 it was found that the lowest compression ratio (14.4) with RG addition produced the widest operating range, however the addition of RG in general allowed for a larger operating range in general. When comparing cases with and without RG while maintaining constant ϕ, EGR, CR and T_{in} it was found that the effect, which the RG had on combustion, was to retard combustion which in turn lowered the maximum in-cylinder pressures and pressure rise rates. Combustion efficiency decreased slightly with RG addition. A continuation of the investigation performed in [33] was conducted in [34] with the primary combustion fuel having a low octane number. Through the work of [34] similar results were found using high octane fuels supplemented with RG; when RG concentrations were increased combustion timing retarded. A slight increase in IMEP was recorded when adding RG which coincided with an increase in thermal efficiency also.

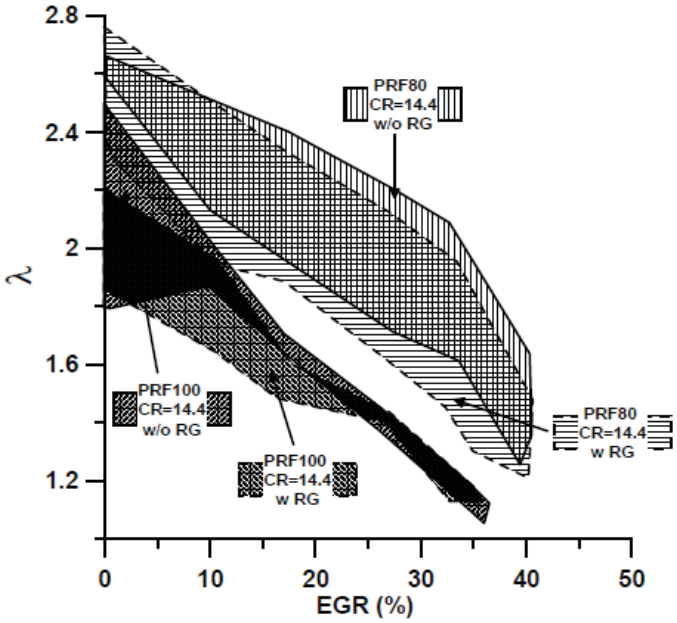

Figure 2.6: Effect of RG replacement on HCCI operating range of PRF100 and PRF80 fuels [33]

Another method to institute reformer gas or reformation products is through in-cylinder partial oxidation. As was identified earlier an effective method to trap combustion products in-cylinder is through the use of NVO [21] and in this work experimentation with fuel reformation strategy is conducted. Here once the exhaust valve closes and hot combustion products are trapped with excess air/O_2 (because HCCI combustion is very lean) a small portion of the total fuel required for the cycle is injected. The remainder of the fuel is injected after the intake stroke is completed and the intake valve cycles. This process is depicted in Figure 2.7 below. This small amount of fuel (~10% & 25 % of total fuel) undergoes a low-temperature partial oxidation reaction where the composition of the mixture changes producing intermediate chemical species. It was found that there was a significant expansion to the lean limit of operation when both the two injections were implemented. In terms of performance it was found that with the 10% NVO fuel injection an IMEP range of 340-400kPa with a valve overlap of 152˚. With 25% NVO injection a range of IMEP = 170-340kPa was achieved. With 100% injection during the intake stroke with the idea of creating a conventional homogeneous charge the IMEP varied between 400-420kPa. For all trials as the IMEP increased the indicated specific fuel consumption (ISFC) decreased. The same concept

for fuel reformation as was used in [21] is presented in [35]. The researchers of [35] found that advancing the NVO injection earlier can affect the main SOC by up to 10˚CA which can be attributed increased amounts of heat release and increased concentrations of intermediate chemical species due to longer reformation times. It was also reported as in [21] that there is an optimal injection timing and % of fuel which should be injected during the NVO period.

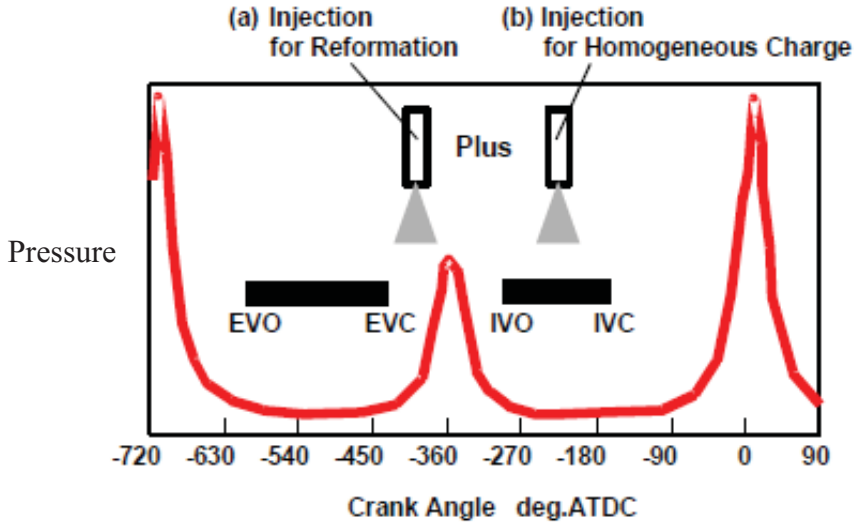

Figure 2.7: Concept of the Combined Injection Method in Negative Valve Overlap & Intake Stroke [21]

2.3 Biogas Production and Characteristics

2.3.1 Biomass and By-Products Overview

Biomass is defined as all organic matter which originates from plants (trees, crops, etc.) [36]. The vegetation itself stems from the reaction between CO_2 in air, water and sunlight which is known as photosynthesis; through biomass growth the solar energy which drives the photosynthesis process is stored in the form of chemical bonds making the structure of the biomass [36]. Researchers classify biomass in various types consisting mostly of: woody plants, herbaceous plants/grasses, aquatic plants, and manures. The fuel gas of interest for this thesis is concentrated on woody plants as the biomass source and subsequent processing to generate the gaseous fuel mixture.

In an extension of the work of [36] a description of technologies used to extract energy back from biomass is provided in the work of [37]. In [37] the conversion processes are broken down in two main categories: thermo-chemical conversion & bio-chemical conversion. Bio-chemical conversion can be broken further into two main processes fermentation and aerobic digestion. Fermentation generally leads to an end-product such as ethanol (liquid fuel) derived from sugar crops or from starch based crops such as corn [37, 38], for this reason fermentation process will not be considered as a source for biomass gas production. Aerobic digestion does provide a proven viable method for conversion of biomass substrate into biogas; however, the AD process is focused on feedstock containing a very high moisture content which in some cases requires extra processes for increasing moisture [37] and therefore for this thesis it will be excluded from the discussion. Thermo-chemical conversion of biomass can be subdivided into three main processes: direct combustion, gasification, pyrolysis [37]. As we are interested in a renewable fuel for HCCI combustion direct combustion is not an option due to the inability of an internal combustion engine to accommodate combustion of a solid feedstock. Pyrolysis is where heating of the feedstock occurs in the absence of air (~500K) which produces a liquid (bio-oil), solid (generally consisting of mostly carbon) and gaseous products [38, 39]. The final thermo-chemical process of biomass gas generation is gasification of the feedstock. Gasification is the partial oxidation of biomass at relatively high temperatures (~800-900˚C) where a LCV gas is generated which then can be burnt directly in a burner type application or potentially fuel an ICE [37]. It is the gasification technology which is the biogas production method of interest.

2.3.2 Gasification Process and Fuel Composition

There are two main gasification technologies which have proven to be viable options for use with wood waste biomass: fixed bed and fluidized bed gasifiers; there are also variations which can be done within each process such as using steam or air [10].

The fluidized bed gasification has one advantage over the fixed bed gasification process; within the gasification zone a uniform temperature can be easily achieved due mainly the fact that the substrate bed consists of finely grained material where air or

steam is introduced insuring a good mixture of material with its oxidant [10]. The researchers in [40] investigated steam to biomass ratio and gasifying temperature on the gas component composition. The results found through the work of [40] are summarized in Table 2.1 below. The fuel compositions shown in [40] have had water vapour and nitrogen filtered out; the compositions tested in this thesis replicate water vapour filtration however retain the nitrogen therefore lowering the % contribution of other components (H_2, CO, etc). At a constant steam biomass ratio of 1.32 as the gasification temperature was increased the H_2 and CO fractions increased while the CO_2 and CH_4 fractions decreased. When the steam biomass ratio was increased the H_2 fraction increased however the CO content decreased, CO_2 increased and CH_4 decreased.

Table 2.1: Carbon balance & gasification efficiency of experimental results of fluidized bed gasifier [40]

Exp. run no.	1	2	3	4	5	6	7	8
Steam biomass ratio	Constant at 1.32				0.60	1.00	1.32	1.70
Gasifier temp. (°C)	650	690	730	770	Constant at 750			
Gas Composition (% of mole)								
H_2	47.25	50.5	52.2	53.08	47.81	48.88	51.17	51.89
CO	11.25	12.83	15.9	17.85	27.48	22.70	19.65	17.38
CO_2	31.9	28.51	25.65	23.9	18.09	22.20	23.15	24.81
CH_4	9.6	8.16	6.25	5.17	6.62	6.22	6.03	5.92
HHV of prod. gas (MJ/Nm^3)	11.28	11.23	11.16	11.09	12.21	11.59	11.42	11.18
Gas yield (Nm^3/kg of raw biomass)	1.03	1.12	1.16	1.21	1.05	1.09	1.16	1.21
Carbon conversion (%)	84.10	85.82	85.83	87.88	84.83	86.25	87.68	90.11
Cold gas efficiency (%)	62.99	64.78	65.58	66.06	65.75	65.96	66.10	66.15

It is shown through [40] that fluidized bed gasification is a viable option for generation of biomass gas, however there are several drawbacks which make the process less attractive. The major issue is slagging of material due to the ash content of the biomass in the gasifier [10]; this problem can be reduced by lowering the temperature. Particulate matter formed in fluidized bed reactors is also greater than those formed through fixed bed gasifiers [10].

Fixed bed gasifiers have in general are of simple design, cost effective, can use a wide variety of feedstock with various sizes which still produce a useful gaseous fuel as in fluidized bed reactors, they also can use steam or air as the oxidizing agent [10, 41, 42, 43, 44]. For these reason the gases produced from fixed bed gasification will be the main focus of this thesis. More specifically, woody biomass was selected as the gasification fuel. Generally there are two types of fixed bed gasifiers: updraft and downdraft; in an updraft the feed is introduced at the top and the air or steam is introduced at the bottom,

in a downdraft type the feed and air/steam move in the same direction (down) [10]. General nominal compositions of the gaseous fuel produced through the process of gasification using air is comprised typically of 40-50% N_2, 15-20% H_2, 10-15%CO, 10-15% CO_2, 3-5% CH_4 [10].

In the work of [43] both scale lab experiments and numerical modelling were carried out in order to help quantify the performance of their fixed bed biomass gasifier operating with air at elevated temperatures. As was found with fluidized bed gasification [40] by increasing the feed gas temperature higher fractions of H_2, CO and CH_4 could be achieved therefore increasing the LCV of the gaseous fuel. When comparing the numerical and experimental data obtained in [43] at feed gas temperatures of 623K to 1103K this work showed an optimal feed gas temperature of ~803K where the concentration increase of combustible component gases (CO, H_2 &C_mH_n) was less significant than temperatures below 803K. The predicted concentration of CO was slightly lower than experimentally recorded values but ranged from 20.1% to 26.3% by volume within the temperature limits of 623K to 1103K on a dry basis. The H_2 presence increased from 6.6% to 12.7% by volume within the same temperature range. The C_mH_n component of the biomass gas ranges from ~5.2% to 9.8% by volume.

As in the work of [43], [42] investigated the gasification of wood in an updraft type gasifier only in this work the biomass substrate was “long stick” feed. The idea behind using a larger feedstock size was to reduce waste produced (sawdust generation) for the gasification process. In this study it was found that long stick feedstock could be used as the substrate for gasification to produce LCV gas for use as a fuel at a conversion efficiency of 73%. It is also shown that the production of biomass gas is strongly dependant on the rate at which the oxidizing agent (air in this case) is delivered. This aspect is depicted in Figure 2.8, it is observed that a linear trend is present until 2.99 m/s of air is delivered at which point variations in volume of biomass gas produced occur.

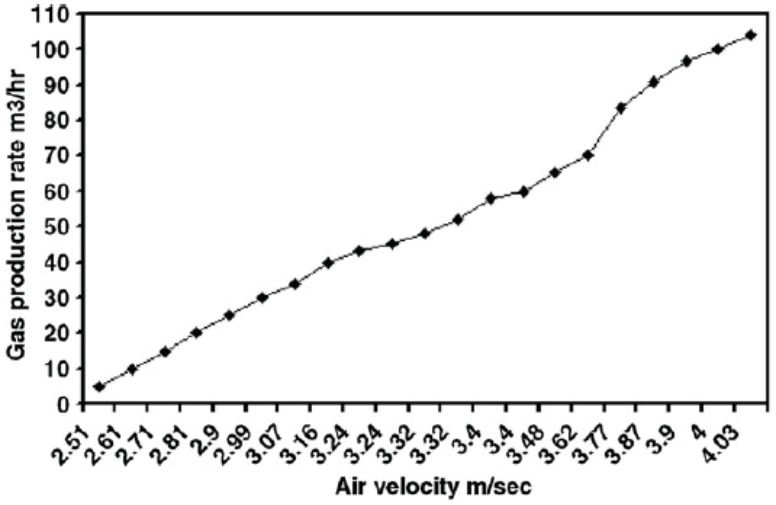

Figure 2.8: Gas production rate vs. air velocity [42]

The composition of the gas produced is listed for the three trials discussed in [42]; the CO content ranged from 10-15%, H_2 was identified as 15-20% of the mixture, CO_2 consisted of 10-14%, the remainder of the compositions was N_2 ranging from 45-50%.

2.3.3 Chemical Kinetic Basics Regarding Hydrogen and Carbon Monoxide Oxidation

As discussed in section 2.3.2 with only a small portion ~2-5 % of the total biomass gas composition consisting of CH_4 and ~65% made of inert species of N_2 and CO_2 the major contributing species to the release of chemical energy from the biomass gas are H_2 and CO. To better understand the auto-ignition of H_2 and CO mixtures with air the chemical reactions of each individual component with air will be considered. Hydrogen oxidation has only eight participating species (H_2, O_2, H, O, OH, H_2O, HO_2, and H_2O_2) and about 20 reactions. Despite of the condense mechanism hydrogen oxidation can be complex [45]. As shown in Figure 2.9 there are three distinct explosive limits for hydrogen oxidation. These limits are drawn by the impact various chemical species and reactions have under certain temperature and pressure conditions. Figure 2.9 represents a stoichiometric mixture, if leaner mixtures are considered the curve would shift to higher temperature and pressure zones.

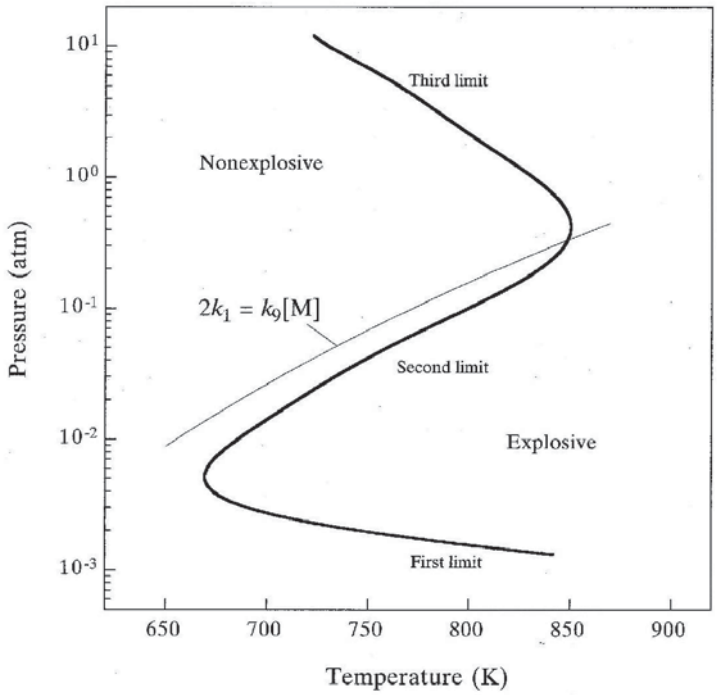

Figure 2.9: Explosion limits of a stoichiometric $H_2 - O_2$ mixture [46]

Basically there are two main initiation reactions; dissociation of H_2, and a H_2-O_2 reaction.

$$H_2 + M \rightarrow H + H + M \quad \text{(Eq. 2.1)}$$

$$H_2 + O_2 \rightarrow HO_2 + H \quad \text{(Eq. 2.2)}$$

Note that intermolecular energy transfer caused by molecule collision is represented by the term M. The most important initiation reaction tends to be Eq. 2.2 which is relevant under almost all conditions; however, the HO_2 molecule being relatively inactive at low temperatures does not lead to any chain branching during combustion on-set [46]. If compression heating (temperature) conditions exist reaction Eq. 2.1 can also contribute to initial stages. With the production of H, a chain reaction is limited leading to further radical formation and finally H_2O production:

$$H + O_2 \rightarrow O + OH \quad \text{(Eq. 2.3)}$$

$$O + H_2 \rightarrow H + OH \quad \text{(Eq. 2.4)}$$

$$OH + H_2 \rightarrow H + H_2O \quad \text{(Eq. 2.5)}$$

These reactions are more dependent on temperature changes than pressure. When H_2O is formed it is considered to be a terminating species as it is relatively unreactive. As the

pressure is increased the frequency of molecule collisions increases leading to accelerated chain branching causing extremely rapid H_2 consumption/oxidation and inherently explosion [46]; this is the first explosion limit in Fig. 2.9. At the second limit reaction Eq. 2.6 occurs as pressure increases and replaces Eq. 2.3 as the H consuming reaction. When the HO_2 molecule is produced it is considered relatively inactive, slowing down overall reactively and therefore can be considered terminating [45].

$$H + O_2 + M \rightarrow HO_2 + M \qquad \text{(Eq. 2.6)}$$

At the third explosive limit with increased temperature and pressure the reactions Eq. 2.7 and Eq. 2.8 emerge and overtake the stability of the generally unreactive HO_2 molecules.

$$HO_2 + H_2 \rightarrow H_2O_2 + H \qquad \text{(Eq. 2.7)}$$

$$H_2O_2 + M \rightarrow OH + OH + M \qquad \text{(Eq. 2.8)}$$

As temperature again increases higher concentrations of OH radicals are produced (Eq. 2.10 and Eq. 2.11) and the chain branching reactions (i.e. Eq. 2.5) between them become more significant.

$$HO_2 + HO_2 \rightarrow H_2O_2 + O_2 \qquad \text{(Eq. 2.9)}$$

$$HO_2 + H \rightarrow OH + OH \qquad \text{(Eq. 2.10)}$$

$$HO_2 + O \rightarrow OH + O_2 \qquad \text{(Eq. 2.11)}$$

It should be noted that reactions Eq. 2.7 through Eq. 2.11 do play an important role at high temperatures and pressures and are the source of the third explosion limit. However, the mechanism itself is somewhat weak relative to other reactions present.

If carbon monoxide is considered to be oxidized only with oxygen the chemical reaction is:

$$CO + O_2 \rightarrow CO_2 + O \qquad \text{(Eq. 2.12)}$$

The energy required to initiate this reaction is fairly high at 48 kcal/mol; this leads to very slow reaction rates. Also, the O atom produced during this reaction does not lead to any rapid chain-branching reactions which does not aid in CO consumption/conversion [46 and 47].

The relatively slow reaction rates when compared to hydrogen are represented in Figure 2.10 in terms of laminar burning velocity [47]. It is observed that under similar conditions (approximately stoichiometric mixtures) the oxidation of CO occurs approximately 6X slower when compared to pure hydrogen.

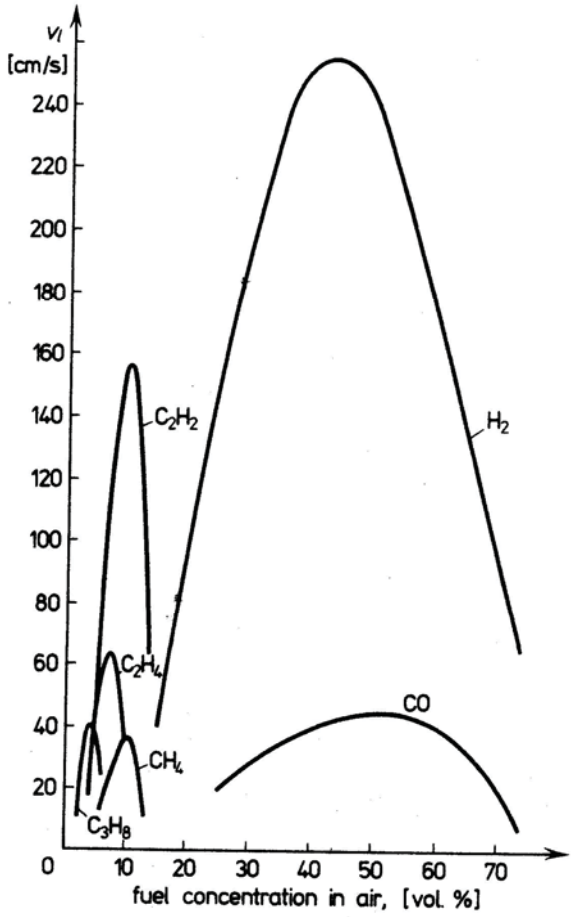

Figure 2.10: Laminar burning velocities for various mixtures [47]

When adding small portions of either water vapour or hydrogen the dynamic of CO oxidation is drastically altered. If water vapour is first considered then the reaction given by Eq. 2.13 [3] becomes significant; this reaction generally requires elevated pressure conditions:

$$CO + H_2O \rightarrow CO_2 + H_2 \qquad \text{(Eq. 2.13)}$$

With the introduction of water vapour, either injected or formed through oxidation of hydrogen i.e. Eq. 2.5, hydrogen can be freed from the H_2O molecule leading to H-O reactions. This will allow for chain branching in turn speeding up the process of CO oxidation. Another potential avenue for water vapour to aid in carbon monoxide oxidation is:

$$O_2 + M \rightarrow O + O + M \qquad \text{(Eq. 2.14)}$$

followed by:

$$O + H_2O \rightarrow OH + OH \quad \text{(Eq. 2.15)}$$

Through the disassociation of O_2 molecules and the formation of OH radicals the most commonly considered dominant path for CO oxidation can be carried out [48]:

$$CO + OH \rightarrow CO_2 + H \quad \text{(Eq. 2.16)}$$

The final potential oxidation path for CO is:

$$CO + HO_2 \rightarrow CO_2 + OH \quad \text{(Eq. 2.17)}$$

The usually chain-branching terminating species of HO_2 will become reactive under certain conditions, generally high pressure, leading to the formation of CO_2 accompanied by OH which will drive both hydrogen and carbon monoxide oxidation reactions [45].

2.3.4 H_2:CO Biomass Gas Combustion Characteristics

The biomass gas produced from the gasification of wood generates a mixture where the combustible components of the gas are dominated by hydrogen and carbon monoxide as reported in previous sections of this thesis. Due to a majority of the chemical energy released in the combustion of biomass gas being attributed to the oxidization of these two components a review of characteristics concerning the mixture of these will now be carried out.

The goal of the researchers in the investigation of [49] was to establish flammability limits of various homogeneous mixtures of H_2 and CO; the experiments were conducted on a dry basis and at atmospheric pressure. The experiments are conducted in a shock tube with the ability to manipulate the temperature of the air/H_2/CO mixture. Figures 2.11 and 2.12 are extracted from the work conducted in [49] and show the effects that not only H_2 has on the flammability of the mixture but also how the charge temperature affects them. For both the lean limit and the rich limit as the temperature of the charge was elevated the operational range is expanded. For the rich limit it is shown that for small amounts of H_2 addition (~4%) an increase in the limit is observed, however as the H_2 concentration is increased the rich limit is decreased slightly. The effect of increased concentrations of H_2 on the lean limit is clearly identified in Figure 2.12; as the H_2 addition increases the lean limit of operation is extended.

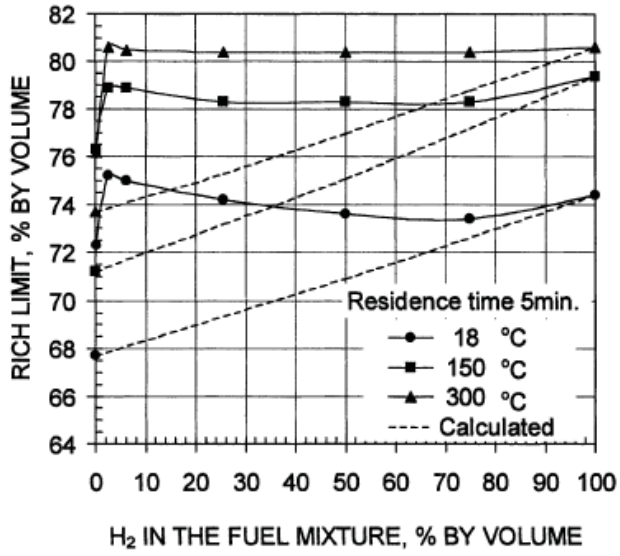

Figure 2.11: Rich flammability limits of H_2-CO mixtures in air at different temperatures [49]

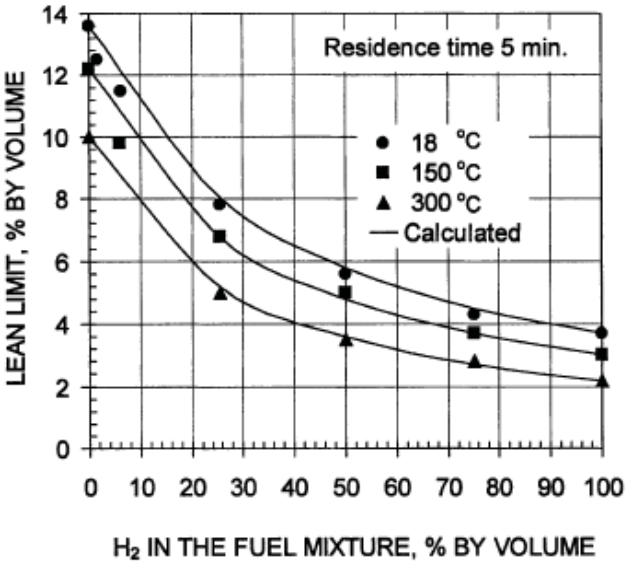

Figure 2.12: Lean flammability limits of H_2-CO mixtures in air at different temperatures [49]

An investigation into the ignition properties of H_2/CO mixtures was conducted in [11]. Using a rapid compression machine ignition properties of only H_2 and CO mixtures (ratios ranging from 0.25-4.0) were tested in simulated air over a range of equivalence ratios (0.1-2.0) at various pressure (7.1-26.4atm) with a span of temperatures (752-1051K). Increasing temperature at a constant pressure of 15atm and $\phi = 0.4$ shortened

the ignition delay time of the charge. The ignition delay time was then quantified with respect to changes in pressure at a constant temperature of 980K and $\phi = 0.4$; it was found that as the pressure was increased the ignition delay time decreased. The pressure and temperature were then held constant at 980K and 15 atm with different equivalence ratios; it was found that as the mixture approached the lean limit the ignition delay time increased.

The work of [50] implements a chemical kinetic model to analyze the main reactions involved in the combustion of various compositions of biomass gas as listed in Table 2.2; F_{rg} is the biomass/air ratio which would be inside the gasifier.

Table 2.2: Mole Fractions of the Producer Gas Components for Different F_{rg} Values [50]

	$F_{rg} = 3$	$F_{rg} = 3.5$	$F_{rg} = 4$	$F_{rg} = 4.5$	$F_{rg} = 5$
X_{H2O}	0.05857	0.04220	0.03745	0.03418	0.03127
X_{N2}	0.41195	0.38699	0.37195	0.35901	0.34719
X_{CO2}	0.09003	0.10166	0.11458	0.12719	0.13928
X_{CH4}	0.00049	0.01613	0.04022	0.06402	0.08663
X_{H2}	0.19937	0.20917	0.19355	0.17584	0.15861
X_{CO}	0.23958	0.24385	0.24226	0.23976	0.23701

Through the modelling work of [50] charge temperature and pressure were key parameters for the investigation of ignition delay time. In Figure 2.13 it is shown that charge temperature plays an important role in the kinetics which control ignition delay; as the temperature is increased the ignition delay decreases. The effect of pressure is not as clearly depicted; at low temperatures (T<1200K) and in the high temperature range (T>1500K) the ignition delay time decreased as pressure increased, for the intermediate temperature range (1200K<T<1500K) there were no significant changes in ignition delay time. Also reported in [50] was the effect of fuel gas/air ratio in an engine; the engine equivalence ratio appeared to play a dominant role in the chemical kinetics at temperatures below 1200K and in the lean region of operation ($\phi < 1$). This point is important for the work in this thesis as HCCI combustion only operates lean through low temperature combustion.

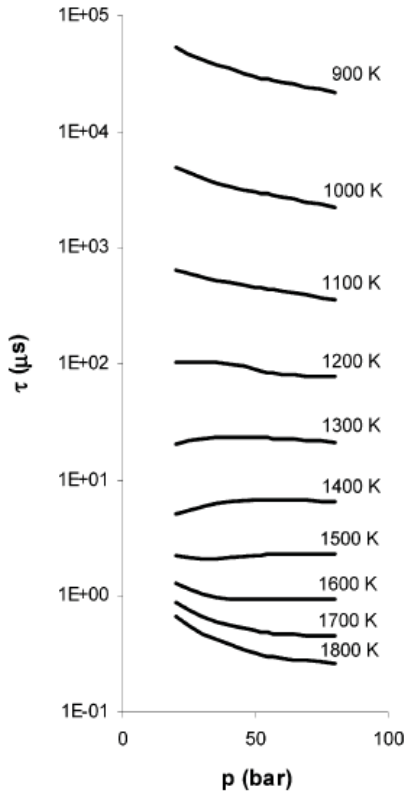

Figure 2.13: Auto-ignition delay time (in microseconds) of a stoichiometric producer gas/air mixture vs. pressure at different temperature values [50]

Another study on the auto-ignition characteristics of H_2/CO mixtures was carried out in [51]. In [51] emphasis was focused on the impact which CO has on combustion. In Figure 2.14 experimental results are plotted showing that for even small fractions of CO addition ignition delay of the mixture is increased with a pressure of 50bar. Similar results are recorded for pressures of 15 and 30 bar under the same mixture and temperature conditions. Due to the lack of experience with such fuel mixtures standard chemical kinetic mechanisms did not correlate well with experimental results where the inhabitation of ignition was not captured at low supplementation rates through the models. Two of the mechanisms were able to capture the suppression of ignition but not until CO constituted 80% of the fuel mixture, on the other hand another mechanism used showed a reduction in ignition delay under the same parameters.

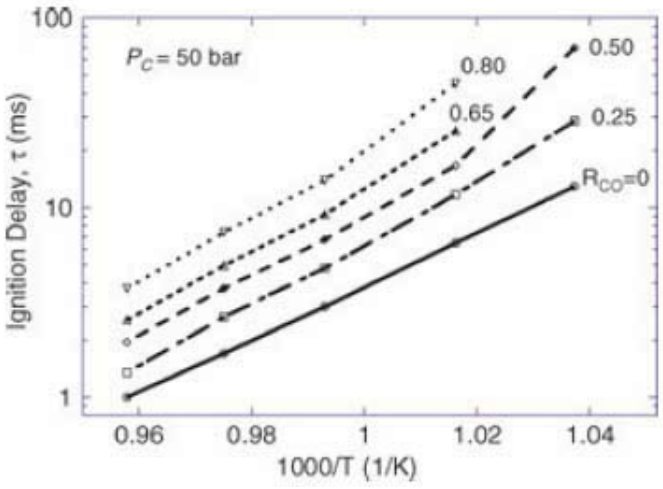

Figure 2.14: Measured ignition delays for H_2/CO auto-ignition. Molar composition: (H_2+CO)/O_2/N_2/Ar=12.5/6.25/18.125/63.125. Pressure at TDC, P_c=50bar [51]

2.4 Biomass Gas as an ICE Fuel

Biomass gas appears to be a viable fuel for internal combustion engines, however practical applications seem to limit the utilization to stationary systems geared toward power generation [52]. There is a misconception that because of the LCV of the biomass gas (4-6 MJ/Nm^3) that there will be a significant derating of the engine performance when compared to conventional liquid fuels or even natural gas with a CV of approximately 30 MJ/Nm^3 [53]. If the biomass + air charge CV is compared to a natural gas + air charge the energy density is only 15-20% lower even though the CV of biomass gas is 1/8 of NG [53]. In the work of [54] a simple model was created to demonstrate the energy density of different fuels for HCCI engines; the results are shown in Figure 2.15. In [54] the CV of the simulated biomass gas used for Figure 2.14 is 4.95 MJ/m^3 when compared to 227.7 MJ/m^3 for gasoline or 57.03 MJ/m^3 for ethanol. The energy density per unit mixture of the biomass gas is only ~25% lower than for a gasoline and air mixture at the equivalence ratio $\Phi = 1$. A reduction of 25% in ideal energy density is not significant when considering the efficiency of the entire energy conversion system; the overall efficiency of an internal combustion engine being fairly low (η_o = 25-40%). As the equivalence ratio decreases from 1 entering an operating range common to HCCI

engines the charge energy density differences become smaller and at Φ = 0.32 they are equal.

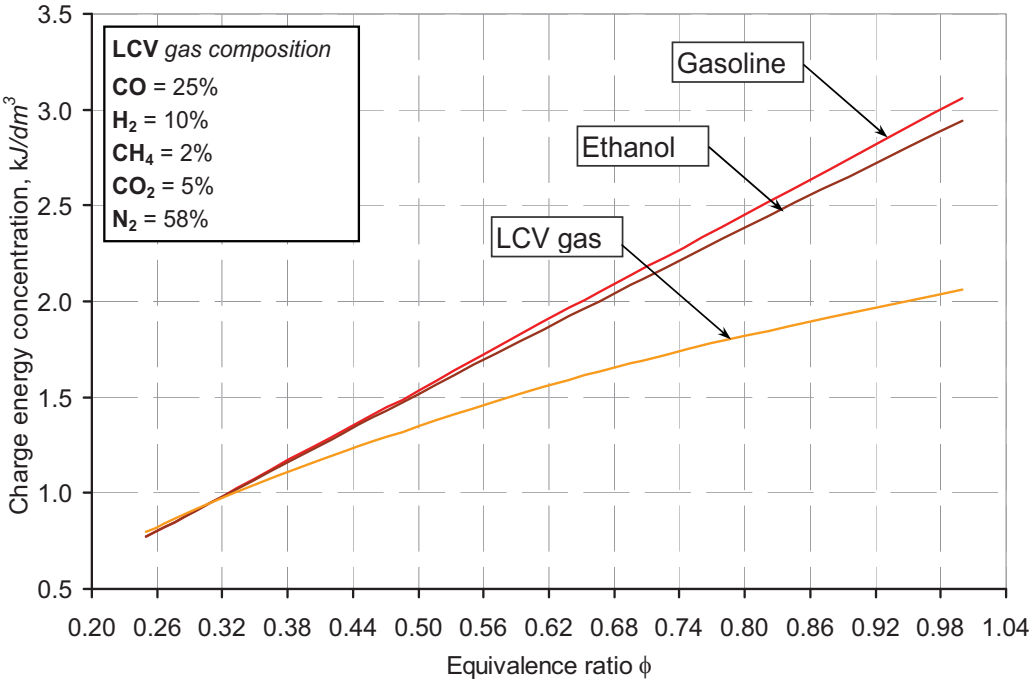

Figure 2.15: Charge energy density of different fuels used in HCCI engine [54]

Due to the composition of the biomass gas where a large fraction consists of inert components (N_2 and CO_2) a higher octane rating these components can act as knock suppressors to allow for use of higher compression ratio therefore leading to potentially higher efficiencies [53]. The most conventional and investigated mode of combustion in engines for LCV gas is currently SI [52, 53, 55, 56] due to very little modification of existing systems for implementation. With the higher octane rating of biomass gas conventional CI or diesel combustion becomes difficult to achieve, however the producer gas can be used for similar processes accomplished by dual fuel natural gas diesel engines.

2.4.1 SI Engine Biomass Gas Utilization

Direct usage of biomass gas in SI combustion is feasible due to its high octane number value despite a lower energy density per unit volume of charge (when compared

to gasoline/air mixtures). In [53] a DI CI engine was converted to SI mode for operation with biomass gas derived from an inline gasification unit. The engine was modified to allow for compression ratio manipulation which was employed for the experiments conducts in [53]. The gas fuel composition was measured in the delivery to the engine with a typical composition of 19% H_2, 19% CO, 2% CH_4, 12% CO_2, and 2% H_2O with the balance being N_2. The stock engine operating on diesel fuel in CI mode with a shaft output power of 24 kW at an overall efficiency of 31%, with a maximum compression ratio 17:1 implemented and the engine operating in SI mode burning the biomass gas 20 kW of power was recorded at 21% overall efficiency. As the compression ratio was reduced a decrease in power output and efficiency occurred. The ignition timing also needed to be advanced with a reduction in compression ratio to maintain maximum performance (quantified here with IMEP).

Another similar study was carried out in [55] on a small single cylinder SI engine. The composition of the LCV gas used was 3% CH_4, 14%H_2, 13% CO_2, 22% CO, 47.3% N_2, and 0.7% containing higher hydrocarbons (acetylene, ethylene, and ethane). Here performance and emission data for biomass gas operation was compared to conventional gasoline at different engine load settings. It was found that a reduction of ~50% in terms of torque occurred leading to a reduction in power when the LCV gas was implemented. This reduction in power can be attributed to two main factors: use of approximately stoichiometric mixtures and reduction in amount of air inducted. Minimal de-rating occurs when the mixture is lean $\Phi < 1$ and the de-rating increases with increases in equivalence ratio. Because [55] utilizes SI combustion the mixture must be around stoichiometric for the flame to propagate through the combustion chamber. Also, as the mixture becomes richer the volume the gaseous fuel charge occupies increases and inherently decreases the flow of air into the engine. SI requires stoichiometric mixtures therefore limiting mass of fuel which can be used (restricting the potential chemical energy to be released); which can lead to de-rating of work output when utilizing biomass gas. Significant reductions in CO and UHC emissions were recorded in [55] when the biomass gas was used compared to gasoline however there was an increase in the CO_2 produced. It is concluded in that LCV gas is a viable option for current commercial engines which employ natural gas or LPG as a fuel with very little modifications.

2.4.2 Biomass Gas Combustion in Diesel Engines

For most of the work concerning implementation of biomass gas for CI combustion it was found that the CI engines were operated in dual fuel mode; this means that there is a premixed charge of some auto-ignition resistant fuel (natural gas, biomass gas, etc.) and air inducted into the engine and then a pilot injection of high cetane fuel times/controls the ignition.

One study which conducts such an investigation is [57], where a mixture of H_2 and N_2 was introduced into the intake airstream and then the amount of diesel fuel directly injected into the cylinder was adjusted in order to produce a specified power output. It was determined through the experiments carried out that the addition of this LCV gas does not significantly affect the efficiency of the engine with the advantage of a substantial reduction in diesel fuel consumption. In terms of emission characteristics it was found that a reduction in NOx production occurred thought to be from an increase in the amount of N_2 present in cylinder and its dilution effects. However, increases in smoke, THC and CO were also recorded; this effect is denoted to be caused by a reduction in the overall O_2 concentration within the charge.

In the work of [58] a biomass gasifier is operated in conjunction with a DI-CI single cylinder engine with the concept of stationary power generation. To better understand how such a dual fuel system operates a schematic is depicted in Figure 2.16.

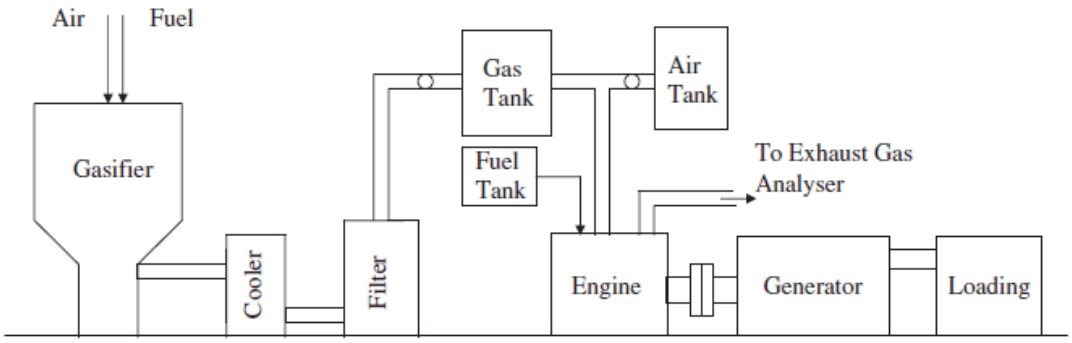

Figure 2.16: Schematic diagram fully renewable fuel engine test setup [58]

The gas produced from the gasifier, which for this study utilized coir-pith as the feedstock, was introduced and mixed in the intake manifold of the diesel engine. The objective of the work was to compare the operation of the DI-CI engine when operating on gas + pilot injection of diesel, gas + pilot injection of rubber seed oil (an alternative renewable liquid fuel), only diesel, and only rubber seed oil. A reduction in performance parameters such as brake thermal efficiency and specific energy consumption was recorded for all alternative fuelling cases when compared to diesel petrol as the sole fuel. The pilot injection fuel consumption savings when comparing the gas + liquid fuel experiments showed that there were lower amounts of petrol diesel required at specific engine outputs (BMEP). The emissions of CO were found to be higher at different engine loadings when using gas + oil vs. gas + diesel and the lowest CO emissions were recorded from the oil only fuelling condition.

2.4.3 Biomass Gas & HCCI Engines

The use of biomass gas for HCCI is extremely limited with only a few papers that incorporate both ideas. One such work was [59]; however this study still did not solely fuel an HCCI with biomass gas. In [59] both diesel and biomass gas were introduced into the intake manifold to create a homogeneous charge which is then inducted into the cylinder for subsequent combustion. The diesel was added as an ignition controller as it was thought that the auto-ignition temperature of only biomass gas/air mixtures would be unfeasible for combustion. The ratio of fuelling ranged from ~40-60% biogas. It was found that this dual fuelling methodology with variations in intake manifold temperature range used was 80-135˚C and was an effective process for controlling combustion. CO_2 in the gaseous fuel suppressed high temperature heat release therefore governing peak pressures and pressure rise rates while the CH_4 was thought to delay combustion to favourable (near TDC) crank angles. A small de-rating in efficiency of 3% was recorded when compared to sole diesel fuel operation. Smoke and NO levels were generally unaffected by dual fuel operation, however a significant increase in UHC was recorded with use of biogas when compared to diesel only fuelling conditions.

There are other works where individual components of a biomass gas mixture are investigated in terms of effects in HCCI combustion, such as H_2 and CO. One such study is [60] where simulated methanol reformed gas (MRG) was used with dimethyl ether (DME) in order to determine how combustion was affected by these mixtures. In this work it was shown that H_2 is an effective ignition controller for HCCI with DME where combustion was delayed due to the higher auto-ignition temperature of H_2 gas mixtures in air. It was also stated that H_2 had a greater effect on retarding combustion that CO did.

Though some of the concepts found in these studies may be applicable to the work done for this thesis none are found to directly relate to HCCI combustion of biomass gas as the sole fuel.

CHAPTER III

DESIGN AND METHODOLOGY

3.1 Engine Experimental Setup

The experimental setup used to carry out this investigation was originally designed and fabricated by a previous M.A.S.c student P. Zoldak and a detailed design of all systems can be found in [61]. Overall small modifications/improvements to the experimental setup have been made but the setup itself for the most part remains as originally designed. The engine and fuelling system are shown in Figure 3.1. For the benefit of the reader of this document a general description of the apparatus will be discussed.

Figure 3.1: Experimental Engine and Fuelling System

The engine itself is a four stroke; three-cylinder compression-ignition engine (Kubota D905) converted to a single cylinder HCCI operation by means of disabling the intake and exhaust valves in for two of the cylinders. The stock engine was an in-direct injection pre-chamber type CI engine. The original pre-chamber was left unmodified; however the entry nozzle from the main chamber was enlarged. The pre-chamber before and after modification for HCCI combustion is shown in Figure 3.2.

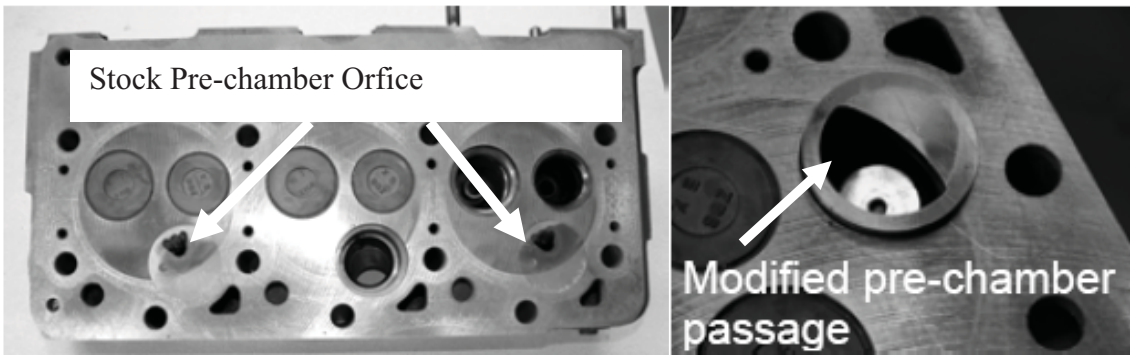

Figure 3.2: Pre-chamber modification for HCCI combustion [61]

The engine is motored using an AC motor with a variable speed drive (VSD). The VSD system is used to maintain the engine speed at a desired RPM during both motoring and firing scenarios. The VSD has in addition a resistor brake which dissipates power generated by the engine during firing conditions.

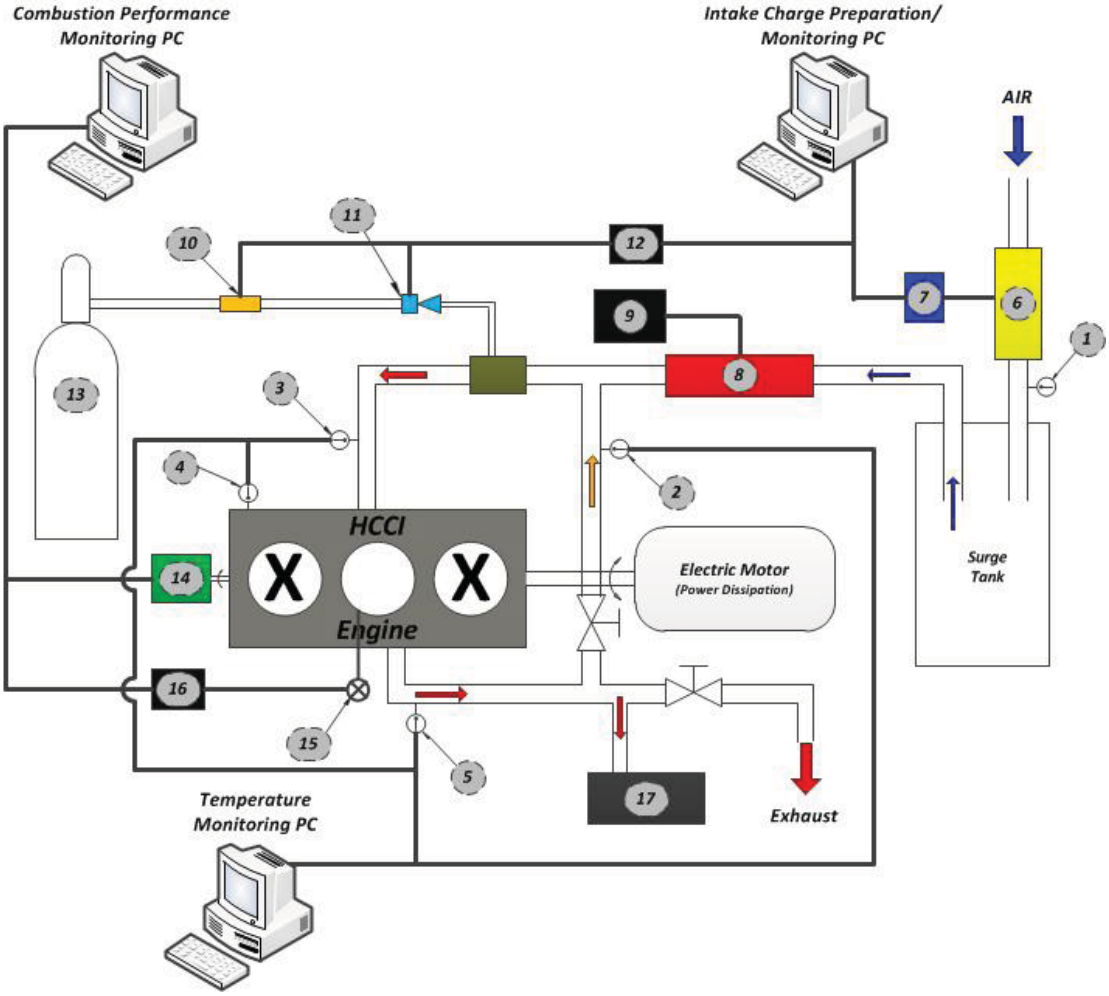

Figure 3.3: Experimental Engine Setup Schematic

The engine is instrumented with various equipement in order to measure and/or control operating conditions and performance. A schematic identifying the core elements of the experimental setup is provided in Figure 3.3 (above). The numbered equipment in Figure 3.3 is identified in Table 3.1 and will be described next.

Table 3.1: Core Experimental Element Identification Corresponding to Figure 3.3

Item Number	Description
1	T_{Room} ***thermocouple*** (measure room air temp.)
2	T_{EGR} ***thermocouple*** (measure temp. of EGR)
3	T_{Intake} ***thermocouple*** (measure temp of fresh charge)
4	T_{Cool} ***thermocouple*** (measure temp of engine coolant)
5	$T_{Exhaust}$ ***thermocouple*** (measure temp of exhaust)
6	***Laminar Flow Element*** (LFE creates differential pressure which correlates with a flowrate)
7	***Differential Pressure Transmitter*** (measures diff. press. Created by LFE)
8	***Intake Charge Preheater*** (preheats intake charge to predetermined temp.)
9	***Temperature Controller*** (controls the Intake Charge Preheater)
10	***Fuel Flowmeter*** (measures the flowrate of fuel being delievered)
11	***Electronic Fuel Injector*** used to deliver the fuel at a specific time dueing the engine cycle
12	The ***ECU*** is used to control the injector timing and monitor some engine parameters (i.e. MAP, coolant temp. etc.)
13	***Gasesous Cylinder*** (contains premixed fuel composition)
14	***Shaft Encoder*** (used to measure the displacement of the crankshaft corresponding to a piston position of TDC)
15	***Pressure Transducer*** (measures the pressure in the cylinder)
16	***Charge Amplifier*** (conditions the signal from the pressure transducer)
17	***Emission Analyzer*** (measures levels of certain engine emissions)

A number of K-Type thermocouples were installed along the intake and exhaust channels to monitor and record the intake and exhaust gas temperatures along with one installed in a cooling channel to monitor engine block temperature. The intake and exhaust system design has the capability of introducing EGR into the intake charge channel. The intake air pre-heater and a laminar flow element in conjunction with a differential pressure transmitter measure and prepare the incoming air for the combustion process. The fuel system designed utilizes a pressure regulator, which maintains the pressure of approximately 255kPa (the suggested operating pressure of the injector) from the gaseous fuel cylinder containing our premixed LCV gas composition(s), to a solenoid valve

(gaseous injector). An electronic control system (ECU) is implemented with a control interface via PC software and was installed to regulate the time of the solenoid valve opening and open duration in order to supply the required demand of LCV fuel dose to the engine cylinder (intake port injection). A Kistler piezoelectric 5mm wall-mounted transducer (6052A1) is mounted in the stock glow plug hole for the acquisition of in-cylinder pressure measurements; the pressure signal is conditioned using a DSP 1104CA charge amplifier. A Gurley optical encoder with a 0.1 degree Crank Angle (CA) resolution is used for engine speed and crank angle measurements. All of the results reported on in this work are a result of the average of 125 consecutive engine cycles. The engine-out emissions were evaluated using a portable MicroGasTM gas analyzer. The emissions data is omitted from the main body of this work as the instrument used is not research calibre; however the emissions results were recorded in Appendix B.

3.2 Data Acquisition and Parameter Control

The data acquisition for this experimental setup has three core systems: combustion performance monitoring, intake charge preparation and monitoring, and system temperature monitoring and control.

The indicated combustion performance of an engine is mainly attributed from the in-cylinder pressure with respect crank angle or cylinder volume. To acquire/process/display the in-cylinder pressure events a MTS CAS (Combustion Analysis System) is utilized and is specifically constructed for experimentation with internal combustion engines. The encoder signal and in-cylinder pressure transducer are routed into this DAQ system where they are used to calculate various performance indicators (IMEP, HRR, HR, etc.).

The intake charge conditions play an extremely important role in the HCCI mode of combustion. The air flowrate and fuel flowrate signals are generated and sent to a NI (National Instruments) SCB 68 terminal box which interfaces with a NI PCI 6251 card in a dedicated PC. A NI LabView program was developed to compare the signals real-time and record the operating equivalence. The rate at which fuel is delivered and how the equivalence is altered is done by the aftermarket EFI ECU and fuel injection system. The engine is naturally aspirated with no need for a throttle as in an SI engine. The intake

charge temperature is manipulated using a Sylvania SureHeat MAX 6kW in conjunction with a standalone temperature controller which utilizes a feedback loop based on the intake thermocouple temperature signal.

The system temperature monitoring and control consists of installed thermocouples to monitor ambient temperature, intake charge temperature, engine coolant temperature, exhaust temperature and the temperature of EGR. The thermocouples are coupled to a NI SCB 100 terminal box which interfaces with a NI PCI 6071E card located in a PC. The software is a Labview based GUI developed in [56] and was not modified for this investigation. There are only two temperatures which currently have specific systems to control them: intake charge (previously discussed) and coolant temperature. The coolant temperature is controlled manually by engaging two electric fans located in front of the engine radiator when the coolant temperature exceeds a high limit predetermined by the operator.

3.3 Operational Conditions

In Table 3.2 the general specification of the Kubota D-905 engine used for this study is listed and also the operating parameters which were applied during the experimental trials.

Table 3.2: General Engine Specifications & Operating Conditions

Engine Parameter	***Description***
Engine Type	Vertical 4-stroke liquid cooled indirect injection compression ignition
Number of Cylinders	3 Cylinder engine [1 cylinder operating, 2 others have values disabled]
Compression Ratio	22:01
Bore & Stroke (mm)	72.0 x 73.6
Engine Speed (RPM)	900-1500
EGR (% by vol.)	0
Coolant Temperature, T_c	~83.5°C (± 0.7°C)
Intake Charge Temperature, T_i	128.6°C to 184.6°C
Equivalence Ratio, Φ	0.346 to 0.513

Identified in Table 3.3 are the compositions of the four biomass gases tested for this study. The gas compositions 1 and 2 emulate real compositions produced from a gasifier system under the operation of my collegue Grzegorz Przybyla in Poland. Fuel

compositions 3 and 4 were designed to test implications of changes in hydrogen and carbon monoxide content in a mixture. For compositions 1, 2, and 3 the CH_4, CO_2 and N_2 fractions are held constant and only the H_2: CO is manipulated. For composition #4 CH_4 and CO_2 are the same but a portion of the N_2 fraction (5%) is redistributed to the H_2/CO fraction. The % fraction of each component is identified on a gravimetric basis and the fuel compositions themselves are supplied by Praxair in a premixed bottle. The flowmeter correlation factor is a value supplied by Alicat Instruments to scale the recorded flowrates in terms of N_2 and convert the readings to the true value of each fuel composition flow based on each mixture's viscosity factor. The stoichiometric AFR (air-to-fuel ratio) is the ratio at which the fuel and air would have to be mixed to form a perfect balanced chemical equation based on complete combustion of the fuel in air with products consisting of only CO_2, H_2O, and N_2. The H_2: CO ratio is the ratio at which the two components will be found in each fuel composition. The LCV is a measure of the energy content for a unit mass of fuel but can also be identified per unit of volume.

Table 3.3: Fuel Compositions & Factors

	Composition #1	Composition #2	Composition #3	Composition #4
CO	25	20	15	25
H_2	10	15	20	15
CH_4	2	2	2	2
CO_2	5	5	5	5
N_2	58	58	58	53
AFR_{Stoich}	***1.144***	***1.204***	***1.271***	***1.344***
H_2:CO Ratio	**1 : 2.50**	**1 : 1.33**	**1 : 0.75**	**1 : 1.67**
LCV (MJ/kg)	***4.271***	***4.413***	***4.570***	***4.987***

3.4 Performance and Combustion Phasing Quantification Methodology

In order to quantify/compare how well an engine operates in terms of performance there are several parameters which are analyzed. These parameters are: (a) maximum in-cylinder pressure, (b) pressure rise rate, (c) IMEP, and (d) indicated efficiency.

(a) Maximum In-cylinder Pressure

- The maximum in-cylinder pressure is simply extracted from the cycle resolved pressure traces experienced by the in-cylinder pressure transducer and recorded by the CAS system.

(b) Pressure Rise Rate

- The pressure rise rates reported on in this study are based on the calculation of the 1st derivative of the pressure curve with respect to CA. The CAS system has a built in function to calculate this data without further post processing; the formula utilized by the MTS CAS System 2005 is:

$$\frac{dP_i}{dCA} = \frac{1}{12 * \Delta CA} * (P_{i-2} - 8 * P_{i-1} + 8 * P_{i+1} - P_{i+2})$$

Where: P_i= in-cylinder pressure

CA= crank angle

ΔCA= change in crank angle

(c) IMEP

- IMEP or Indicated Mean Effective Pressure is a measure of the work done by the expanding gases (combustion products) on the piston per unit of swept volume. Through the utilization of this comparison method researchers can compare engines of different displacements and number of cylinders because the size of the engine is normalized.

$$IMEP = \frac{W_{c,i}}{V_d} = \oint \frac{PdV}{V_d} \qquad [48]$$

Where: $W_{c,i}$= indicated work of the cycle

V_d= displacement volume

P= in-cylinder pressure

(d) Indicated Efficiency (η_i)

- The indicated efficiency is a calculation which is a means of evaluating the thermodynamic process in an engine by isolating and ignoring any mechanical losses.

$$\eta_i = \frac{\dot{W}_i}{\dot{m}_f * CV} \qquad [3]$$

Where: $\dot{W}_i$ = engine indicated power (indicated work*engine speed)

$\dot{m}_f$ = mass flowrate of fuel

CV= calorific value of the fuel

The performance of the engine is dependent on the combustion event itself therefore the phasing of the combustion or release of energy must be analyzed. In this study (i) Net HRR and HR, (ii) SOC, and (iii) combustion duration will be the main focus for quantifying the phasing.

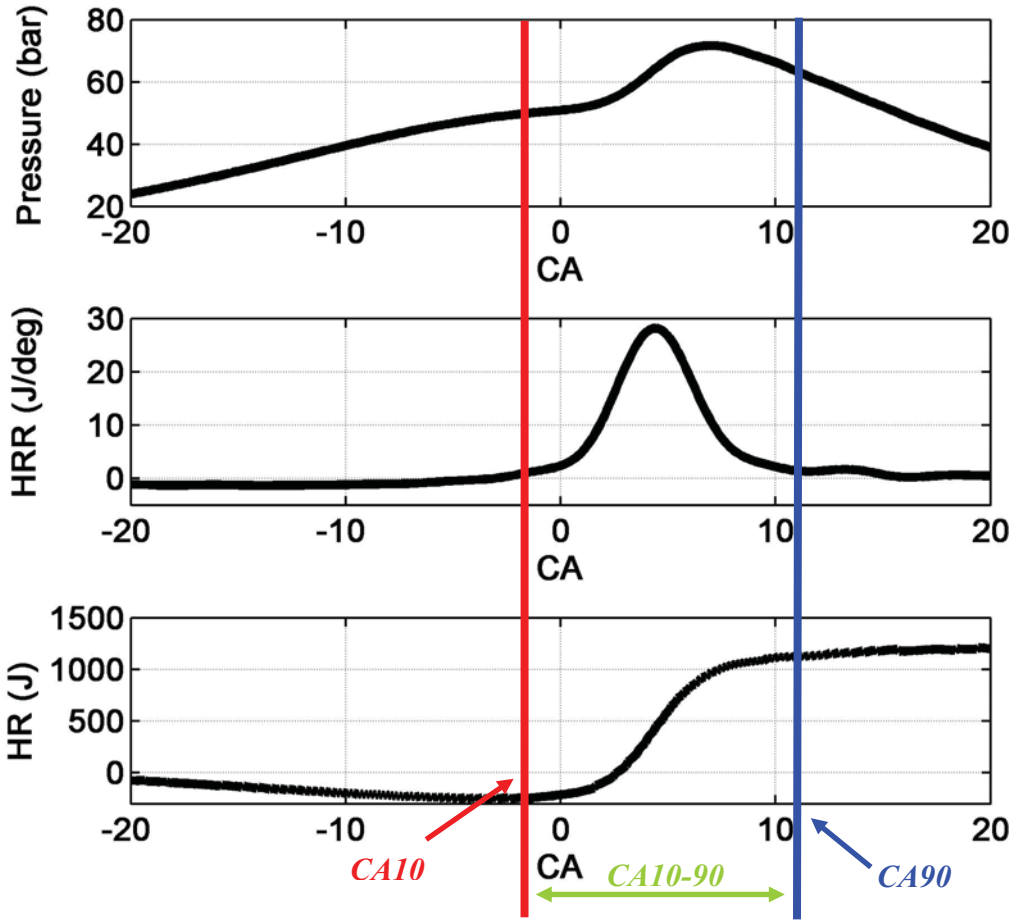

Figure 3.4: Pressure, HRR, and HR traces showing correlation of CA10, CA90, and CA10-90

(i) Net HRR & HR (Heat Release Rate & Heat Release shown in Fig. 3.4)

- The net HRR is calculated from the in-cylinder pressure trace and is the difference between the gross heat release rate and the heat-transfer rate to the walls. This can also be equated to the rate at which work is done on

the piston plus the rate of change of internal energy of the cylinder contents. [48]

$$\frac{dQ_n}{dt} = \frac{dQ_{ch}}{dt} - \frac{dQ_{ht}}{dt} = p\frac{dV}{dt} + \frac{dU_s}{dt} = \frac{\gamma}{\gamma - 1} p\frac{dV}{dCA} + \frac{1}{\gamma - 1} V\frac{dp}{dCA}$$

Where: Q_n= net HR

t= time

Q_{ch}= gross HRR

Q_{ht}= heat transfer to the walls

p= in-cylinder pressure

V= volume

U_s= internal energy

ɣ= ratio of specific heats

CA= crank angle

- The HR is the amount of energy released at a certain crank angle and is the HRR multiplied by the crank angle.

(ii) SOC (Start of Combustion) ***or*** CA10 (shown in Fig. 3.4)

- The SOC is a calculation based on 10% of the total heat released (HR) which is derived from the HRR curve. The CA which correlates to 10% of the total HR is then identified at the point where SOC or the on-set of combustion occurs (CA10) [3].

(iii) Combustion Duration ***or*** CA10-90 (shown in Figure 3.4)

- The combustion duration is the measure of the total crank angle displacement from SOC or 10% of the total heat released to EOC (End of Combustion) or 90% of the total heat released [3].

CHAPTER IV

RESULTS

4.1 Experimental Results Preamble

The fuel compositions identified in Section 3.3 of this study were tested over a range of equivalence ratios, intake charge temperatures and engine speeds as reported in Table 3.2. Table 4.1 listed below shows the specific operating conditions corresponding to each fuel composition (RPM, T_{in}, equivalence ratio). A complete table of results is provided in Appendix A.

Table 4.1: Specific Operating Test Conditions Regarding Fuel Composition

Operating Condition	***Fuel Composition #1***	***Fuel Composition #2***	***Fuel Composition #3***	***Fuel Composition #4***
Engine Speed (RPM)	*Inconclusive*	931.8 to 1530.5	932.6 to 1524.8	935.0 to 1525.3
Intake Charge Temperature, T_i		128.6°C to 162.3°C	130.2°C to 163.4°C	150.9°C to 184.6°C
Equivalence Ratio, Φ		0.346 to 0.513	0.346 to 0.455	0.351 to 0.452

Fuel composition #1 shows not operating conditions. When testing fuel #1 it was found that the fuel was extremely sensitive to engine speed which is postulated to be related to charge mixing. Combustion would only occur for this fuel at 1500 RPM. Because the nature of this study is to compare results for all fuel compositions with respect to equivalence ratio, intake temperature and engine speed the results were inconclusive and excluded from further discussion.

Fuel compositions 2, 3, and 4 ran the engine over the range of engine speeds at various equivalence ratios with corresponding intake charge temperatures. All engine speeds were virtually held constant for all tests at approximately 930, 1220, 1525 rpm. Fuels 2 and 3 operated over the same intake temperature range of approximately 130°C to 160°C; however fuel 4 required a higher intake temperature band of 150°C to 180°C. In terms of equivalence ratio, fuel 2 operated over the largest range from $\Phi = 0.346$ to 0.513. Fuels 3 and 4 were able to maintain a lean operating ratio of $\Phi \approx 0.35$ as with fuel 2 but were limited to $\Phi \approx 0.45$ by maximum in-cylinder pressure conditions.

The graphical technique for data analysis presented in this work is a series of contour plots representing the surface of best fit based on the interplant method to the cubic (3rd) order.

4.2 Individual Fuel Composition Results

4.2.1 Fuel Composition 2 Results – T_{in} and Φ Parameters at various Engine Speeds

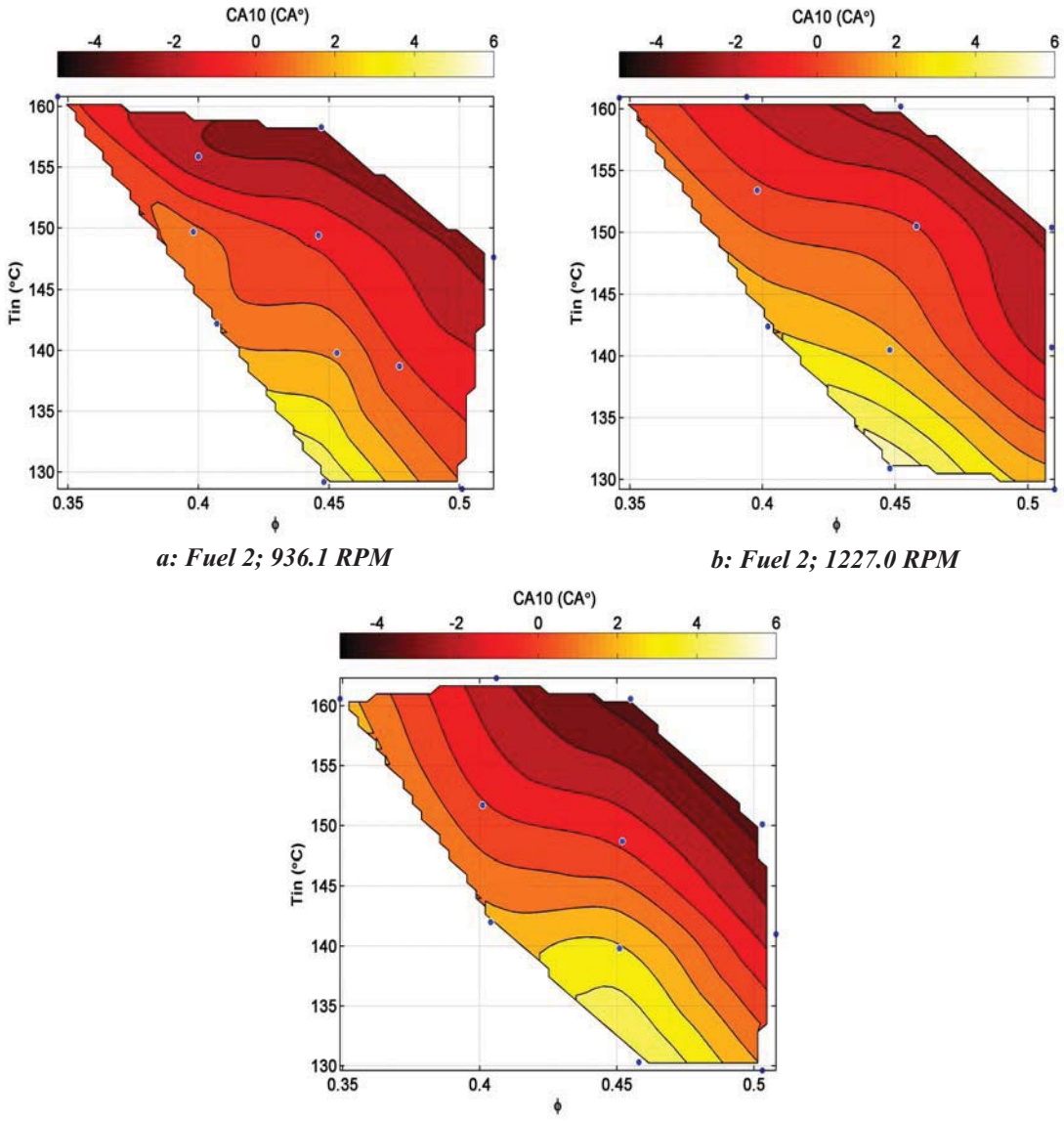

a: Fuel 2; 936.1 RPM

b: Fuel 2; 1227.0 RPM

c: Fuel 2; 1524.7 RPM

Figure 4.1: CA10 for Fuel Composition 2 with respect to intake charge temperature and equivalence ratio at engine speeds of 936.1, 1227.0 and 1524.7 RPM

In order to quantify the phasing of combustion the heat release is calculated from the recorded in-cylinder pressure data. SOC is denoted as CA10; the crank angle position at which 10% of the heat is released. 0 °CA represents the piston's position as top dead center (TDC) in the cylinder following the compression stroke; a negative CA value indicates a position before the piston reaches TDC. Figure 4.1 shows results obtained regarding SOC corresponding to combustion of fuel 2. The most advanced SOC timing recorded was approximately -3.50 °CA where the highest equivalence ratio of 0.503 was used at the highest temperature (150.1°C) tested for that mixture. The most retarded SOC was 5.8 °CA where the minimum temperature of 130.9°C was tested at the minimum equivalence ratio ($\Phi = 0.448$) corresponding to that temperature. At any constant equivalence ratio with fixed engine speed as the intake charge temperature is increased the SOC advances. As equivalence ratio is increased at a constant intake temperature with fixed engine speed the SOC generally is advanced. When comparing Figs. 4.1.a, 4.1.b, and 4.1.c engine speed has no significant impact on SOC phasing.

Figure 4.2 shows CA10-90 which is the duration of heat release from 10% heat release to 90% heat release measured in crank angle degrees; this value can also be thought of as the duration of combustion. The shortest duration of heat release was 2.1 °CA occurring at equivalence ratio 0.452 with a peak intake temperature of 160.2°C at the lowest engine speed of 936 rpm. The maximum duration of heat release was 23.7 °CA at the lowest intake charge temperature of 129.2°C with an equivalence ratio of 0.448 and engine speed of 936 rpm. In Figure 4.2 the lowest intake charge temperatures with the leanest mixtures produce the longest heat release durations for all engine speeds. As the equivalence ratio is increased utilizing minimum intake temperature preheating the duration of heat release is decreased. As the intake charge temperature is increased at constant equivalence ratio CA10-90 decreases until a minimum value of ~2 °CA is achieved. At the rich limit of these experiments it is found the intake temperature has little affect on CA10-90 with minimal engine speed as the duration has already reached a minimum value of ~2 °CA. Over the range of engine speeds tested with intake temperatures above 136°C variations in engine speed showed very little impact on the duration of combustion.

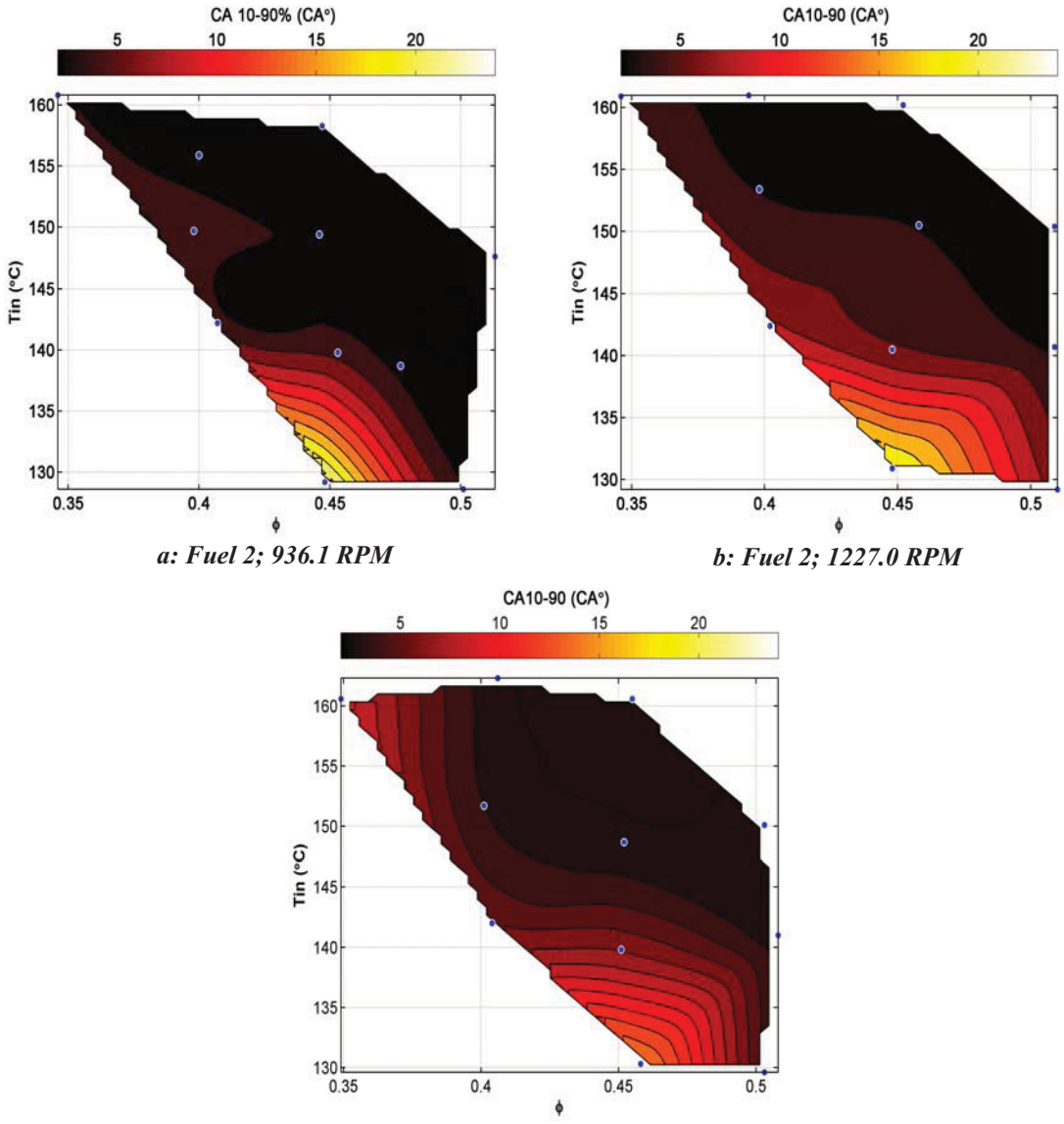

a: Fuel 2; 936.1 RPM

b: Fuel 2; 1227.0 RPM

c: Fuel 2; 1524.7 RPM

Figure 4.2: CA10-90 for Fuel Composition 2 with respect to intake charge temperature and equivalence ratio at engine speeds of 936.1, 1227.0 and 1524.7 RPM

The pressure rise rate is a result related to combustion phasing. If SOC advances while CA10-90 duration decreases combustion shifts before TDC. Therefore, because the piston is still rising decreasing the cylinder volume which increases the pressure with additional pressure increases due to expanding combustion products the pressure rise increases. The maximum pressure rise rate of 11.5 bar/°CA using fuel 2 occurred at with the richest mixture of $\Phi = 0.503$ and at a maximum intake charge temperature of 150.1°C

with the maximum engine speed tested. The minimum pressure rise rate recorded was 1.8 bar/°CA and occurred at the lowest intake charge temperature of 130.9°C with the leanest mixture of Φ = 0.448.

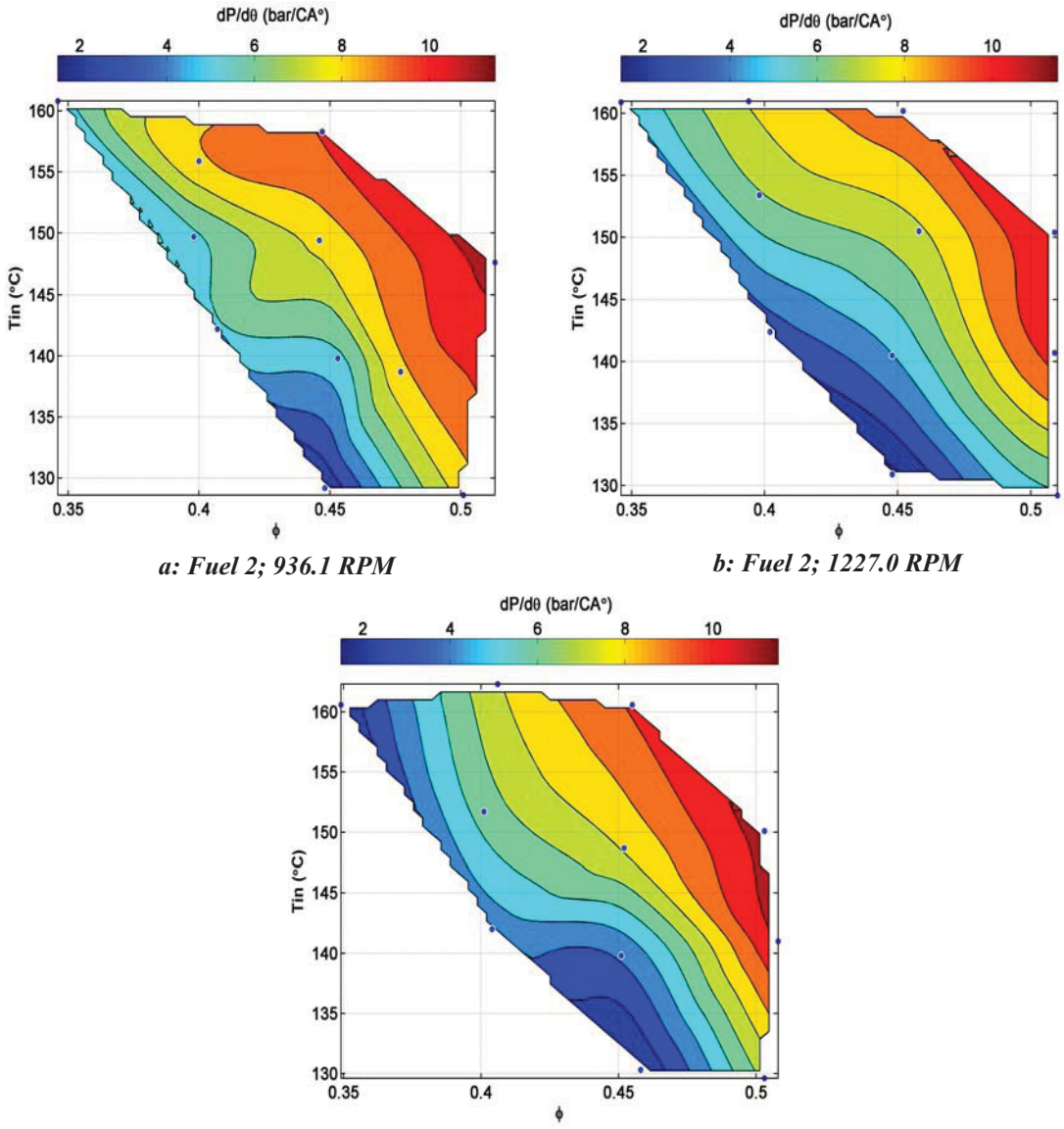

a: Fuel 2; 936.1 RPM

b: Fuel 2; 1227.0 RPM

c: Fuel 2; 1524.7 RPM

Figure 4.3: Maximum Pressure Rise Rate for Fuel Composition 2 with respect to intake charge temperature and equivalence ratio at engine speeds of 936.1, 1227.0 and 1524.7 RPM

Figure 4.3 contains the results regarding the maximum in-cylinder pressure rise rate. If intake temperature is maintained constant and equivalence ratio is increased the maximum pressure rise rate increases. If the air-to-fuel mixture is constant at any

equivalence ratio and the intake charge temperature is increased the maximum pressure rise rate increases. If variations in engine speeds at fixed equivalence ratio and intake charge temperature are considered there is very little effect. At the lean limit of operation a wider range of pressure rise rates occur (1.8 to 5.7 bar/°CA) compared with other fixed equivalence ratio and intake temperature fixed conditions. This result is most predominant at equivalence ratio ~0.35 and intake temperature ~160°C.

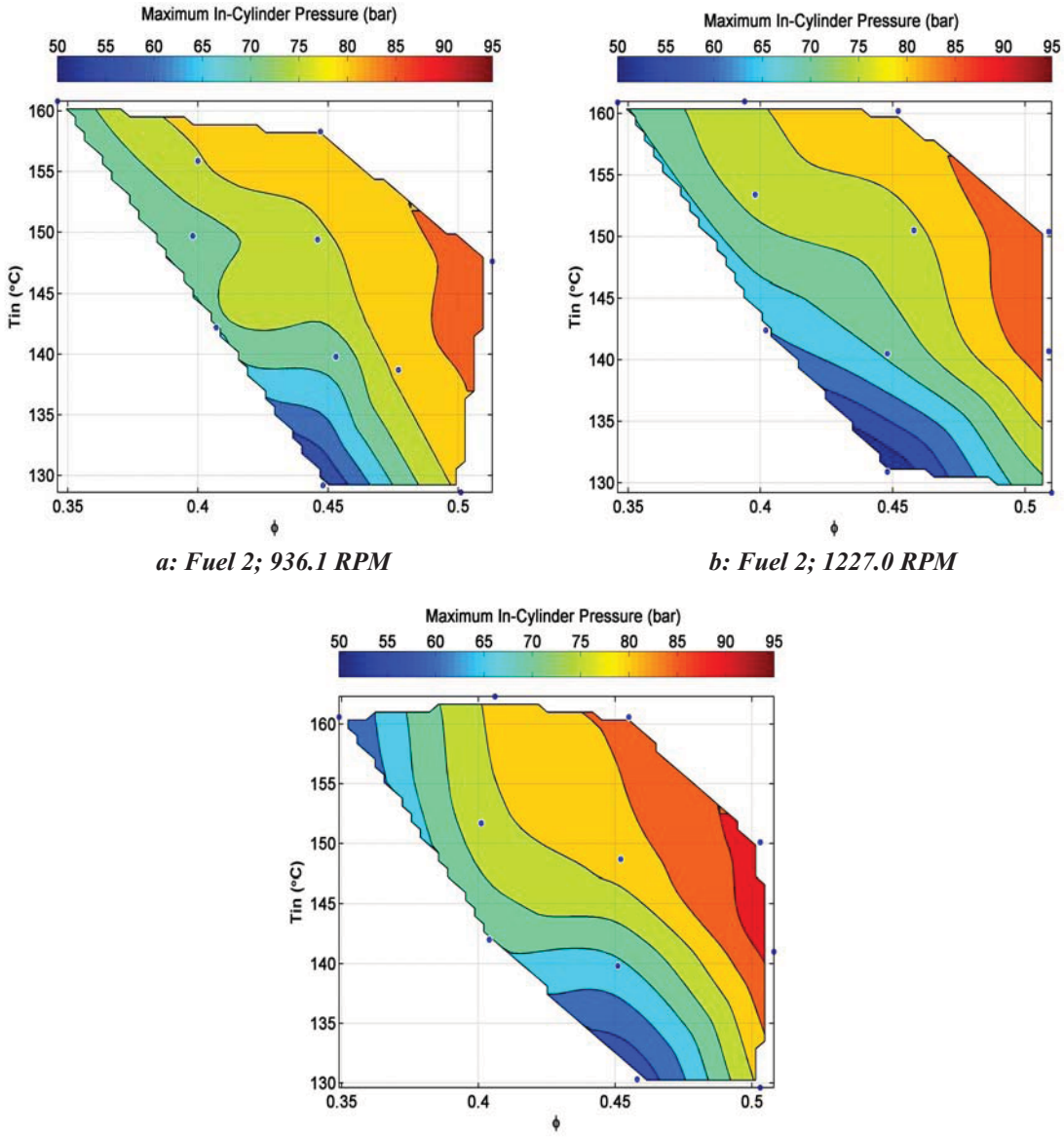

a: Fuel 2; 936.1 RPM

b: Fuel 2; 1227.0 RPM

c: Fuel 2; 1524.7 RPM

Figure 4.4: Maximum In-Cylinder Pressure for Fuel Composition 2 with respect to intake charge temperature and equivalence ratio at engine speeds of 936.1, 1227.0 and 1524.7 RPM

Both combustion phasing and pressure rise rates affect maximum in-cylinder pressure; results are shown in Figure 4.4. Similar occurrences are observed in maximum in-cylinder pressure as was recorded with $dP/d\theta$. The lowest pressure 51.0 bar occurred at the lowest temperature of 130.9°C with the leanest mixture of $\Phi = 0.451$ while the maximum pressure (92.3 bar) occurred at the richest mixture of $\Phi = 0.503$ with the highest temperature of 150.1°C. As with SOC and $dP/d\theta$ if intake charge temperature is maintained constant and increase the equivalence ratio the maximum in-cylinder pressure increases. If a constant equivalence ratio is maintained and the intake temperature is increased the maximum in-cylinder pressure again increases. The highest range of maximum in-cylinder pressure (56.7 to 92.3 bar) occurs at the highest engine speed tested of 1525 rpm. At the lower engine speeds of 1227 and 936 rpm the maximum pressure was limited to 88 bar.

IMEP results are displayed in Figure 4.5 with values ranging from 2.32 bar to 3.67 bar; both the maximum value is recorded at an engine speed of 1227 and minimum occurred at an engine speed of 1524 rpm. At the engine speed of 936 rpm IMEP ranges from 2.51 bar to 3.41 bar; the minimum value is achieved using the leanest mixtures at the highest temperatures ($\Phi = 0.349$ and $T_{in} = 160.6$°C) and maximum occurs with richest mixtures at lowest temperatures ($\Phi = 0.505$ and $T_{in} = 129.1$°C). The most obvious observation is that as intake charge temperature is increased the IMEP decreases; this result can be related to poor combustion phasing (SOC BTDC, Fig. 4.1) and reduced volumetric efficiency. The decrease in IMEP as intake temperature increases is consistent for all engine speeds [($IMEP_{1524rpm,\ \Phi=0.45}$ = 3.45 bar {130.3°C} to 2.71 bar {160.6°C}), ($IMEP_{1227rpm,\ \Phi=0.45}$ = 3.17 bar {130.9°C} to 2.74 bar {160.2°C}), ($IMEP_{936rpm,\ \Phi=0.45}$ = 3.28 bar {129.2°C} to 2.69 bar {158.3°C})]. If the intake temperature is held constant at the engine speed of 936 rpm there is not much effect of varied equivalence ratio (i.e. $\Delta IMEP_{150°C\text{-}936rpm}$ = 0.16 bar). As the engine speed is increased to ~1230rpm the trend of little variation in IMEP due to changes in the equivalence ratio is present above intake temperatures of 145°C ($\Delta IMEP_{160°C\text{-}1227rpm}$ = 0.12 bar). When lower temperatures below 145°C are used equivalence ratio variations seem to impact IMEP for 1227rpm; as the equivalence ratio is increased IMEP increases ($\Delta IMEP_{130°C\text{-}1227rpm}$ = 0.57 bar). At the constant engine speed of 1524 rpm as the

equivalence ratio increases at a constant intake temperature IMEP values increase ($\Delta IMEP_{140°C\text{-}1525rpm}$ = 0.47 bar). With changes in engine speed from 936 rpm to 1227 rpm under generally constant conditions the IMEP achieved increased as engine speed was increased most predominantly occurring with richer mixtures (i.e. $IMEP_{936rpm,\ \Phi=0.50,\ Tin=130°C}$ = 3.41 to $IMEP_{1227rpm,\ \Phi=0.50,\ Tin=130°C}$ =3.67 bar). With further increases to engine speed after 1227 rpm a larger range of IMEP occurred, however there were no further increases in maximum IMEP recorded ($\Delta IMEP_{130°C,\ 1227\text{-}1525rpm}$ = 0.06 bar).

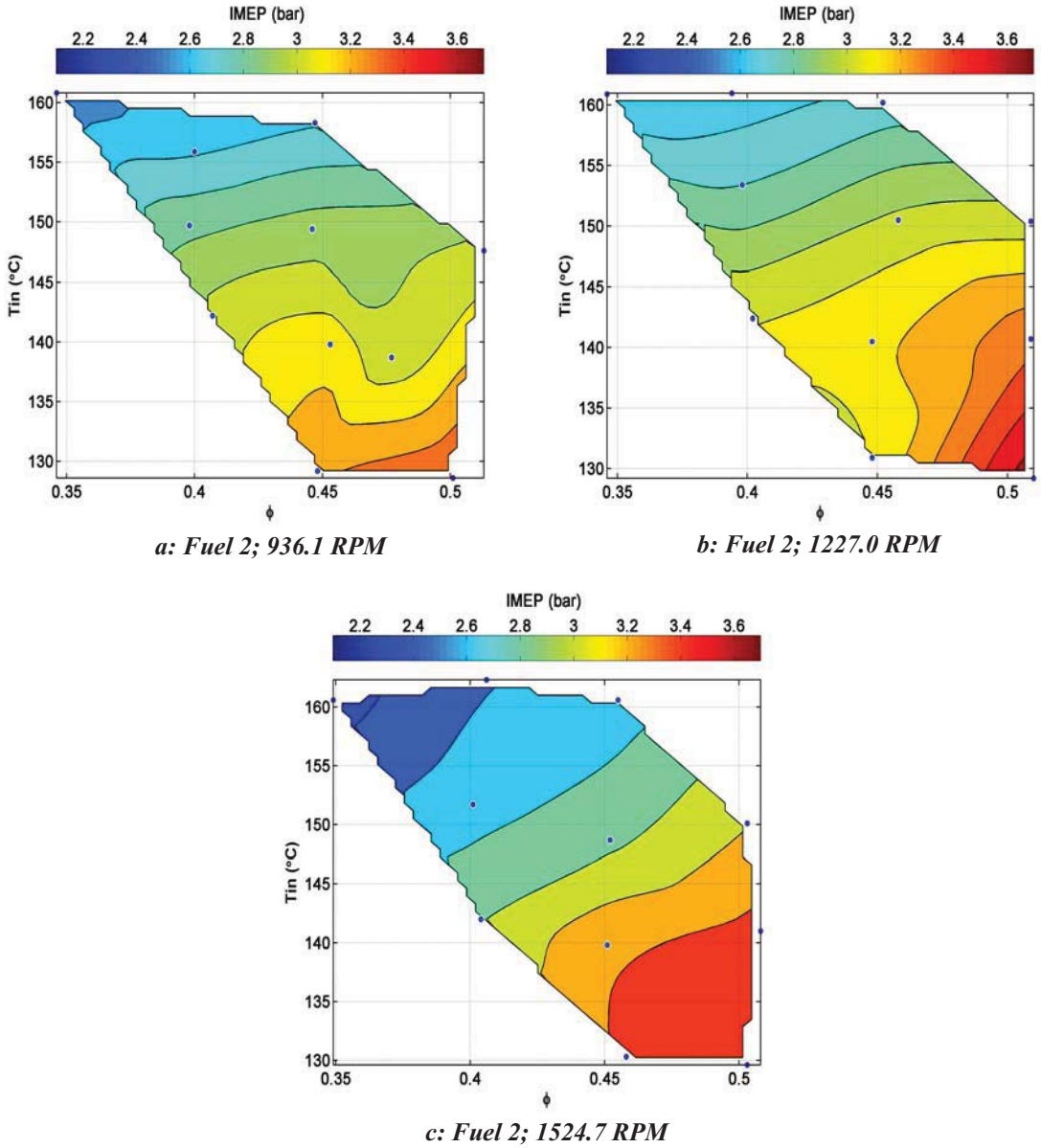

a: Fuel 2; 936.1 RPM

b: Fuel 2; 1227.0 RPM

c: Fuel 2; 1524.7 RPM

Figure 4.5: IMEP for Fuel Composition 2 with respect to intake charge temperature and equivalence ratio at engine speeds of 936.1, 1227.0 and 1524.7 RPM

Figure 4.6 depicts the changes in indicated efficiency which vary from 27.8% occurring with the richest mixture at the highest temperature and engine speed (Φ=0.455, 160.6°C, 1525rpm) to 33.9% with the leanest mixture at the lowest temperature, highest speed (Φ=0.458, 130.3°C, 1525rpm). For Fig. 4.6.a (936rpm) at any constant temperature if the equivalence ratio is increased the indicated efficiency decreases ($\eta_{i150°C,\ 936rpm}$ = 31.7% drops to 28.1%). Alternatively if the equivalence ratio is maintained constant and the intake temperature is increased the indicated efficiency again decreases ($\eta_{i\Phi=.045,\ 936rpm}$ = 32.7% drops to 28%). When considering the engine speed of 1227rpm (Fig. 4.6.b) if constant temperatures above 140°C are considered as equivalence ratio is increased the indicated efficiency decreases ($\eta_{i160°C,\ 1227rpm}$ = 32.5% drops to 27.9%). Utilizing the lowest temperature at 1227rpm the efficiency actually increases with increases in equivalence ratio which is contradictory to trends which were previously observed ($\eta_{i130°C,\ 1227rpm}$ = 30.7% drops to 33.3%); this result could be attributed to insufficient mixing and will be discussed further in Chapter 5. Evaluating Figure 4.6.c. the most significant observation is there are no changes in indicated efficiency with respect to equivalence ratio variations; at 1525rpm indicated efficiency is independent of equivalence ratio. With a fixed equivalence ratio and increasing intake temperature the indicated efficiency decreases for all equivalence ratio cases at 1525 rpm ($\eta_{i\Phi=.045,\ 1525rpm}$ = 33.9% drops to 27.7%). With respect to varying engine speed at higher temperatures using weaker mixtures and engine speeds lower than 1227rpm there is very little effect on efficiency ($\Delta\eta_{i\Phi=0.40,\ 936\text{-}1227rpm,\ 160°C}$ = 0.5%). If the engine speed is further increased to 1525rpm under lean operation and high temperature there is a significant decrease in the efficiency relative to the lower engine speed conditions. As temperature decreases and mixtures become richer the variations in efficiency over the span of engine speeds tested diminishes.

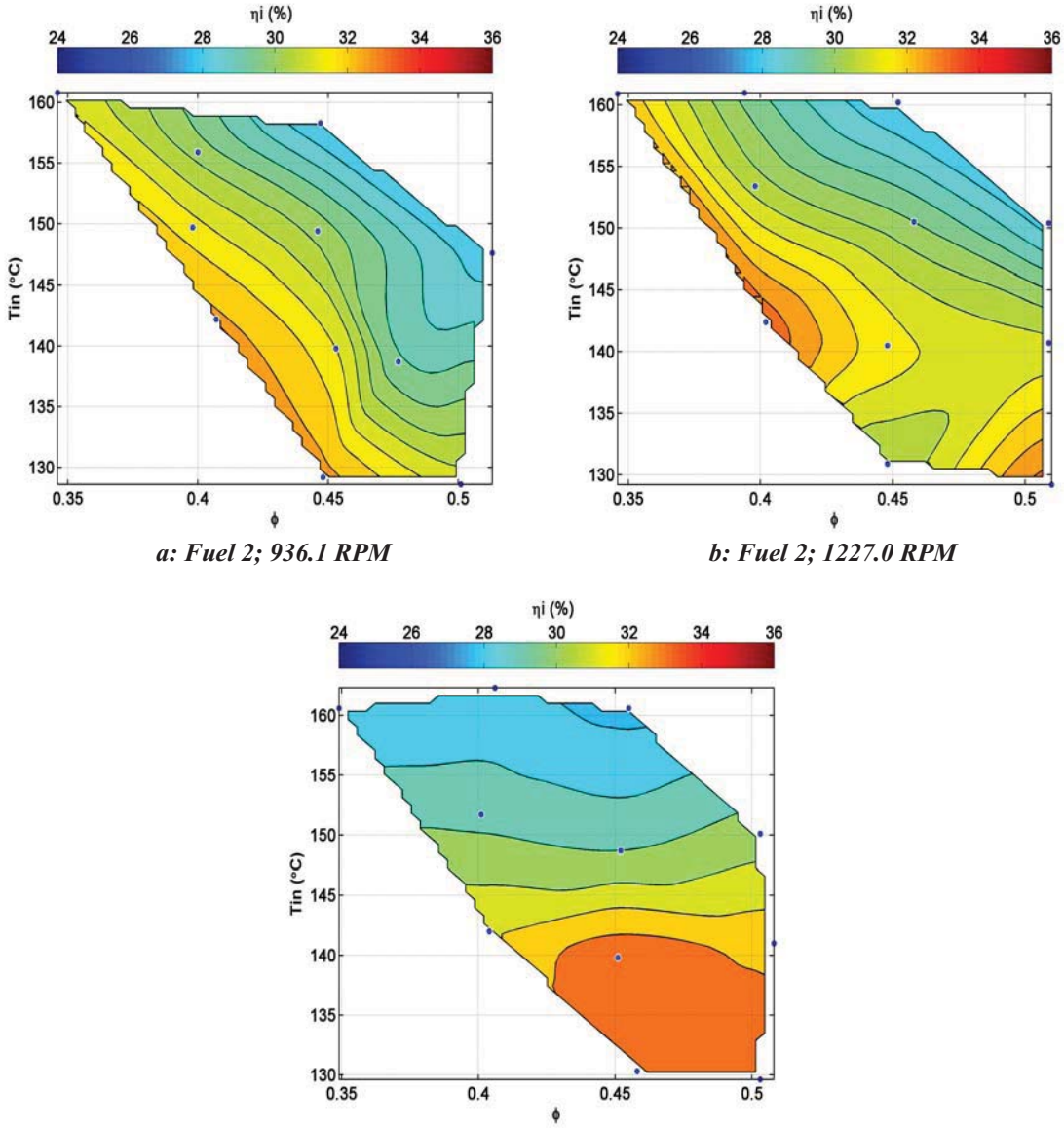

a: Fuel 2; 936.1 RPM

b: Fuel 2; 1227.0 RPM

c: Fuel 2; 1524.7 RPM

Figure 4.6: Indicated Efficiency for Fuel Composition 2 with respect to intake charge temperature and equivalence ratio at engine speeds of 936.1, 1227.0, and 1524.7 RPM

4.2.2 Fuel Composition 3 Results – T_{in} and Φ Parameters at various Engine Speeds

The operating conditions under which fuel 3 combusted are slightly different compared to those used to react fuel 2 where the same intake charge temperature range used was common. However, the maximum equivalence ratio for fuel 3 was Φ = 0.455

(limited by peak in-cylinder pressures and pressure rise rates) compared to fuel 2 which reached 0.513. The fuel composition effects themselves will be discussed in Chapter 5.

Figure 4.7 shows the changes in SOC for fuel composition 3. The most advanced SOC timing was -4.1°CA where intake temperature was a maximum of 161.4°C and equivalence ratio was $\Phi = 0.391$. The most retarded combustion of 3.2°CA was observed at the lowest intake temperature of 131.1°C with an equivalence ratio of $\Phi = 0.395$. The combustion onset timing can then altered within a range of 7.3°CA. For the engine speed of 935rpm, when the intake temperature are held constant and the equivalence ratio is increased the SOC advances (i.e. $CA10_{Tin=140°C,\ 935rpm} = 1.4°CA$ advances to -1.7°CA). If the equivalence ratio is then held steady ($\Phi = 0.396$) while intake temperature is increased there again is advancement of the SOC timing; the lowest temperature of 131.1°C produces a CA10 timing of 1.1°CA then as temperature is increased to 161.4°C the SOC advances by 5.0°CA. When the engine speed is increased to 1226rpm the actual time required to travel through 1°CA is reduced. If the ignition delay time of the fuel/air mixtures is assumed to remain constant with the auto-ignition temperature of the mixtures remaining constant and no change in compression ratio or intake temperature, then it would be concluded that the results should indicate a delay in SOC as engine speed increases. This prediction holds true when evaluating Fig. 4.7.b. At a constant temperature of 140°C as equivalence ratio is increased the SOC advances (i.e. $CA10_{Tin=140°C,\ 1226rpm} = 2.6°CA$ advances to -0.4°CA); comparing this range to the data at 935rpm it is shown that with an increase in engine speed translates to a retardation of SOC. When the equivalence ratio is held constant at $\Phi = 0.396$ and the intake charge temperature is increased the SOC again advances (i.e. $CA10_{Tin=140°C,\ 1226rpm} = 2.6°CA$ advances to -0.4°CA); when compared again compared to results at 935rpm a delay in SOC occurs. Results regarding a further increase to 1522rpm of the engine speed are shown in Fig. 4.7.c. Predicated on the idea regarding a reduction in actual time for travel through 1°CA as engine speed increases leading to more delayed timing does not seem to be observed in the results for 1522rpm; this result will be discussed with regards to fuel composition effects later. At the constant intake temperature of 140°C with increasing equivalence ratio the SOC timing does advance as with the other engine speeds tested (i.e. $CA10_{Tin=140°C,\ 1522rpm} = 2.4°CA$ advances to -2.0°CA). When compared to results for

1226rpm the most delayed case with the leanest mixture of Φ = 0.349 the SOC remains virtually the same (ΔSOC=0.2°CA), however at the maximum equivalence ratio of Φ = 0.451 the advancement of SOC with the higher engine speed of 1522rpm significantly sooner (1.6°CA). At the constant equivalence ratio of Φ = 0.396 as the temperature increases from 130.2°C to 160.6°C the SOC advances from 2.3°CA to -3.8°CA; this creates a shift of 6.1°CA which is the largest change at a constant engine speed regarding fuel 3.

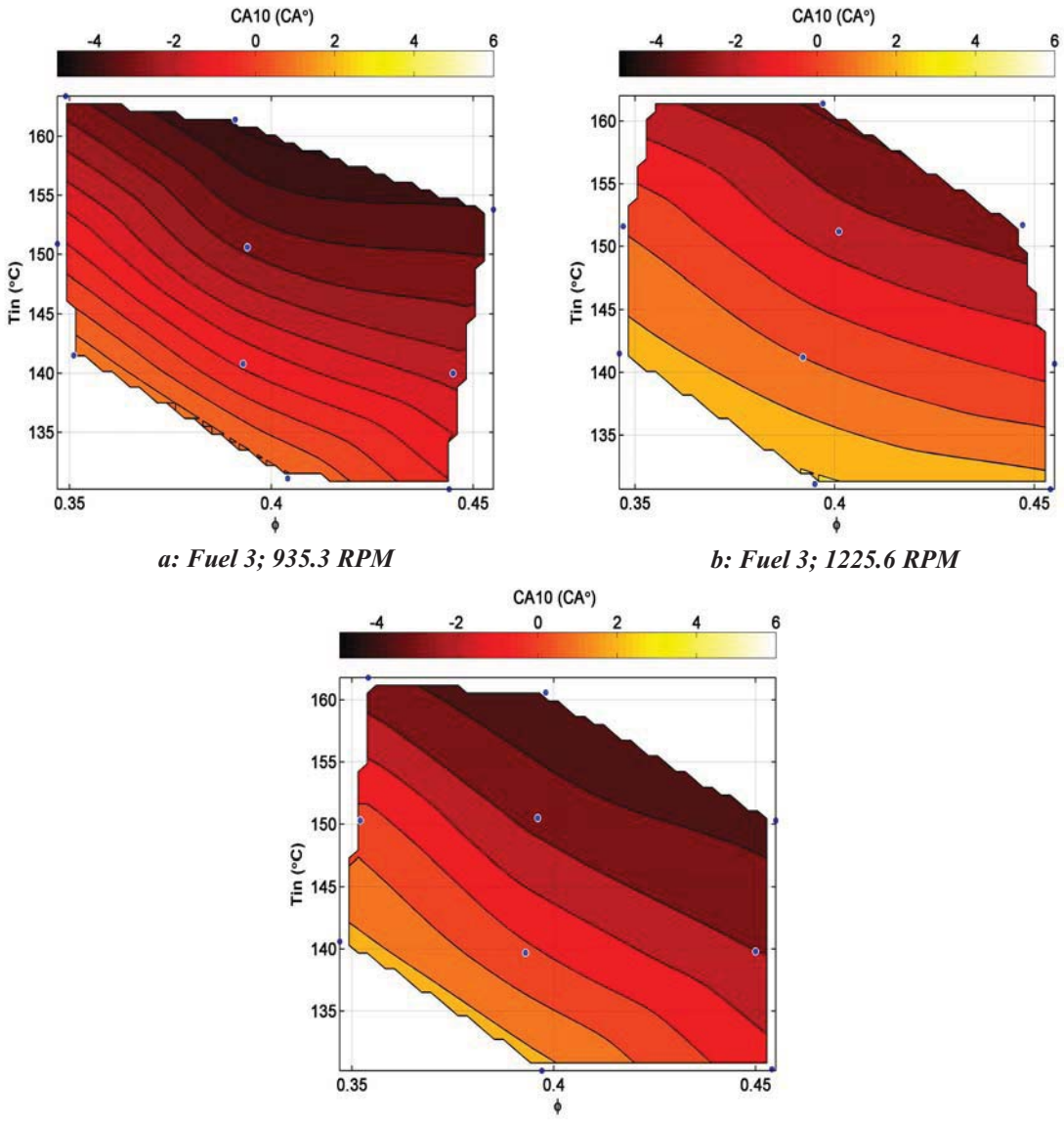

a: Fuel 3; 935.3 RPM

b: Fuel 3; 1225.6 RPM

c: Fuel 3; 1521.9 RPM

Figure 4.7: CA10 for Fuel Composition 3 with respect to intake charge temperature and equivalence ratio at engine speeds of 935.3, 1225.6, and 1521.9 RPM

With the only the change in engine speed at constant conditions a delay in CA10 occurs with an increase from 935rpm to 1226rpm. When the speed is further increased to 1522rpm a slight advance occurs compared to 1226rpm. With changes in engine speed it is not only the residence time which changes but also mixing characteristics and heat transfer. As engine speed increases turbulence should increase with the range of speeds tested and the heat transfer to the walls will be reduced due to decreases residence time. The improved quality of mixing at 1522rpm and reduction in heat transfer attribute to the slight advancement of SOC when compared to similar operating conditions at 1226rpm.

In Figure 4.8 the duration of combustion (CA10-90) for fuel composition 3 is shown. At the engine speed of 935rpm there is very little change in the duration of combustion; the total range of duration is 5.7°CA to 2.1°CA resulting in ΔCA10-90 of 3.6°CA. However, with what little change there is as with CA10 as intake temperature increases at constant equivalence ratio the duration gets shorter as the SOC timing advances (i.e. $CA10\text{-}90_{\Phi=0.40,\ 935rpm}$ = 4.6°CA decreasing to 2.2°CA). If the intake temperature is held constant and the equivalence ratio is increased the length of combustion duration shortens (i.e. $CA10\text{-}90_{Tin=140°C,\ 935rpm}$ = 5.7°CA decreasing to 2.7°CA). The same trends are found as engine speed is increased to 1226rpm, however the duration range is larger and generally durations are longer (11.4°CA to 2.3°CA, $\Delta CA10\text{-}90_{1226rpm}$= 9.1°CA). The largest change at 1226rpm is found with constant equivalence ratio; as the intake charge temperature is increased the combustion duration decreases (i.e. $CA10\text{-}90_{\Phi=0.40,\ 1226rpm}$ = 11.4°CA decreasing to 2.4°CA). At the constant intake temperature of 140°C as the equivalence ratio is increased the duration length is decreased (i.e. $CA10\text{-}90_{Tin=140°C,\ 1226rpm}$ = 8.8°CA decreasing to 3.2°CA). When the engine speed is again increased to 1522rpm again at constant equivalence ratio as the intake charge temperature is increased the duration length decreases (i.e. $CA10\text{-}90_{\Phi=0.40,\ 1522rpm}$ = 5.6°CA decreasing to 2.7°CA). Also as the equivalence ratio is increased at constant intake temperature the duration of combustion decreases (i.e. $CA10\text{-}90_{Tin=140°C,\ 1522rpm}$ = 7.2°CA decreasing to 2.9°CA). When compared to the previous engine speed of 1226rpm the CA10-90 durations are shortened, however when compared to 935rpm the durations are still longer.

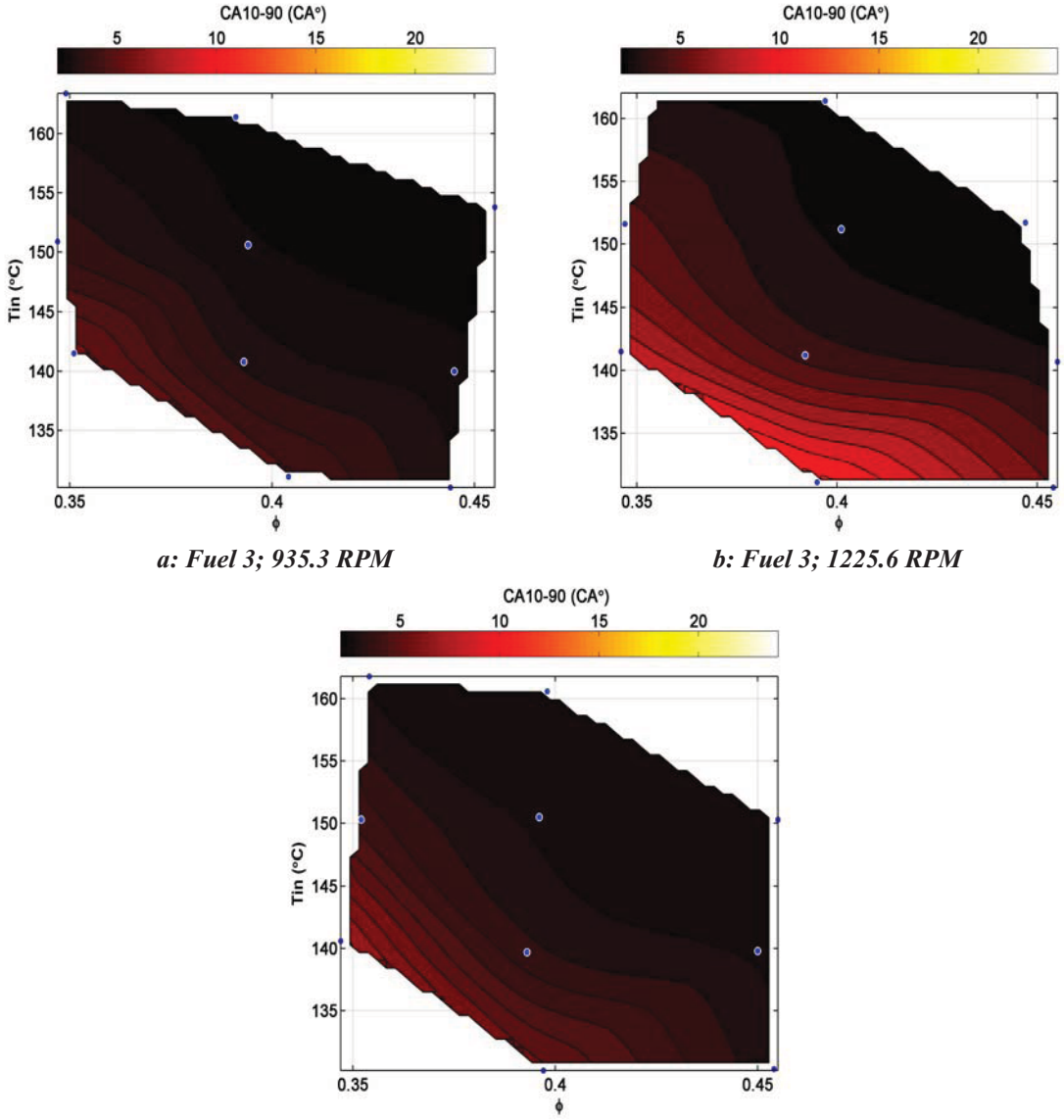

a: Fuel 3; 935.3 RPM

b: Fuel 3; 1225.6 RPM

c: Fuel 3; 1521.9 RPM

Figure 4.8: CA10-90 for Fuel Composition 3 with respect to intake charge temperature and equivalence ratio at engine speeds of 935.3, 1225.6, and 1521.9 RPM

The maximum in-cylinder pressure rise rate at various operating conditions is shown in Figure 4.9(a-c). The peak pressure rise rate range obtained varies from 2.52 bar/°CA to11.02 bar/°CA. Pressure rise rate is directly attributed to the phasing and speed of combustion which cause the production of expanding combustion products and in turn raising pressure. This pressure rise is compounded BTDC by increases in pressure due to the compression stroke, and therefore the phasing of combustion becomes

important. The trends found in dP/dθ should resemble results previously found with SOC.

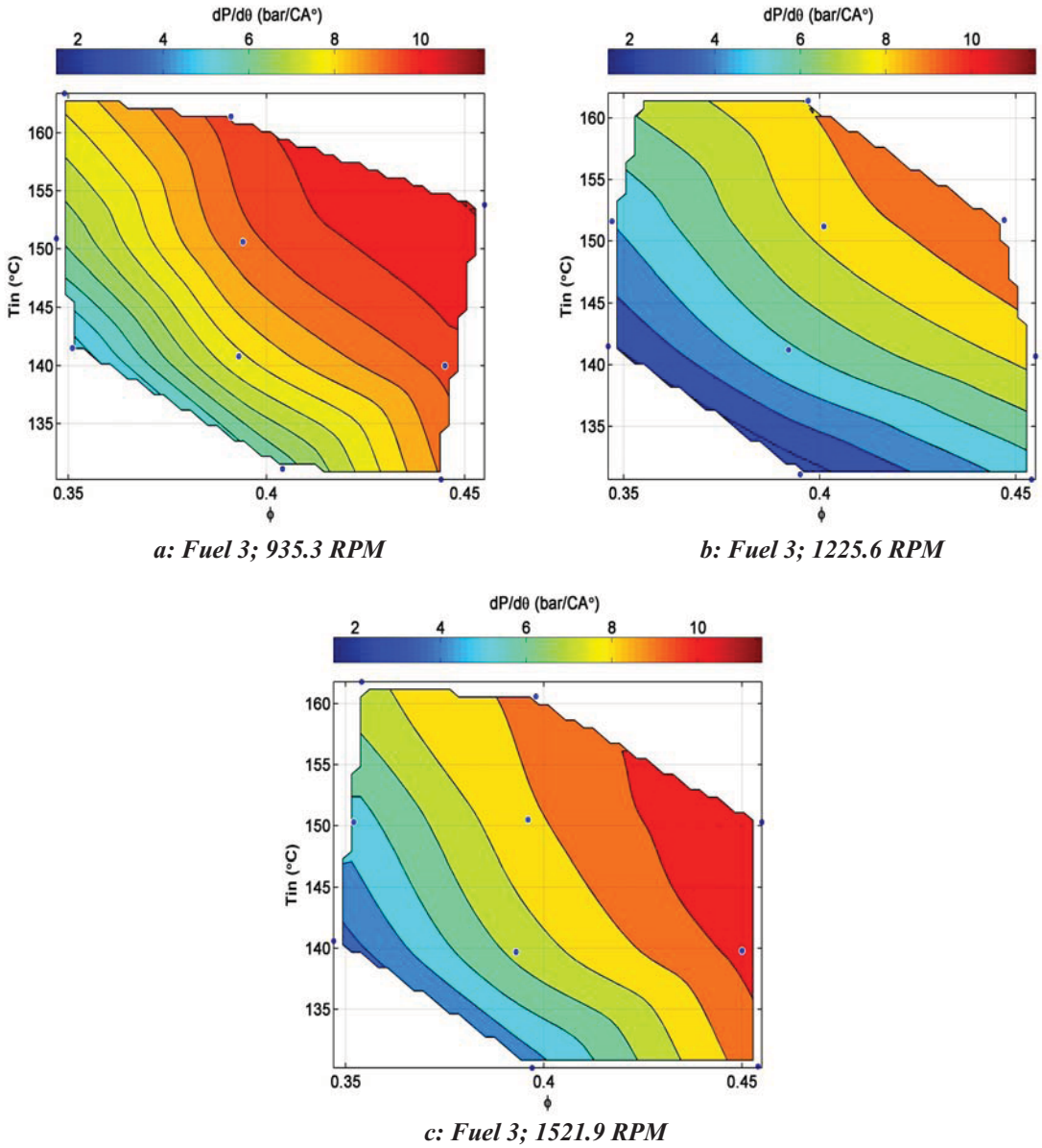

a: Fuel 3; 935.3 RPM

b: Fuel 3; 1225.6 RPM

c: Fuel 3; 1521.9 RPM

Figure 4.9: Pressure Rise Rate for Fuel Composition 3 with respect to intake charge temperature and equivalence ratio at engine speeds of 935.3, 1225.6, and 1521.9 RPM

At 935rpm as either intake temperature or equivalence ratio are increased the pressure rise increases. At a constant intake temperature of 140°C as the equivalence ratio increases from 0.349 to 0.451 the pressure rise rate increases from 4.75 bar/°CA to 9.68 bar/°CA. As the intake temperature is increased from 131.1°C to 161.4°C at constant

equivalence ratio of 0.396 the pressure rise increases from 6.20 bar/°CA to 9.76 bar/°CA. When the engine speed is increased to 1226rpm the maximum pressure rise (9.85 bar/°CA) decreases when compared to 935rpm (10.58 bar/°CA); the range of $dP/d\theta$ increases with the increase in engine speed ($\Delta dP/d\theta_{935rpm}$= 5.83 bar/°CA, $\Delta dP/d\theta_{1226rpm}$= 7.32 bar/°CA). Again as the equivalence ratio is increased at constant temperature or the temperature is increased at constant equivalence ratio the pressure rise is increasing. If the engine speed is further increased to 1522rpm a large range of pressure rise values is observed similar to results for 1226rpm ($\Delta dP/d\theta_{1522rpm}$=7.54 bar/°CA). However, unlike the results at 1226rpm the range shifts to larger $dP/d\theta$ values reaching the maximum value recorded for the fuel 3 tests (3.5 bar/°CA to 11.02 bar/°CA). This shift could be attributed to improved mixing quality with increased engine speed from 1226rpm to 1522rpm.

The maximum in-cylinder pressures are depicted in Figure 4.10 and range from 59.9 bar to 89.7 bar over the conditions tested. With an engine speed of 935rpm the maximum in-cylinder pressure ranged from 68.0 bar to 83.5 bar or ΔP_{max}=15.5 bar. As the equivalence ratio was increased at constant temperature the maximum in-cylinder pressure increased (i.e. $P_{max,\ Tin=140°C,\ 935rpm}$= 68.0 bar to 83.0 bar). With the equivalence ratio held constant and increasing the intake temperature the maximum in-cylinder pressure again increased (i.e. $P_{max,\ \Phi=0.40,\ 935rpm}$= 74.3 bar to 80.7 bar). With an increase in engine speed to 1226rpm the range of peak pressure increased ΔP_{max}= 24.5 bar with a decrease in the minimum pressure changing from 68.0 bar to 59.9 bar. The highest value obtained was only slightly higher than the maximum obtained for 935rpm at 84.4 bar. Following the trends identified with 935rpm as either equivalence ratio or intake charge temperature are increased while holding the other fixed there was a resulting increase of maximum in-cylinder pressure. Increasing the engine speed to the final speed tested of 1522rpm it was observed that a larger range of pressure values was maintained (ΔP_{max}= 24.2 bar), however the range shifted to overall higher pressures (P_{max}= 65.5 bar to 89.7 bar). At 1522 rpm it is observed in Fig. 4.10.c. that with elevated temperatures (above ~140°C) and richer mixtures ($\Phi > 0.40$) increases in intake temperature have very little

affects on P_{max} and the only changes recorded in this zone correspond to variations with equivalence ratio.

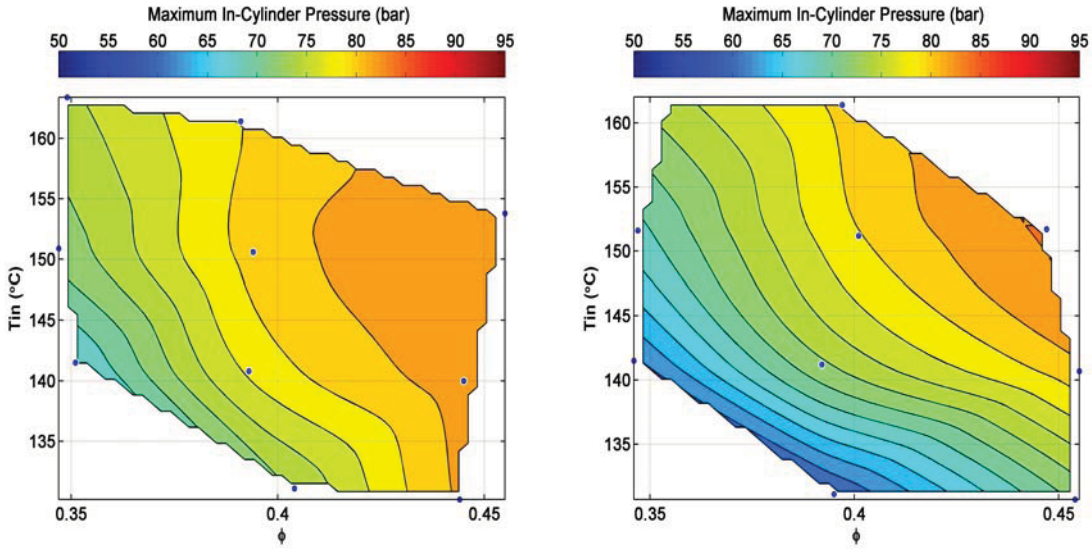

a: Fuel 3; 935.3 RPM

b: Fuel 3; 1225.6 RPM

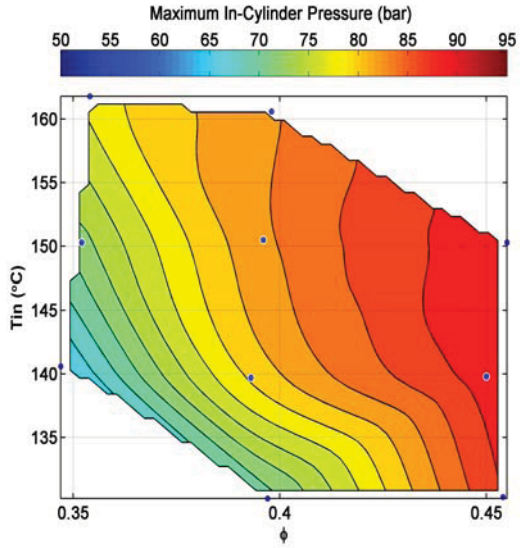

c: Fuel 3; 1521.9 RPM

Figure 4.10: Maximum In-Cylinder Pressure for Fuel Composition 3 with respect to intake charge temperature and equivalence ratio at engine speeds of 935.3, 1225.6, and 1521.9 RPM

IMEP results for fuel 3 are shown in Figure 4.11 and range from 2.23 bar to 3.16 bar over the entire operating range tested. At the lowest engine speed tested (935rpm) the IMEP achieved range from 2.23 bar, resulting from the leanest mixture and highest intake temperature conditions, to 2.92 bar where the lowest temperatures and richest mixtures

are utilized. At 935rpm with increases of temperature at any constant equivalence ratio there is a resultant decrease in IMEP produced (i.e. $IMEP_{935rpm,\ \Phi=0.40}$=2.84 bar decreases to 2.37 bar). With increases of equivalence ratio at constant intake temperature there is an increase in IMEP values (i.e. $IMEP_{935rpm,\ Tin=140°C}$=2.56 bar increases to 2.68 bar).

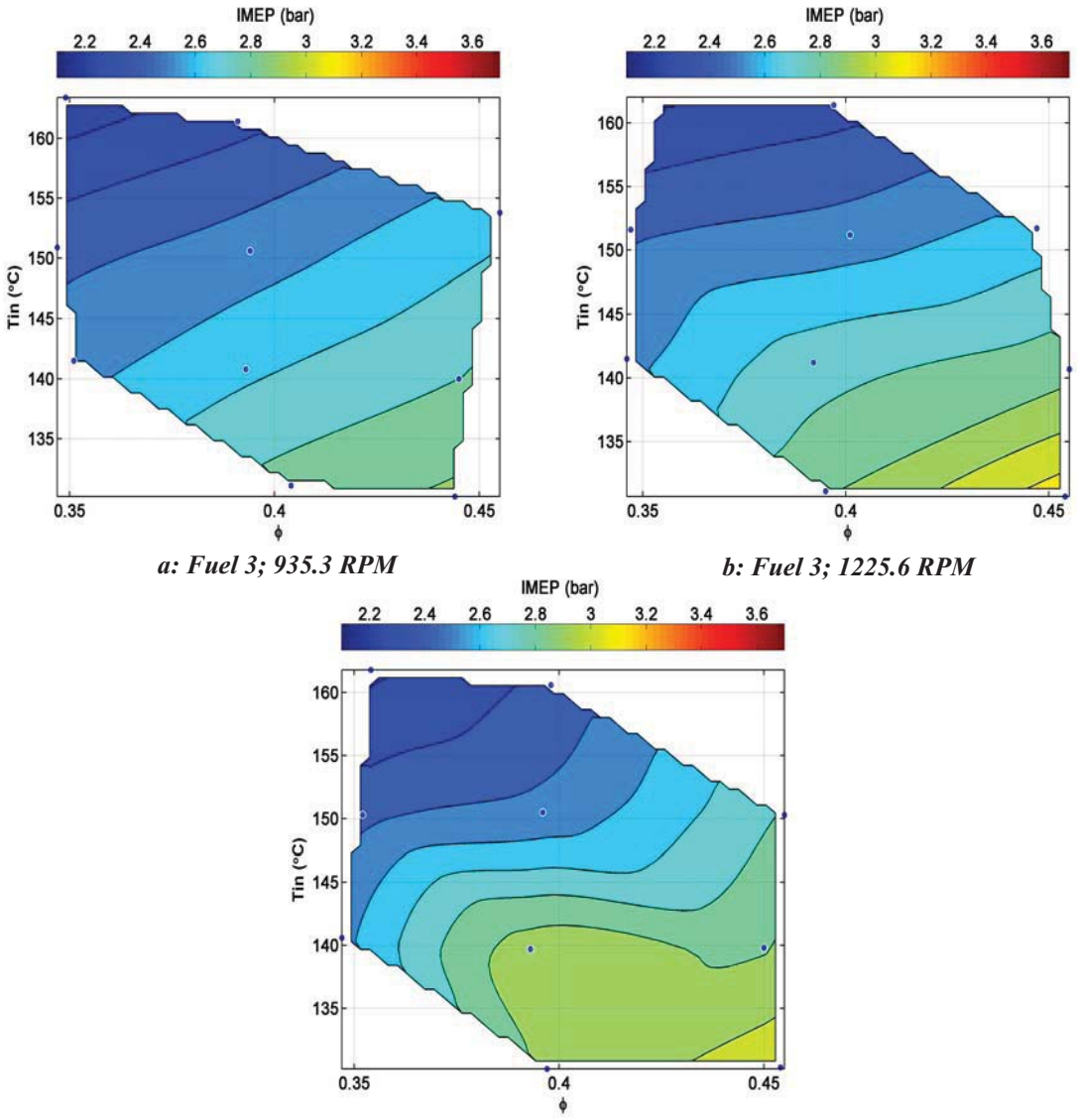

a: Fuel 3; 935.3 RPM

b: Fuel 3; 1225.6 RPM

c: Fuel 3; 1521.9 RPM

Figure 4.11: IMEP for Fuel Composition 3 with respect to intake charge temperature and equivalence ratio at engine speeds of 935.3, 1225.6, and 1521.9 RPM

When going to the higher engine speed of 1226rpm maximum IMEP reached 3.16 bar (greater than $IMEP_{max}$ at 935rpm) and decreases to 2.28 bar ($\Delta IMEP_{1226rpm}$=0.86 bar). When compared to 935rpm the results follow the same trends with regards to changes of

intake charge temperature and equivalence ratio (i.e. $IMEP_{1226rpm,\ Tin=140°C}$ = 2.57 bar increases to 2.87 bar, $IMEP_{1226rpm,\ \Phi=0.40}$ = 2.89 bar decreases to 2.36 bar). However, with the increased engine speed a larger operating zone (richer mixtures at low temperatures) allows for peak IMEP near 3 bar. By increasing the engine speed further to 1522rpm similar characteristics relative to the lower engine speeds tested are present. As the intake temperature is increased at constant equivalence ratio IMEP decreases ($IMEP_{1522rpm,\ \Phi=0.40}$ = 2.92 bar decreases to 2.43 bar). When the intake temperature is held constant and the equivalence ratio is increased the IMEP increases ($IMEP_{1522rpm,\ Tin=150°C}$ = 2.47 bar increases to 2.81 bar). One observation which can be made regarding the effect of increasing engine speed from 1226rpm to 1522rpm is that at the higher engine speed while using low intake charge temperatures (T_{in} < ~140°C) and above Φ = 0.396, IMEP values remain fairly constant at 2.96 ± 0.09 bar. With higher intake temperatures with all equivalence ratios there are no effects from increasing engine speed.

Indicated efficiency results are presented in Figure 4.12; fuel 3 produced a maximum η_i of 33.0% but suffered a decrease to 26.6% under high temperature and rich limit operating conditions. For the lowest engine speed of 935rpm the best efficiency was obtained using the leanest mixture at the lowest temperature ($\Delta\eta_{i\Phi=0.35,\ 140°C}$ = 31.1%). From this point if either the equivalence ratio is increased or if the intake temperature is increased the efficiency decreases. With an increase in engine speed to 1226rpm the maximum efficiency decreases but only slightly to 31.2% still occurring with minimum equivalence ratio of 0.346 and minimum temperature of 141.5°C. With an increase of equivalence ratio or intake temperature or both the efficiency again decreases. At the maximum engine speed tested an optimal point of 33% is observed at 139.7°C and Φ = 0.393. With any change in equivalence ratio or intake temperature the efficiency decreases. With regard to engine speed, as engine speed increased it was shown that efficiency generally increased for consistent operating conditions. Speeds of 935 and 1226 rpm compared very closely whereas at the maximum speed tested an optimal tradeoff between intake temperature and equivalence ratio produced the highest recorded η_i value for fuel 3.

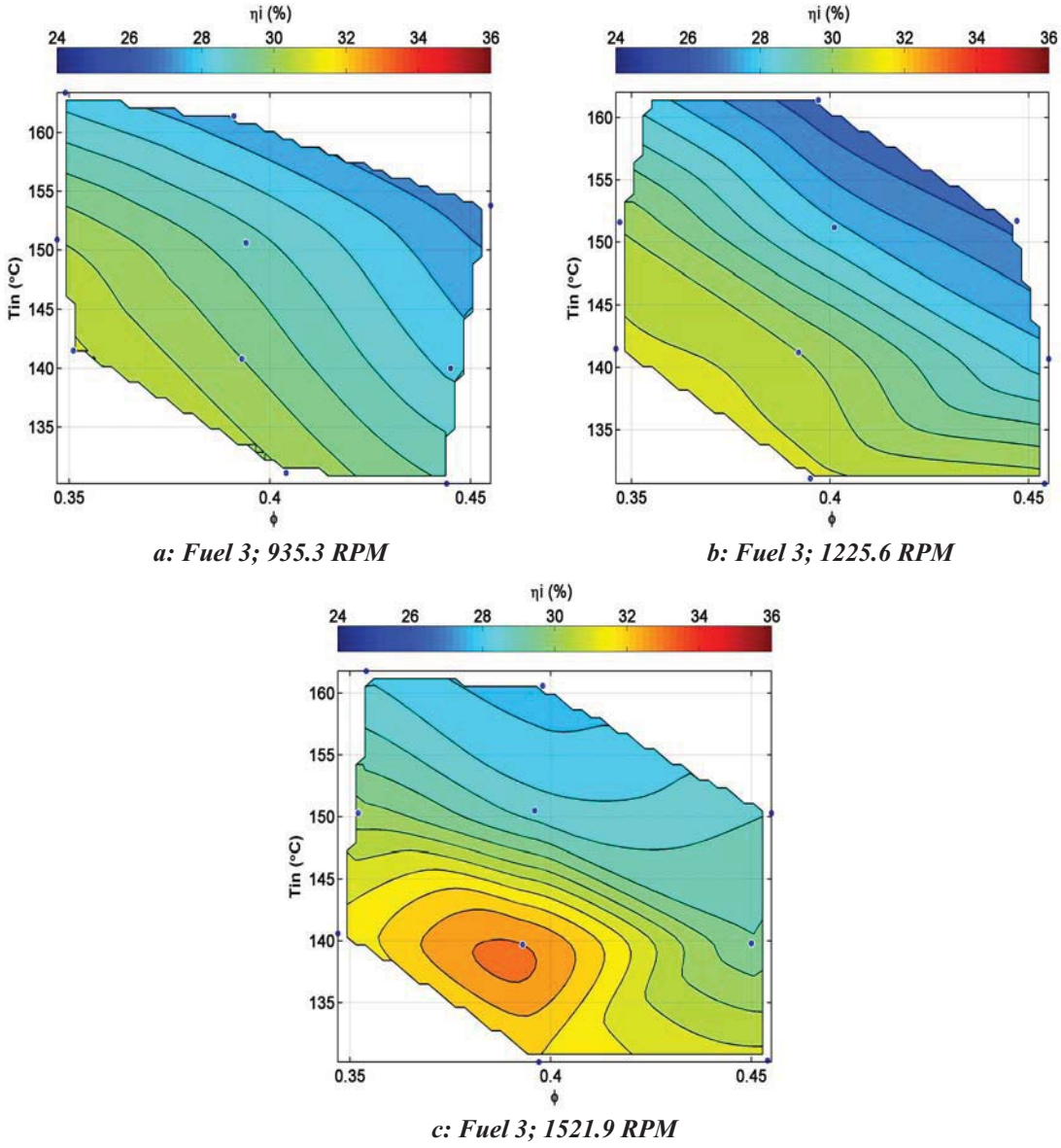

a: Fuel 3; 935.3 RPM

b: Fuel 3; 1225.6 RPM

c: Fuel 3; 1521.9 RPM

Figure 4.12: Indicated Efficiency for Fuel Composition 3 with respect to intake charge temperature and equivalence ratio at engine speeds of 935.3, 1225.6, and 1521.9 RPM

4.2.3 Fuel Composition 4 Results – T_{in} and Φ Parameters at various Engine Speeds

Fuel composition 4 was the final fuel which was tested. In terms of the equivalence ratio used fuel 4 operation was similar to fuel 3 igniting between Φ = 0.351 and Φ = 0.448. The engine speeds tested (939, 1227, and 1523) remained approximately

constant compared to tests for both fuel 2 and fuel 3. The largest discrepancy in operating conditions between fuel 4 and the other two fuels occurred for the intake temperature range. Fuel 4 required a higher temperature range (150.9°C to 184.6°C); the lowest temperature used is approximately 20 degrees higher compared to fuels 2 and 3. In the following section the direct results will be discussed and an explanation regarding the required increased intake temperature will be addressed in Chapter 5.

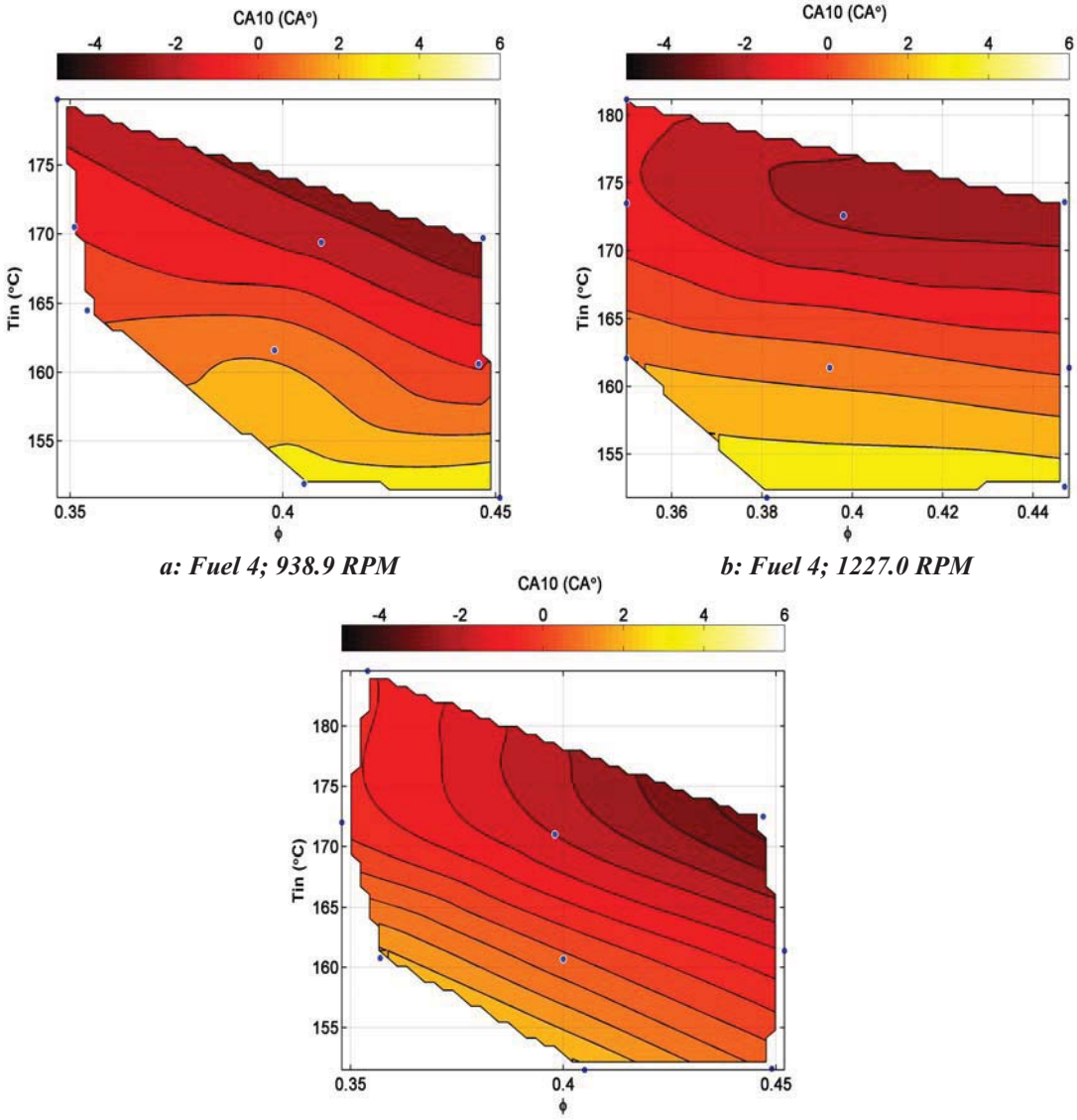

a: Fuel 4; 938.9 RPM

b: Fuel 4; 1227.0 RPM

c: Fuel 4; 1523.4 RPM

Figure 4.13: CA10 for Fuel Composition 4 with respect to intake charge temperature and equivalence ratio at engine speeds of 938.9, 1227.0, and 1523.4 RPM

Displayed in Figure 4.13(a-c) are the results regarding SOC related to fuel composition 4. Figure 4.13.a., at the lowest engine speed tested (939rpm), it is observed that at the lowest intake temperature used (151.4°C) if the equivalence ratio is increased there is no change in SOC timing. If the intake temperature is held constant at some value above 160°C then as the equivalence ratio is increased the resulting SOC advances (i.e. $CA10_{Tin=172°C,\ 939rpm}$ = -0.1°CA advances to -2.8°CA). At any equivalence ratio for the engine speed of 939rpm if the intake temperature is increased the SOC advances (i.e. $CA10_{\Phi=0.40,\ 939rpm}$ = 3.6°CA advances to -1.4°CA). The change in SOC timing at 939rpm shows a higher dependence on intake temperature variations rather than equivalence ratio changes. When the engine speed is increased to 1227rpm the trends and magnitude of SOC remains fairly consistent. With constant low temperature scenarios of T_{in} < 160°C if the equivalence ratio is modified there appears to be no effect on SOC timing. If the intake temperature is increased then held constant with increased equivalence ratio the SOC advances (i.e. $CA10_{Tin=172°C,\ 1227rpm}$ = -0.8°CA advances to -2.6°CA). When the equivalence ratio is held constant for an engine speed of 1227rpm and the intake temperature is increased the SOC advances (i.e. $CA10_{\Phi=0.40,\ 1227rpm}$ = 4.0°CA advances to -2.2°CA). With a further increase in engine speed to 1523rpm the impact of equivalence ratio seems to change. As observed with previous engine speeds (939 and 1227rpm) at low intake charge temperatures equivalence ratio had no effect on SOC. However, at the engine speed of 1523rpm over the entire range of intake temperatures if the intake temperature is held constant and the equivalence ratio is increased the SOC advances (i.e. $CA10_{Tin=152°C,\ 1523rpm}$ = 2.6°CA advances to -0.9°CA and $CA10_{Tin=172°C,\ 1523rpm}$ = -0.1°CA advances to -3.3°CA). As with the engine speeds of 939 and 1227rpm, at 1523rpm and constant equivalence ratio when the intake temperature is increased the SOC advances (i.e. $CA10_{\Phi=0.40,\ 1523rpm}$ = 2.6°CA advances to -1.5°CA). With respect to engine speed effects there is no change in the trends or little to no change in the magnitude of values obtained for 939 and 1227rpm. With the increase to 1523rpm equivalence ratio has a greater impact and the overall range of SOC is advanced compared with the lower engine speeds tested.

The combustion duration for fuel 4 with different engine speeds is shown in Figure 4.14; the durations range between 2.4°CA and 13.5°CA. At the engine speed of

939rpm the longest recorded CA10-90 duration is 13.5°CA and it occurs at the lowest temperature (150.9°C), which should be expected, but with the richest mixture; this is attributed to fuel compositions (CO) affects and will be discussed in Chapter 5. As was shown with both fuels 2 and 3 as the equivalence ratio is increased the duration decreased; for now this will be attribute to chemical kinetics of the mixture and explained in detail in Chapter 5.

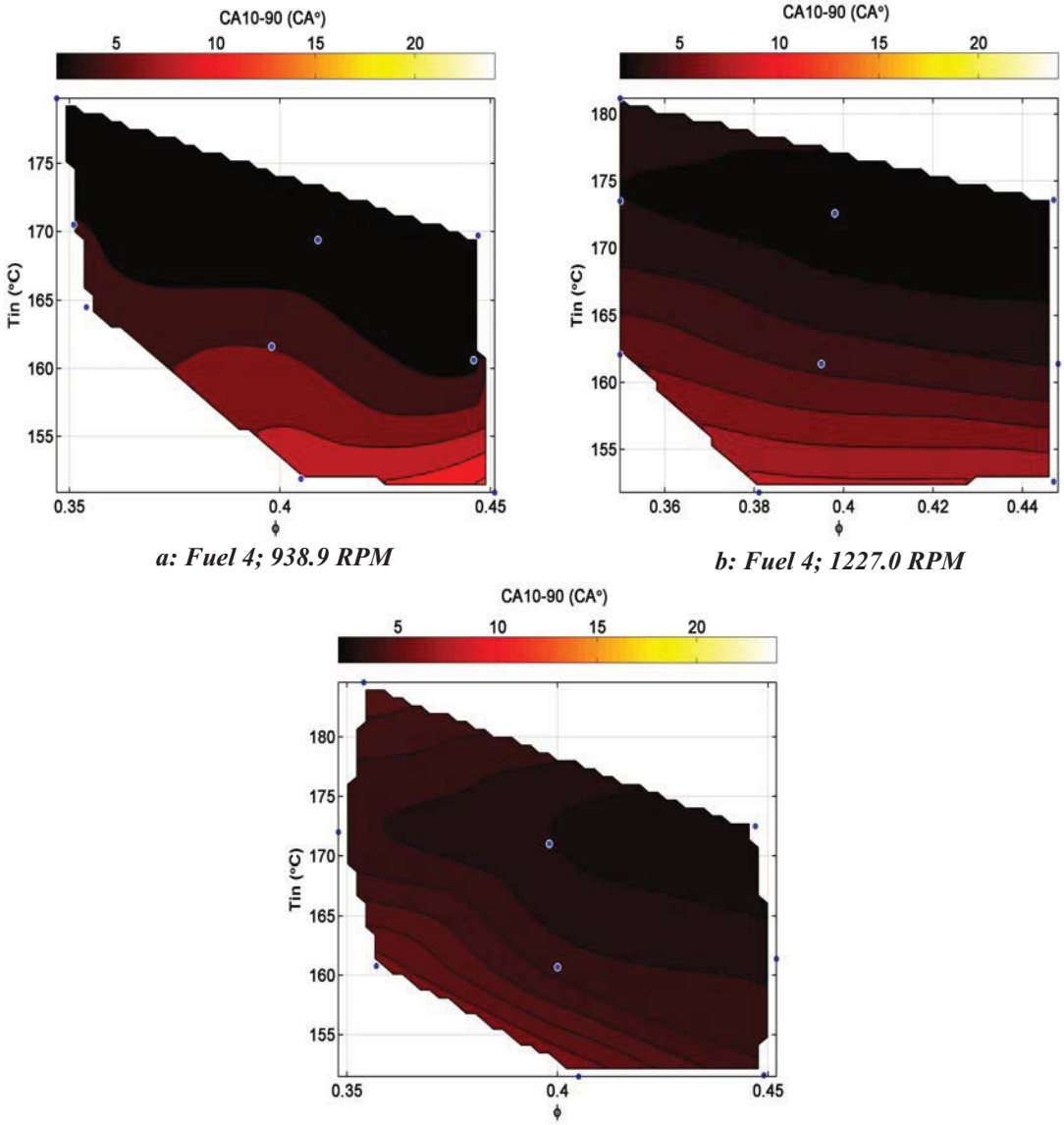

a: Fuel 4; 938.9 RPM

b: Fuel 4; 1227.0 RPM

c: Fuel 4; 1523.4 RPM

Figure 4.14: CA10-90 for Fuel Composition 4 with respect to intake charge temperature and equivalence ratio at engine speeds of 938.9, 1227.0, and 1523.4 RPM

In general at the engine speed of 939rpm and constant intake charge temperature as equivalence ratio is varied there is little effect on the duration of combustion. However, consistent will all other findings so far at a constant equivalence ratio as the intake temperature is increased, the CA10-90 duration decreases (i.e. $CA10\text{-}90_{\Phi=0.40,\ 939rpm}$ = 9.9°CA decreases to 2.7°CA). With an increase in the engine speed to 1227rpm as it was observed with results for CA10 using constant low intake temperatures (T_{in} < 160°C) and varied equivalence ratio has little to no effect on combustion duration. Again, at constant equivalence ratio and increasing intake charge temperature the CA10-90 duration decreases until a minimum duration of 2.4°CA is reached (i.e. $CA10\text{-}90_{\Phi=0.40,\ 1227rpm}$ = 8.6°CA decreases to 2.4°CA). At the engine speed of 1523rpm there was no combustion duration longer than 6.0°CA even though there was less actual time to react the fuel and air mixture. A local minimum CA10-90 duration of 2.4°CA can be identified in Fig. 4.14.c. in the region with equivalence ratio great than 0.40 and using temperatures higher than 165°C. If intake temperature is reduced from this region at constant equivalence ratio the duration of combustion increases (i.e. $CA10\text{-}90_{\Phi=0.40,\ 1523rpm}$ = 6.0°CA increases to 3.0°CA). Over the entire range of equivalence ratios tested at 1523rpm if the intake temperature remains constant and the equivalence ratio is increased the duration of combustion decreases (i.e. $CA10\text{-}90_{Tin=162°C,\ 1523rpm}$ = 5.7°CA decreases to 3.3°CA). This trend is not consistent with the lower engine speeds tested for fuel 4; however it does correlate well with results previously discussed corresponding to fuels 2 and 3.

The resultant pressure rise rate due to combustion phasing is shown in Figure 4.15; values range from 2.8 bar/°CA to 11.4 bar/°CA. The largest range of pressure rise actually occurs while using the lowest engine speed (939rpm). Similar to the results obtained regarding phasing as the intake temperature is increased at constant equivalence ratio the pressure rise increases ($dP/d\theta_{\Phi=0.40,\ 939rpm}$ = 3.2 bar/°CA increases to 9.2 bar/°CA). With increases in equivalence at constant temperature there is also an increase in the pressure rise ($dP/d\theta_{Tin=172°C,\ 939rpm}$ = 6.6 bar/°CA increases to 11.4 bar/°CA). At the engine speed of 1227rpm if the equivalence ratio is first held constant the intake temperature is increased the resulting pressure rise rate increases ($dP/d\theta_{\Phi=0.40,\ 1227rpm}$ = 2.9 bar/°CA increases to 9.7 bar/°CA). At constant intake temperature and increasing equivalence ratio the pressure rise again increases ($dP/d\theta_{Tin=172°C,\ 1227rpm}$=7.5 bar/°CA

increases to 10.7 bar/°CA). The effect of equivalence ratio is relatively week when compared to the change in pressure rise rate induced by increasing the intake charge temperature at 1227rpm.

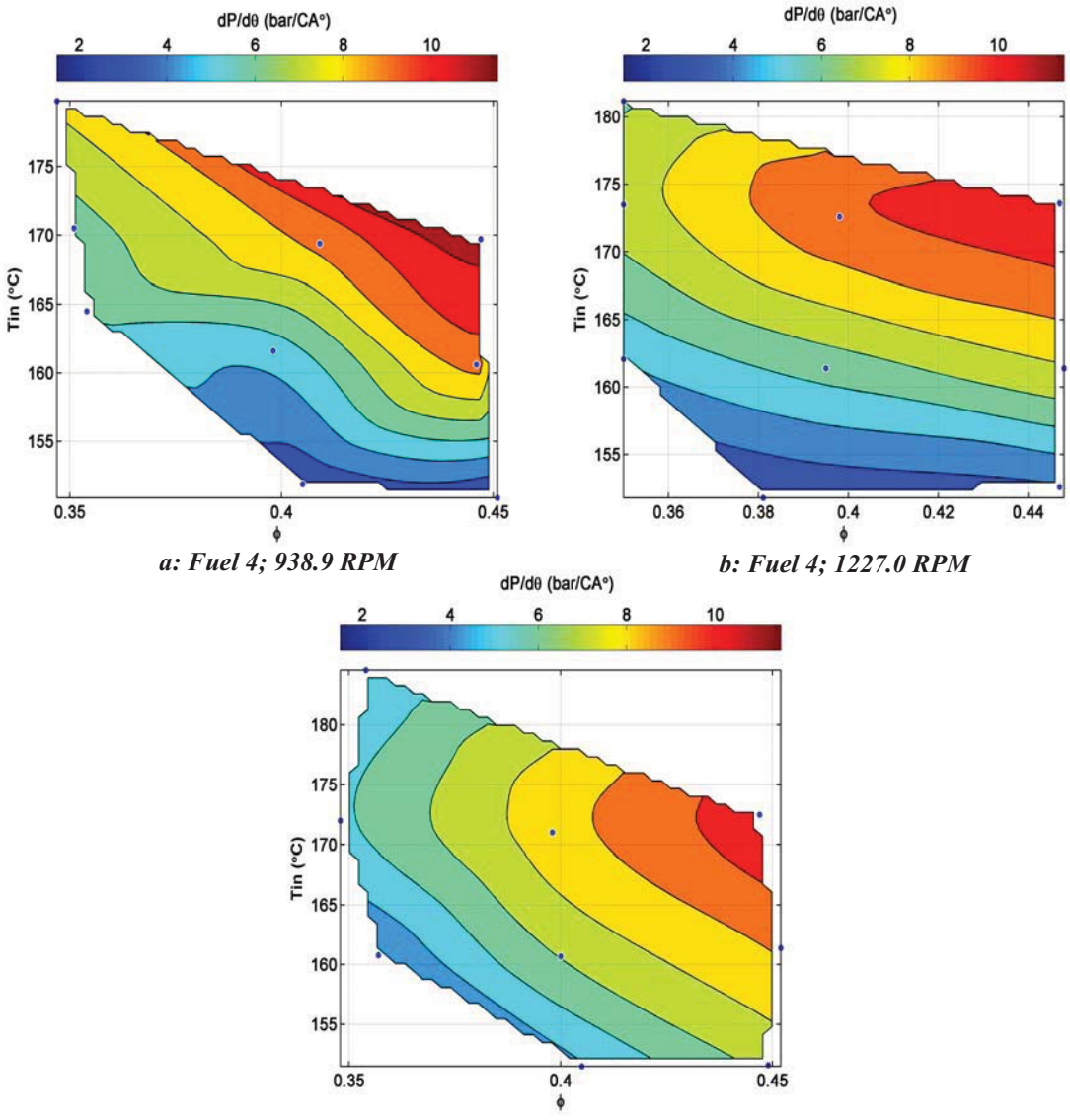

a: Fuel 4; 938.9 RPM

b: Fuel 4; 1227.0 RPM

c: Fuel 4; 1523.4 RPM

Figure 4.15: Maximum Pressure Rise Rate for Fuel Composition 4 with respect to intake charge temperature and equivalence ratio at engine speeds of 938.9, 1227.0, and 1523.4 RPM

Moving to an engine speed of 1523rpm the first observation made is the range of values is smaller when compared to the lower engine speed ($\Delta\ dP/d\theta_{1532rpm} = 6.6$ bar/°CA, $\Delta\ dP/d\theta_{1227rpm} = 7.8$ bar/°CA, and $\Delta\ dP/d\theta_{939rpm} = 8.6$ bar/°CA). However the effects of both, increasing equivalence ratio and intake temperature are the same; if either intake

temperature or equivalence ratio are increased while maintaining the other as a constant the pressure rise rate will increase (i.e. $dP/d\theta_{\Phi=0.40,\ 1523rpm}$ = 4.9 bar/°CA increases to 8.5 bar/°CA and $dP/d\theta_{Tin=172°C,\ 1523rpm}$ = 5.8 bar/°CA increases to 10.6 bar/°CA). As the engine speed was increased the maximum pressure rise was reduced even though was generally phased sooner and over a shorter duration. Also when increasing the engine speed the range/changes with pressure rise rate decreased.

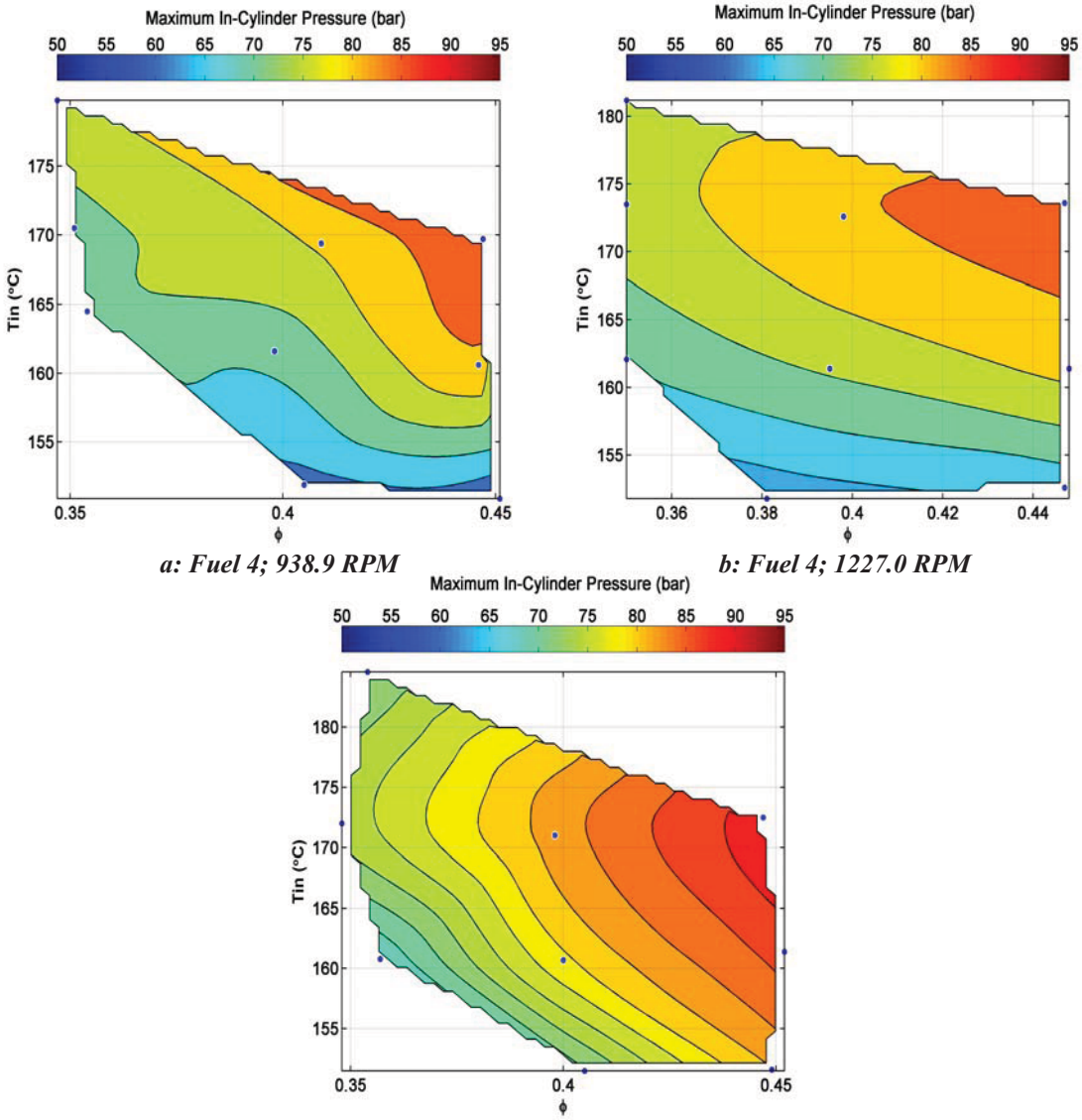

a: Fuel 4; 938.9 RPM

b: Fuel 4; 1227.0 RPM

c: Fuel 4; 1523.4 RPM

Figure 4.16: Maximum Pressure Rise Rate for Fuel Composition 4 with respect to intake charge temperature and equivalence ratio at engine speeds of 938.9, 1227.0, and 1523.4 RPM

Maximum in-cylinder pressure data for fuel 4 is plotted in Figure 4.16 and results range from 60.2 bar to 89.1 bar. At the engine speed of 939rpm operating at fixed equivalence ratios and increasing the intake temperature results in increasing maximum in-cylinder pressure (i.e. $P_{max\ \Phi=0.40,\ 939rpm}$ = 63.1 bar increases to 80.6 bar). At constant intake temperature as equivalence ratio is increased the maximum pressure increases (i.e. $P_{max\ Tin=172°C,\ 939rpm}$ = 73.4 bar increases to 87.4 bar). An increase in engine speed to 1227rpm results in a similar range of pressures when compared to results for 939rpm ($P_{max939rpm}$ = 60.2 bar to 87.4 bar and $P_{max1227rpm}$ = 62.0 bar to 87.6 bar). At 1227rpm when the equivalence ratio is maintained at a constant and the intake temperature is increased the maximum in-cylinder pressure increases ($P_{max\ \Phi=0.40,\ 1227rpm}$=62.0 bar increases to 84.0 bar). When the intake temperature remains constant and the equivalence ratio the maximum pressure is again increased (i.e. $P_{max\ Tin=172°C,\ 1227rpm}$=77.5 bar increases to 87.6 bar). There is again a shift in values observed with regard to maximum in-cylinder pressure and the highest engine speed tested of 1523rpm. The pressure conditions at 1523rpm remain higher under all equivalence ratio and intake temperature conditions compared to the lower engine speed trials and the range of values is also smaller ($P_{max1523rpm}$= 68.4 bar to 89.1 bar, $\Delta P_{max1523rpm}$= 20.7 bar). Consistent trends however do occur corresponding to changes in equivalence ratio and intake temperature variations when compared to the other engine speeds, the values are simply of higher magnitude ($P_{max\ \Phi=0.40,\ 1523rpm}$ = 71.8 bar increases to 82.9 bar and $P_{max\ Tin=172°C,\ 1523rpm}$ = 74.7 bar increases to 89.1 bar).

The performance parameter IMEP is plotted in Figure 4.17. IMEP values range from 3.56 bar occurring with the richest mixture of Φ = 0.451 at the lowest intake temperature (150.9°C) and lowest engine speed (939rpm) down to 2.22 bar at the highest engine speed (1523rpm) leanest mixture (Φ = 0.354) and highest intake temperature (184.6°C). Individually looking at the engine speed of 939rpm the largest span of IMEP is produced ($\Delta IMEP_{939rpm}$ = 1.0 bar). The lowest IMEP recorded at 939rpm is 2.6 bar occurring at the lean limit of operation (Φ = 0.357) using the highest intake temperature (179.8°C). As the intake temperature is decreased at any constant equivalence ratio the IMEP achieved increases ($IMEP_{\Phi=0.40,\ 939rpm}$ = 2.9 bar increases to 3.3 bar). Increases in

equivalence ratio at fixed intake temperature also produce an increase in IMEP ($\Delta IMEP_{Tin=172°C,\ 939rpm} = 0.3$ bar).

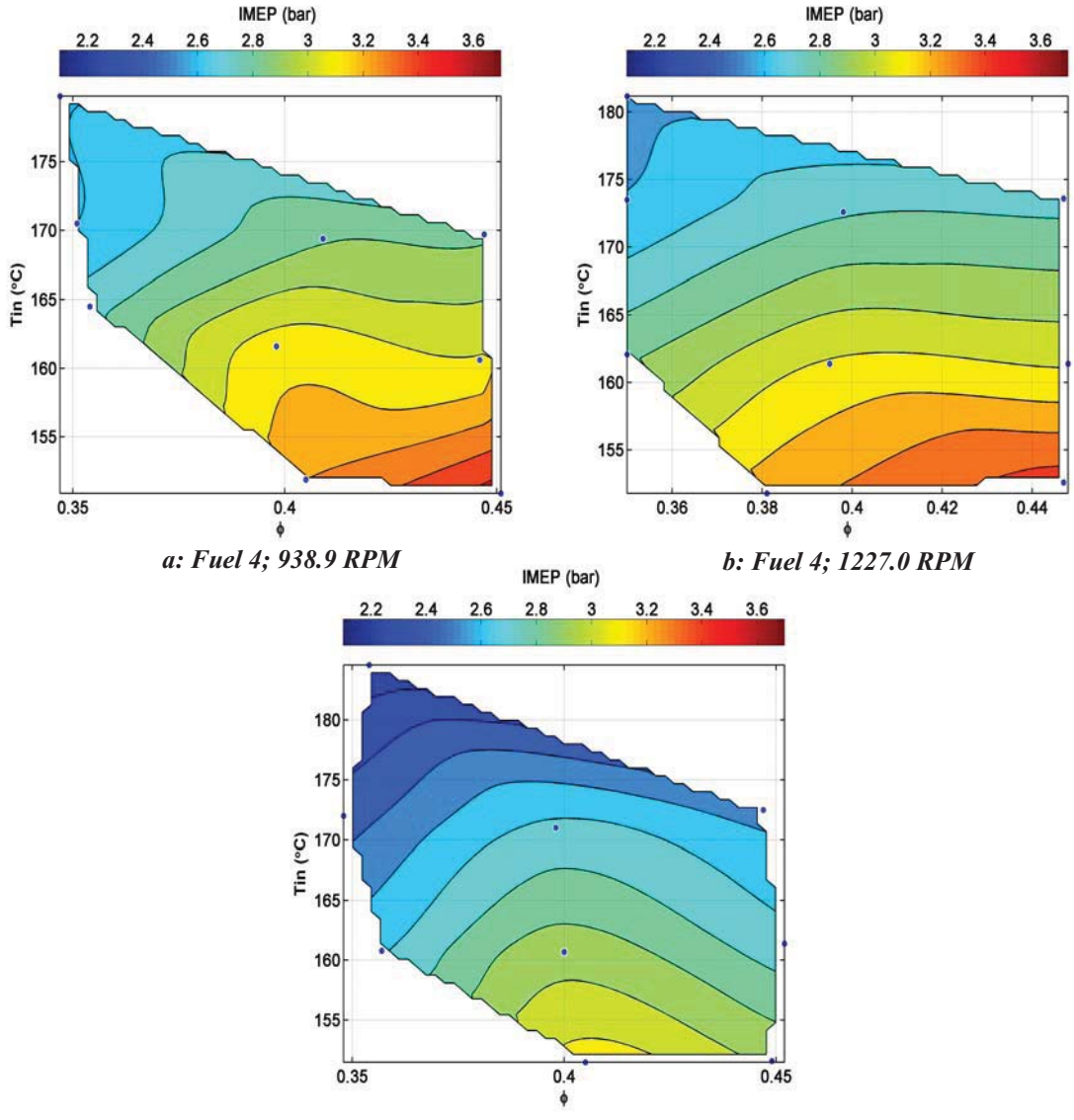

a: Fuel 4; 938.9 RPM

b: Fuel 4; 1227.0 RPM

c: Fuel 4; 1523

Figure 4.17: IMEP for Fuel Composition 4 with respect to intake charge temperature and equivalence ratio at engine speeds of 938.9, 1227.0, and 1523.4 RPM

Increasing the engine speed to 1227rpm decreases the IMEP span to 0.9 bar, still maintaining a relatively high value of 3.4 bar compared to 3.56 bar at 939rpm. In general at constant intake temperatures using the engine speed of 1227rpm there is very little to no effect as equivalence ratio is increased on IMEP ($\Delta IMEP_{Tin=172°C,\ 1227rpm} = 0.2$ bar). However, a strong effect is observed when the intake temperature is modified and the

equivalence ratio remains fixed; as the intake temperature increases from ~152°C to 172°C the resulting IMEP values decrease ($IMEP_{\Phi=0.40,\ 1227rpm}$ = 3.3 bar decreases to 2.8 bar). The final increase in engine speed to 1523rpm shows significant reduction in IMEP with a maximum of 3.1 bar compared to the lower speeds attaining maximum values of 3.4 bar or greater. This prominent reduction IMEP is attributed to poor combustion phasing (Figs. 4.13.c. and 4.14.c) where SOC generally occurred BTDC and combustion durations were short. The maximum IMEP value (3.1 bar) for 1523rpm is observed at the lowest intake temperature and leanest mixture; inverse of results previously recorded were IMEP maximums occurred at maximum equivalence ratios. If the intake temperature is increased at constant equivalence ratio the IMEP decreases ($IMEP_{\Phi=0.40,\ 1523rpm}$ = 3.1 bar decreases to 2.7 bar). When the intake temperature is maintained at a constant and the equivalence ratio is increased it seems that there is an optimal equivalence ratio in terms of IMEP at 0.399, all other values at constant temperature result in a reduction of IMEP. The highest IMEP values occur with the lowest engine speed and as engine speed is increase under constant operating conditions the IMEP values will decrease.

Compared to all other fuel compositions under any operating conditions fuel 4 achieved the highest indicated efficiencies ranging from 25.8% up to 35.9%; the indicated efficiency results for fuel composition 4 are shown in Figure 4.18. Starting with 939rpm the best efficiencies (29.7% to 35.0%) are achieved around T_{in} < 160°C and 0.399 equivalence ratio. At minimum intake temperature, high efficiency (35.0%) can even be achieved with an increase in equivalence ratio. As intake temperature increases at constant equivalence ratio over the range tested the indicated efficiency decreases (i.e. $\eta_{i\ \Phi=0.45,\ 939rpm}$ = 35.0% decreases to 29.7%). Generally with fixed intake temperature as equivalence ratio increases there is a decrease in efficiency; as was previously stated for minimum intake charge heating efficiency remains basically unchanged. As engine speed increases to 1227rpm trends found with the previous fuels show themselves. The maximum efficiency obtained through any of the experiments conducted in the study is 35.9% and corresponded to the lowest temperature (151.8°C) used for fuel 4 at 1227rpm and the leanest mixture at that temperature (Φ = 0.381). With an increase in the intake

charge temperature at constant equivalence ratio the indicated efficiency decreases (i.e. $\eta_{i\ \Phi=0.45,\ 1227rpm}$ = 34.0% decreases to 28.2%). Under constant intake temperature conditions if the equivalence ratio is increased the efficiency again drops (i.e. $\eta_{i\ Tin=172°C,\ 1227rpm}$ = 31.5% decreases to 28.2%).

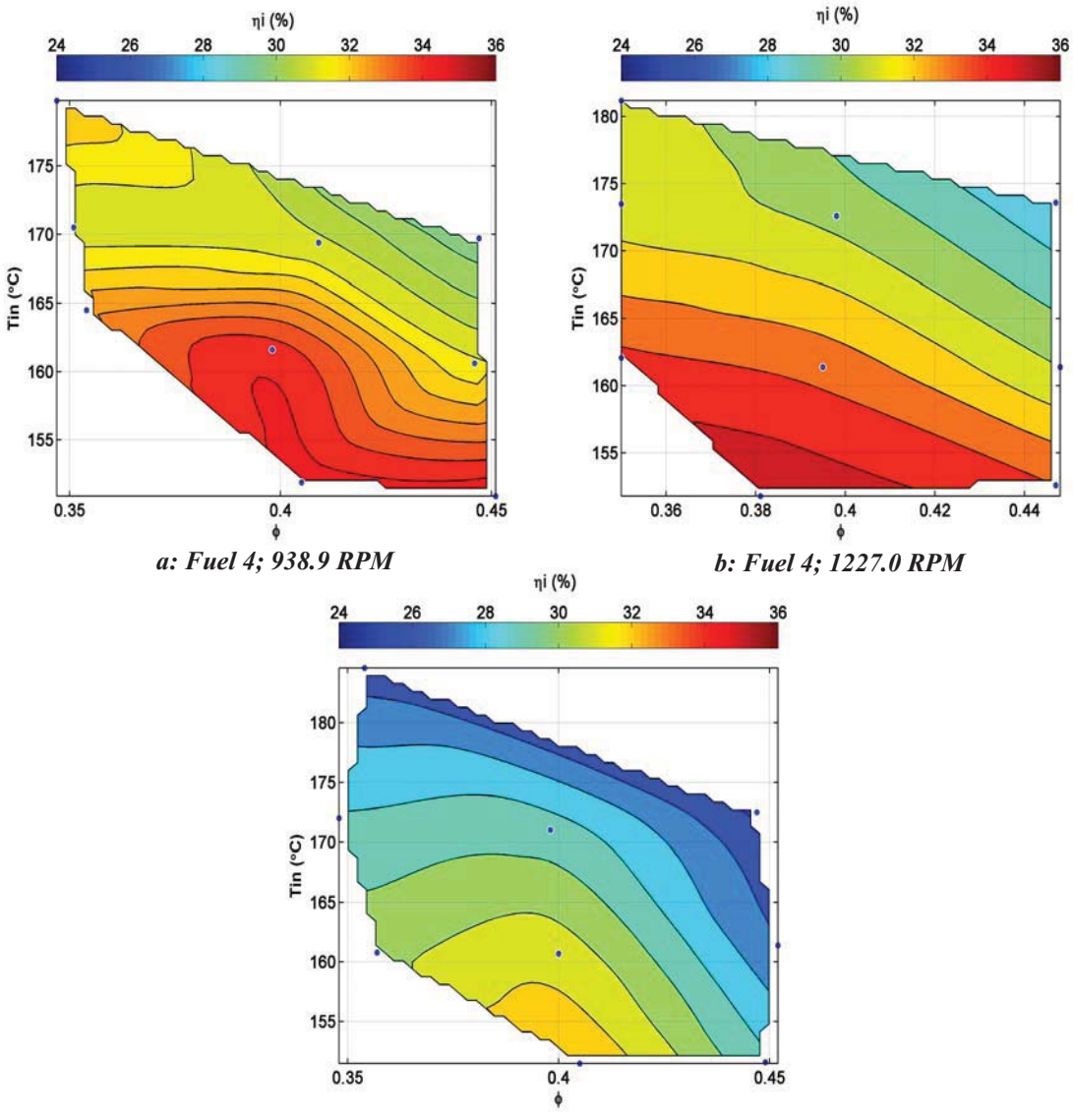

a: Fuel 4; 938.9 RPM

b: Fuel 4; 1227.0 RPM

c: Fuel 4; 1523.4 RPM

Figure 4.18: Indicated Efficiency for Fuel Composition 4 with respect to intake charge temperature and equivalence ratio at engine speeds of 938.9, 1227.0, and 1523.4 RPM

Considering the engine speed of 1523rpm indicated efficiency is reduced related to the other engine speeds tested. A maximum value of 32.7% is achieved using minimum

intake heating (151.6°C) and lean mixtures ($\Phi = 0.399$). With an increase in intake temperature at constant equivalence ratio a decrease in indicated efficiency occurs (i.e. $\eta_{i\ \Phi=0.40,\ 1523rpm} = 32.7\%$ decreases to 29.4%). As was observed in Figure 4.17.c. IMEP at the equivalence ratio $\Phi = 0.399$ seems to exhibit an optimal operating point when intake temperature remains constant. With either increases or decreases in equivalence ratio from this point indicated efficiency will decrease. The increasing engine speed presents itself as a negative variation in terms of indicated efficiency.

CHAPTER V

ANALYSIS AND DISCUSSION

5.1 Fuel Composition Effects

In this section the effects of fuel composition variations will be analyzed and discussed. Based on the results reported on in Section 4.2 of this work it was discovered that the highest IMEP values obtained for each fuel generally occurred with maximum equivalence ratio and utilized minimum intake charge preheating. The highest common equivalence between the different fuel compositions is $\Phi = 0.450 \pm 0.004$. However, the premise of HCCI is lean combustion in order to obtain high efficiency. Again when minimum intake heating is employed as observed in Section 4.2 the highest efficiencies were achieved with the leanest mixtures at said lowest temperatures; the lowest common equivalence ratio is $\Phi = 0.398 \pm 0.006$. When HCCI engines are compared to similarly sized CI or SI engines the work output is significantly reduced, therefore the approach of optimized IMEP will be taken here. In this section $dP/d\theta$ and P_{max} will be eliminated from the discussion and the focus will be on combustion phasing (CA10 and CA10-90) and the resulting performance parameters (IMEP and η_i).

The first topic which needs to be addressed is the range of intake charge temperature used corresponding to each fuel composition. Revisiting the ideal that HCCI auto-ignition is kinetically controlled this factor becomes extremely important when discussing combustion of these biomass gas mixtures. In Section 2.3.3 the principles of H_2 and CO oxidation were discussed. Literature showed that realistic CO oxidation is heavily dependant on the presence of H_2 and hydrogen based radicals. The oxidation of hydrogen can have explosive tendencies under certain pressure and temperature conditions based on rapid chain branching reactions. If these oxidization principles are then applied to the mixtures and combustion mode in this work, the less hydrogen in the fuel and more carbon monoxide, the slower the chain branching occurs. Also, if the amount of hydrogen is reduced relative to carbon monoxide, higher temperatures will need to be employed in order to maintain auto-ignition characteristics. As was mentioned in Chapter 4 fuels 2 and 3 operate between the approximate intake temperature limits of 130°C to 160°C, fuel 4 on the other hand requires a higher range of intake temperatures

152°C to 172°C. When Table 3.3 is recalled fuels 2 and 3 have higher contents of H_2 relative to CO (H_2:CO_{Fuel2} = 0.752 and H_2:CO_{Fuel3} = 1.333); fuel 4 has the lowest hydrogen content relative to the carbon monoxide present (H_2:CO_{Fuel4} = 0.599). Due to the dilution of fuel 4 with higher CO concentrations, higher intake charge temperatures are required in order to initiate the H_2 oxidation leading to H and O radical formation which in turn enhances CO oxidation. It should also be noted that fuels 2 and 4 do not vary drastically with regards to H_2:CO and they both contain the highest fractions of CO. Specifically fuel 4 contains the same amount of H_2 as fuel 2 but has an increased amount of CO resulting from a reduction in its N_2 fraction.

In Figure 5.1 SOC is shown regarding the three different fuel compositions; each subplot is held at $\Phi = 0.450 \pm 0.004$, the highest common equivalence ratio between all the fuel compositions in order to optimize IMEP. Consistent with results found in Section 4.2 for all the fuel compositions at any engine speed as the intake temperature increases the SOC timing advances (i.e. $CA10_{Fuel2,\ 1227rpm,\ Tin=130\text{-}160°C}$ = 5.8°CA to -2.7°CA; $CA10_{Fuel3,\ 1226rpm,\ Tin=130\text{-}160°C}$ = 2.4°CA to -2.6°CA; $CA10_{Fuel4,\ 1227rpm,\ Tin=150\text{-}170°C}$ = 3.6°CA to -2.6 °CA). Fuel 2 with the lowest amount of both H_2 and CO produced the largest range shift of CA10 timing (9.3°CA). When the CO is increased while holding the H_2 fraction constant (Fuel 4) the second largest shift is produced (7.5°CA) even though the temperature range used for fuel 4 is ~20°C higher. Fuel 3, containing the highest fraction of H_2 (20%) produced earlier CA10 timings compared with the other two fuels utilizing minimum intake charge heating and a smaller overall shift range (5.8°CA). As was explained earlier the initial reactions at combustion onset are governed by H_2 oxidization therefore if the hydrogen content increases (as with fuel 3) it is not surprising that the SOC would advance as rapid chain branching occurs. At maximum individual intake temperature correlating to each fuel all the fuels were advanced to approximately the same time (3.4°CA). Fuels 2 and 4 are affected similarly with respect to engine speed; results show little no CA10 changes as engine speed is varied. With a smaller amount of hydrogen present in fuels 2 and 4 lower instances of locally rich H_2 zones (caused through insufficient mixing) would occur limiting the rate of chain branching throughout the reaction zone. Fuel 3 does show effects caused by engine speed variations as retardation of SOC occurring in the region of ~1200rpm over the entire range of intake

temperatures. This effect is speculated to be related to poor mixing which creates locally rich H_2 zones that lead to rapid chain branching.

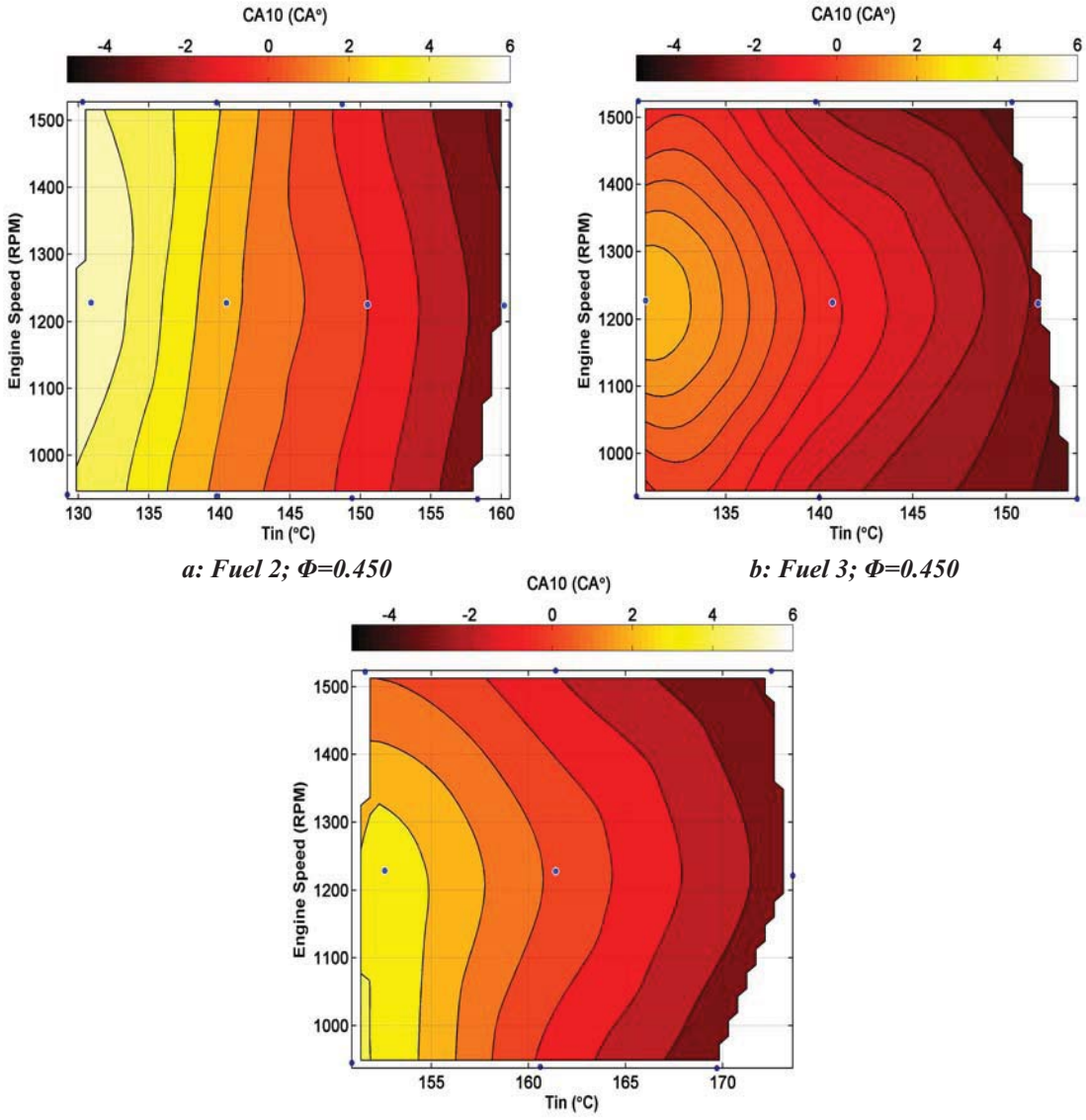

a: Fuel 2; Φ=0.450

b: Fuel 3; Φ=0.450

c: Fuel 4; Φ=0.450

Figure 5.1: CA10 at constant equivalence ratio 0.450 ± 0.004 with respect to intake charge temperature and engine speed regarding fuel compositions 2, 3, and 4

Combustion duration is plotted in Figure 5.2; CA10-90 is thought of to be an indication of the overall rate of burn.

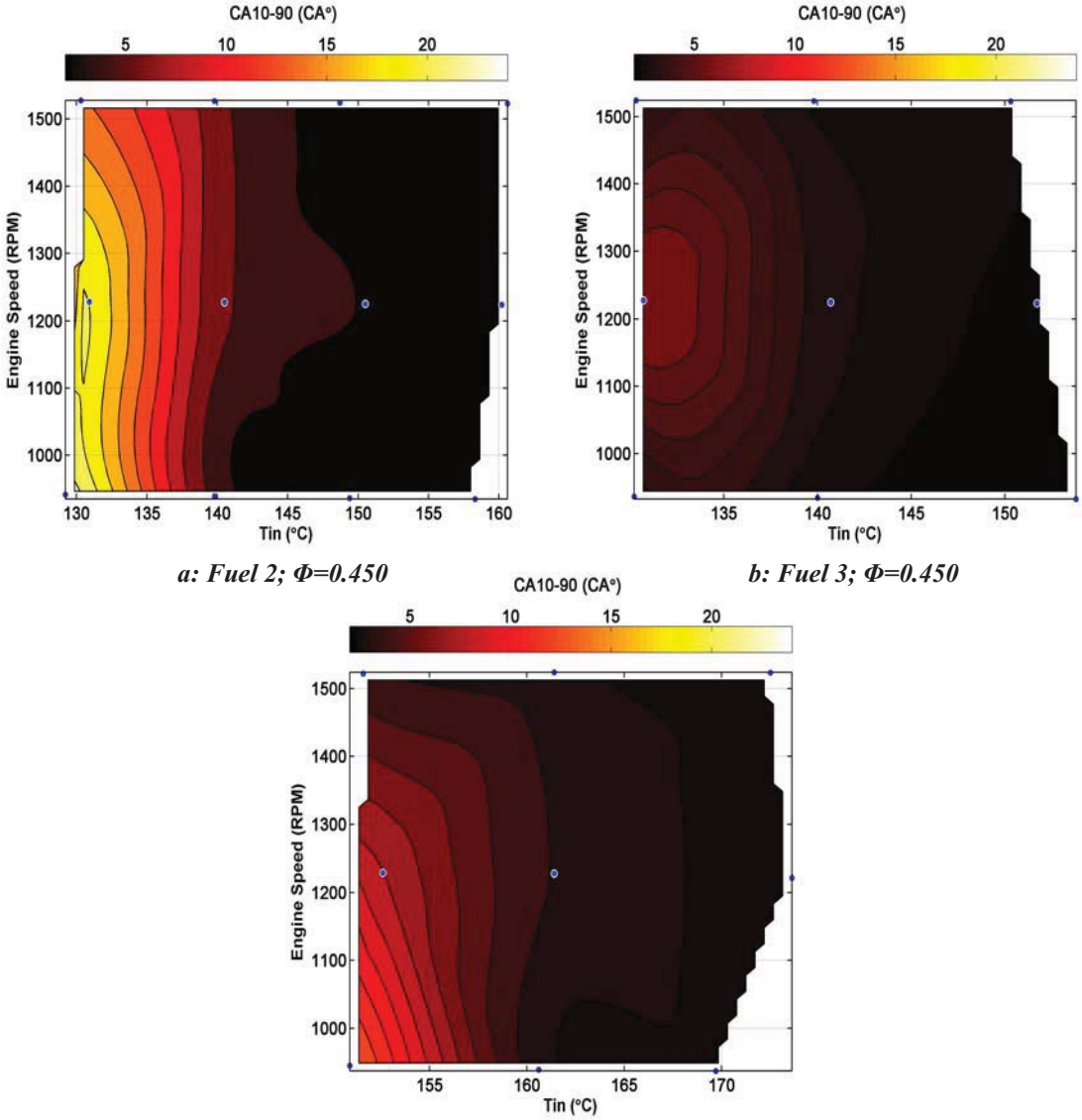

a: Fuel 2; Φ=0.450

b: Fuel 3; Φ=0.450

c: Fuel 4; Φ=0.450

Figure 5.2: CA10-90 at constant equivalence ratio 0.450 ± 0.004 with respect to intake charge temperature and engine speed regarding fuel compositions 2, 3, and 4

First looking at Fig. 5.2.a. regarding Fuel 2, it is shown that long combustion durations (23.7°CA to 14.2°CA) occur at low intake temperature (130°C). As the intake temperature is increased no duration lasts longer than 7°CA and engine speed has no effect on combustion duration at fixed intake temperature. With an increase in H_2 and a reduction in CO (fuel 3) combustion durations are significantly reduced when compared to Fuel 2 ($CA10\text{-}90_{max}$ = 6.0°CA). This decrease in duration can be attributed to the increase in H_2 content. With the increase of hydrogen more H radicals can be produced

simultaneously; as the intermediate species are produced and react further with hydrogen, carbon monoxide and oxygen the reaction rates speed up (similar process when approaching the explosion limit in Fig. 2.8). The reactants are then consumed at a much faster rate leading to these shortened durations. As with CA10 regarding fuel 3, engine speed does affect CA10-90; the total combustion duration for fuel 3 changes from 6.0°CA to 2.1°CA. If fuel 4 CA10-90 results are examined the combustion duration length increases at low intake temperatures compared to fuel 3 ($T_{inFuel4}$= 151.7°C which is roughly 20°C higher than fuel 3) which resembles results obtained with fuel 2. The maximum CA10-90 duration is still shorter for fuel 4 (13.5°CA), this could be a result of the increased intake temperature used corresponding to an increased chemical reaction rate. Fuel 4 shows very little change with respect to variations in engine speed, similar to the results regarding fuel 2.

Next the results of IMEP regarding the three different fuel compositions are shown in Figure 5.3. If both Fig. 5.3.a and 5.3.b are analyzed it appears that there is little difference in IMEP corresponding to fuel compositions 2 and 3 when in fact there is. As shown in fig. 5.1.a and 5.2.a regarding fuel 2 the on-set of combustion was relatively late (ATDC) and the durations of combustion were long (up to 23.7°CA). This corresponds to the pressure trace being poorly phased (retarded) and high peak pressures (60-65 bar and above) not being consistently reached; subsequently the piston does not experience higher pressures leading to a reduction in applied force and effective work output. However, there is no negative work being done on the piston during compression stroke caused from phasing BTDC which is a benefit to performance. IMEP values for fuel 2 do reach as high as 3.5 bar and are maintained above 2.7 bar. Observed in Figs. 5.1.b. and 5.2.b. regarding fuel composition 3, the combination of earlier SOC timing and short durations does not lead to higher performance; shown in Fig. 5.3.b. Combustion phasing again dictates the reduced IMEP for fuel 3, only in this case phasing was too early and short. By phasing combustion BTDC and having very short CA10-90 durations the pressure created BTDC is actually doing negative work on the piston as it is trying to complete the compression stroke. Even though all maximum pressures were above 72.3 bar because combustion was phased to early the benefits of short (volumetric) combustion were not achieved. When analyzing fuel 4 results in terms of IMEP

consistently higher IMEP values were achieved even though higher intake charge temperatures were utilized. This increased performance is a result of the combination of slightly retarded SOC (description of Fig. 5.1) but fairly short combustion durations (Fig. 5.2). The maximum IMEP achieved for fuel 4 under the conditions specified is 3.6 bar (lowest temperature and speed conditions) and does not decrease below 2.6 bar (highest temperature and speed conditions).

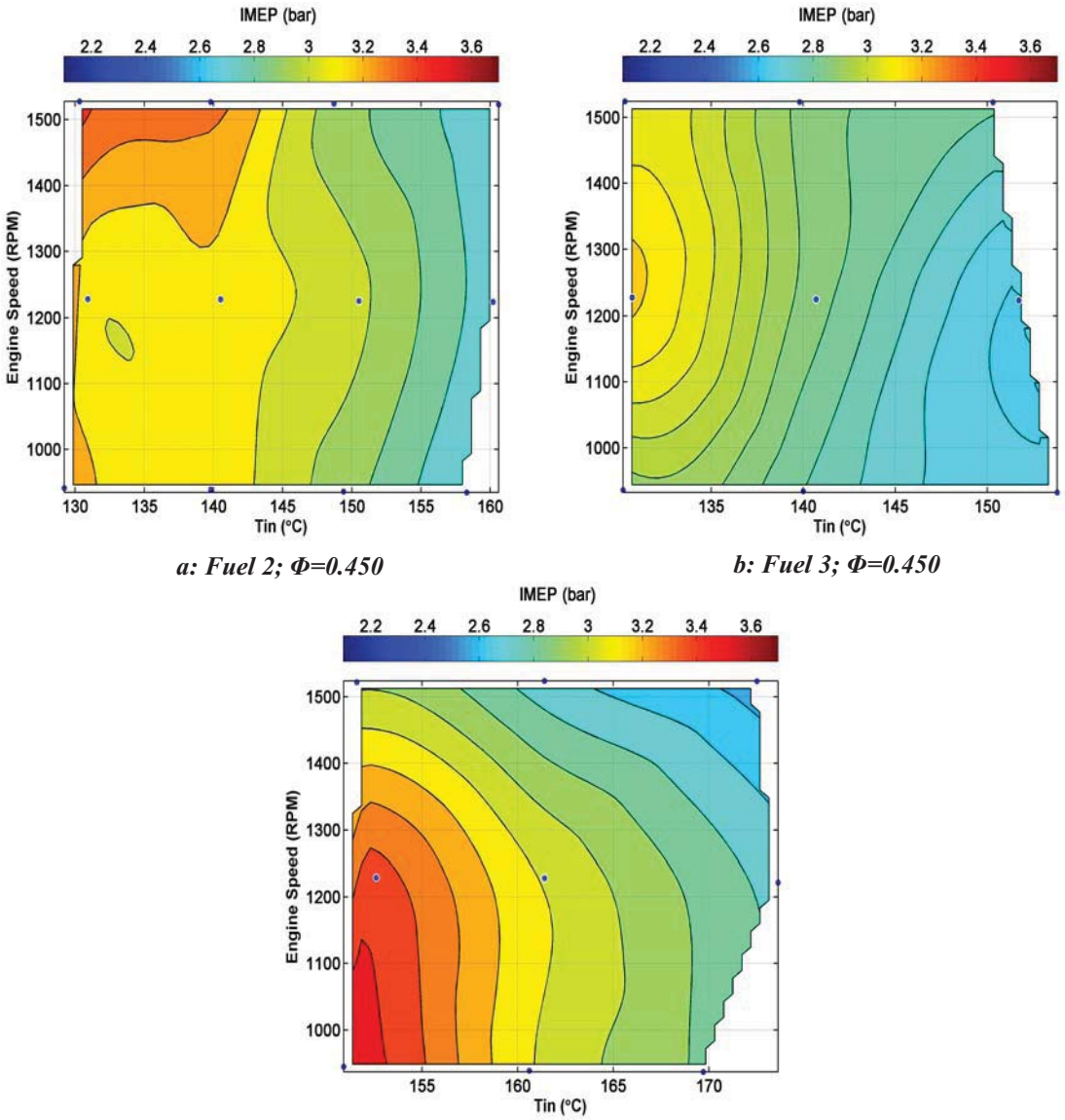

a: Fuel 2; Φ=0.450

b: Fuel 3; Φ=0.450

c: Fuel 4; Φ=0.450

Figure 5.3: IMEP at constant equivalence ratio 0.450 ± 0.004 with respect to intake charge temperature and engine speed regarding fuel compositions 2, 3, and 4

In terms of optimal phasing relating to fuel composition, the utilization of the ignition delay characteristics of CO with the increased kinetics of H_2 of fuels 2 and 4 under similar operating conditions (engine speed and equivalence ratio) proves to enhance work output.

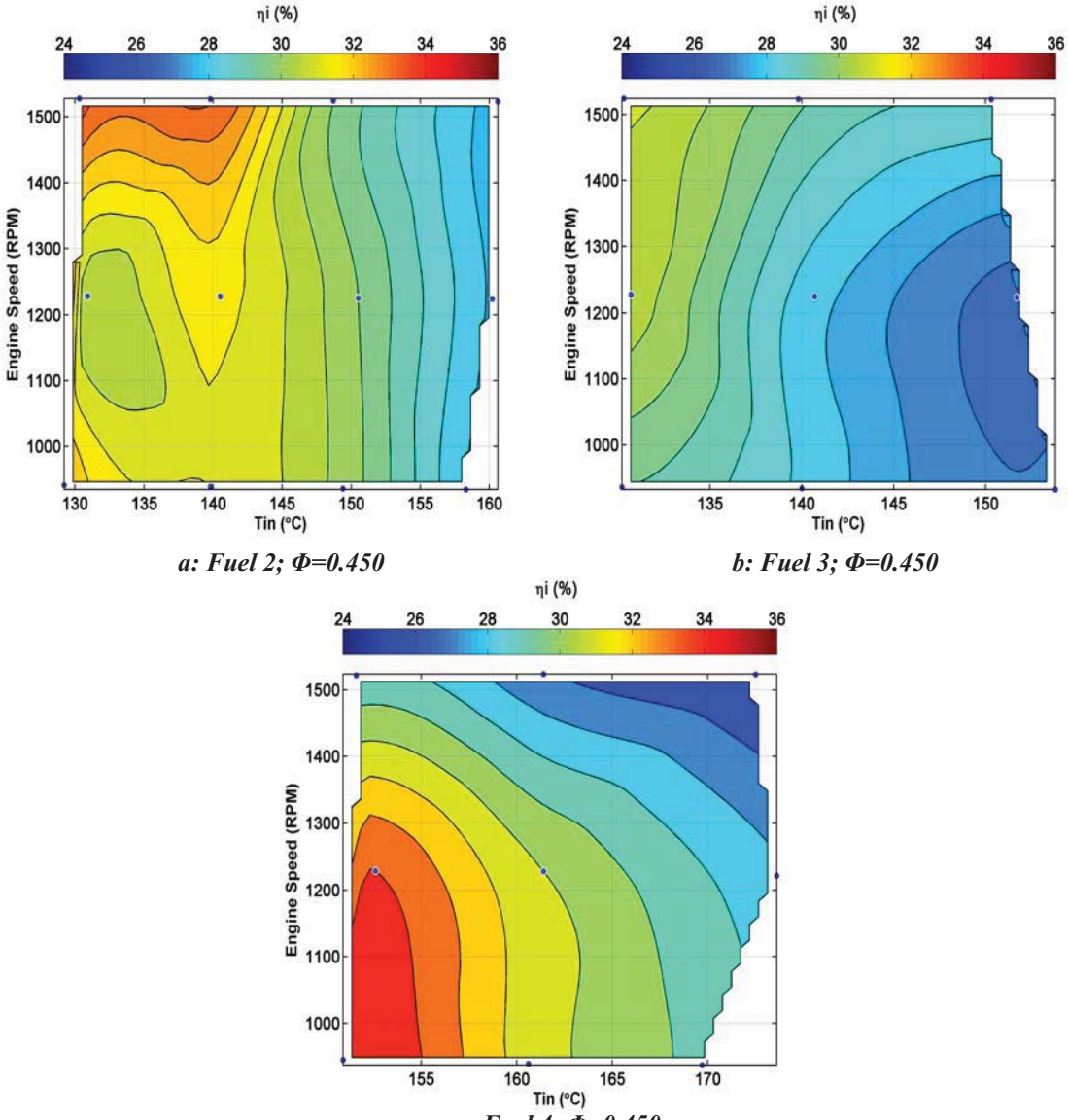

Figure 5.4: Indicated Efficiency at constant equivalence ratio 0.450 ± 0.004 with respect to intake charge temperature and engine speed regarding fuel compositions 2, 3, and 4

Indicated efficiency data are shown in Figure 5.4 and resemble the results obtained for IMEP (Fig. 5.3). The maximum efficiency obtained by fuel 2 was 33.9%

and decreased to 27.7%. The indicated efficiencies obtained for fuel 2 based on the results of IMEP are somewhat higher than might be assumed. This higher efficiency trend can be attributed to fuel 2 having the lowest calorific value and similar IMEP results compared to the other fuel compositions which have higher LCVs. As is to be expected indicated efficiency decreases with increases in intake temperature due to advanced on-set of combustion (BTDC) and reduced volumetric efficiency occurs as intake temperature increases. Engine speed variations have no effect on indicated efficiency of fuel 2 at intake temperatures above 145°C but at lower intake temperatures there appear to be some deficiencies. The maximum indicated efficiency which can be achieved with fuel 3 is 31.2% occurring at the highest engine speed and lowest intake temperature. From this point if the intake temperature is increased the efficiency decreases (minimum of 26.8%) as phasing becomes more advanced. In general engine speed does not have much of an effect on efficiency for fuel 3; one could speculate that there is a very weak effect of better efficiencies with increased engine speed being a resultant of increased charge mixing quality (i.e. $\eta_{iTin=140°C}$ = 28.4% increases to 29.6%). Fuel 4 shows somewhat similar results when compared to fuel 2. The highest attained efficiency value for a fuel tested here (fuel 4) occurs at the lowest engine speed and minimum intake charge preheating (35.0 %). If the engine speed is increased the indicated efficiency decreases and at any engine speed if the intake temperature is increased the efficiency again decreases.

5.2 Discussion of Operating Conditions Effects on Combustion

5.2.1 Effects of Intake Charge Temperature Variations

Results shown in Section 4.2 regarding intake temperature show that variations in the charge preheat temperature significantly affect combustion parameters. One factor behind the results is that increased temperature represents an increased internal energy. If a constant compression ratio is used (the same internal energy increase caused by compression) and the intake temperature is increased the charge reaches auto-ignition

temperature sooner, therefore advancing the combustion phasing. Advanced ignition is shown through the CA10 analysis conducted in Figures 4.1, 4.7, 4.13, and 5.1. As the intake temperature was increased the SOC timing advanced. One other effect that increased intake charge temperature has is decreased charge density which will lower volumetric efficiency and potentially equivalence ratio, which will be discussed in section 5.2.2. Since the phasing of combustion plays such an important role in engine performance, the intake charge preheating constitutes a primary factor that affects engine performance. The most important indicators of performance are IMEP and indicated efficiency. In Figures 4.5, 4.11, 4.17, and 5.3 it was shown that IMEP is negatively affected by increases in intake charge temperatures. This is a result of excessively advanced SOC timing along with shorter CA10-90 durations, where combustion is occurring sooner before TDC and finishing closer to TDC, which translates into more work being done against the piston as the compression stroke is ending. Due to the fact that more positive net work output is being produced at lower intake temperatures the mass of the fuel brought into the cylinder is being utilized more efficiently which is verified through indicated efficiency values shown in Figures 4.6, 4.12, 4.18, and 5.4.

5.2.2 Equivalence Ratio Effects on Phasing and Performance

The equivalence ratio is the comparison of theoretical AFR (air-to-fuel ratio) and actual AFR. Since the theoretical or stoichiometric AFR doesn't change (unless the fuel composition changes) for the individual fuels it is only the actual AFR which changes during the trials. With conventional liquid fuelling this is not necessarily as a complex process as the volume of fuel injected is very small because of the large density of the liquid fuel (about 900 times difference) and the AFR is evaluated on a mass basis. The densities of the gaseous fuels used in this study are very low, in fact lower than air. Therefore if the amount of fuel injected increases the result is less air that is inducted leading to an increase in equivalence ratio. However, to benefit from the HCCI mode of combustion the fuelling must be very lean due to the auto-ignition process limitation. Because of this factor there is always an excess amount of oxygen in HCCI and therefore the engine is not starved for air. As the equivalence ratio increases, a larger mass of fuel

is injected and the amount of total chemical energy which can potentially be released increases. Because the HCCI mode of combustion is an auto-ignition process, the ignition is solely dependent on the chemical kinetics (temperature and concentration) of the air-fuel mixture. When increasing the amount of injected fuel the fuel concentration increases and oxidizer decreases which effects the phasing of combustion. For all constant intake charge temperature conditions for all fuel compositions it was shown that CA10 was advanced and CA10-90 shorter with higher equivalence ratios (Figs. 4.1, 4.2, 4.7, 4.8, 4.13, and 4.14). In addition, the use of richer mixtures also allows for utilization of lower intake charge temperatures which in turn lead to higher engine outputs. The IMEP analysis conducted in Figures 4.5, 4.11, 4.17, and 4.23 shows that this holds true and the maximum IMEP values obtained for each fuel were at the lowest intake charge temperatures and highest equivalence ratios. The efficiency however was negatively affected by increases in equivalence and the highest efficiencies were recorded for the leanest mixtures at the lowest temperatures. This indicates that the increase in the amount of work output is not necessarily proportional to the increase in the amount of fuel mass increased which can be attributed to incomplete conversion to ideal combustion products (CO_2 and H_2O). It shows that the extra fuel's chemical energy was not all converted into the engine's useful work.

5.2.3 Engine Speed Variation Effects on Combustion

Changes in the engine speed affect flow and mixing of the air and fuel charge. One would think that with engine speed increases the duration of combustion in terms of CA° should increase as there is less time per degree crank angle change. One assumption must be made for the previous statement to hold true: HCCI combustion is kinetically controlled and turbulence does not aid in flame propagation or combustion rate. One aspect which should be noted is that ICE technology requires a heat rejection in order to complete a cycle. This occurs through removal of hot combustion products/gases from the cylinder when the exhaust valve opens. Another aspect is heat transfer to the coolant to ensure the engine itself does not overheat and reach it mechanical limit in terms of temperature. The heat transfer losses are proportional to the temperature difference

between the hot gases (combustion products) and the cylinder walls; as long as there is ΔT there will be some magnitude of heat transfer loss. However, amount of heat transfer is dependant on both the difference in temperature between the gas and wall and the time (rate transfer) the two components are exposed to one another. HCCI combustion is considered low temperature combustion (T_{max}<~1500K [5]) compared to conventional combustion modes which use much richer air-to-fuel mixtures. Therefore the temperature gradient between the hot product gases and surfaces are lower than those found in SI or CI engines. Considering the actual time the two components are exposed to each other, as the engine speed increases the time decreases; for the same air-to-fuel mixtures and the same intake charge temperatures there should be less heat transfer to the engine coolant. On the other hand the gain (less heat transfer losses) can be off-set by increases in the heat transfer coefficient due to increased charge velocity. Speculating that there is lower heat transfer does not necessarily translate into more useful work produced; the combustion product enthalpy could be rejected through the exhaust port or the reduction in heat transfer could phase the combustion event sooner leading to a loss in expansion work. Another aspect which should be considered is that with changes in engine speed, the quality of mixing of the charge varies.

The volumetric efficiency of an engine is an evaluation of the amount of charge actually inducted into a cylinder with respect to the volume which that cylinder displaces. If a reduction in volumetric efficiency occurs an automatic reduction in the available charge mass for reaction occurs. The volumetric efficiency of the engine in this work is not 100% and decreases with increases in intake temperature and engine speed (shown in Figure 5.5). Experiments to obtain data for Fig. 5.5 were carried out inducting only preheated air into the engine. The volumetric efficiency decreases with increases in intake temperature because the charge density decreases. For any constant intake temperature curve shown in Fig. 5.5 there is an overall decrease of ~2% in volumetric efficiency from 900rpm to 1500rpm which is the range tested for this study. With only a 2% decrease in volumetric efficiency any effects caused from this condition are considered negligible.

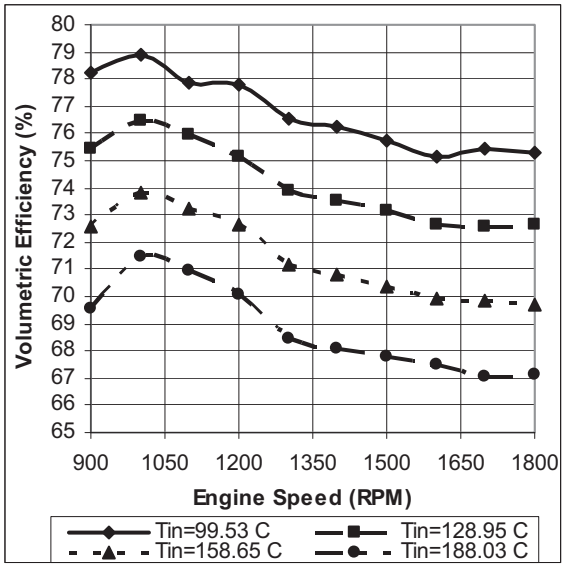

Figure 5.5: Volumetric Efficiency investigation utilizing Only Air (no fuel injection)

The position of the fuel injector is approximately 0.572 m away from the intake port. This distance corresponds to a volume approximately 2.2x the cylinder displacement volume. This suggests that combustion could be dependent on multiple cycles of injection and less than perfect mixing of the intake air and injected fuel. The injection duration is held constant for each test therefore some deviations in combustion are a result of airflow changes and mixture formation. The intake air-flow is intermittent and occurs only when the intake valve is open as this is a single cylinder engine. It is suspected when the gaseous fuel is introduced into the intake piping the charge becomes stratified as there is no mixing promoting flow in the piping and the fact that a gaseous fuel jet does not disperse readily [62]. Another key factor when discussing mixing is that the engine is a converted IDI CI; the original/stock turbulence in the pre-chamber (which aids in mixing and therefore combustion) is a result of the transfer port geometry connecting with the main cylinder volume (recall Fig. 3.2). In this experimental setup that orifice has been enlarged and therefore is it speculated that charge which ends up in the combustion chamber will retain some stratification formed in the intake piping. Engine speed is also suspected to play a role in the severity of stratification. As engine speed is increased better mixing of the fuel/air should occur as the flow itself becomes

steadier and increased turbulence is expected, this will lead to reduced stratification effects and more homogeneity in the charge.

CHAPTER VI

CONCLUSIONS AND RECOMMENDATIONS

6.1 Conclusions

Several specific results were derived in this study and are listed in the following section:

- The results regarding fuel composition effects seem to indicate that higher CO levels in the fuel are beneficial for phasing combustion. These results indicate that CO acts as a reaction inhibitor. The rapid chain branching mechanisms of hydrogen are slowed as some the hydrogen oxygen radicals formed are consumed through the oxidization of carbon monoxide.
- A more ideal volumetric heat input processes can be achieved with higher concentrations of hydrogen basically independent of operating parameters. With an increased fraction of H_2 the kinetics of the mixture change and CO becomes a reaction enhancer. The inefficient advanced nature of combustion onset is greater than the benefits of short combustion. With variations in the fuel compositions and the AFR used, the ignition properties will change under various operating conditions (i.e. equivalence ratio, intake temperature).
- Increasing the intake charge temperature irrespective of any other operating condition advanced the phasing of the combustion eventually leads to negative impact on pressure derived performance parameters. This occurred for all fuels and at all operating conditions.
- With increased equivalence ratio more fuel mass was injected allowing for more chemical energy to potentially be released. Increased equivalence ratio allowed for operation with lower intake temperatures maximizing IMEP. The fuel inducted however was not as efficiently utilized with rich mixtures and maximum efficiencies were observed with lean mixtures.
- Because mixing cannot currently be quantified with the existing experimental setup the results are somewhat speculative. However, it is shown that at constant equivalence ratio and intake temperature engine speed does have some effects.

Charge homogeneity is thought to be greatest impacted by insufficient mixing. Variations of engine speed leading to locally rich or lean zones in the combustion chamber effect chemical kinetics and ultimately combustion phasing.

6.2 Technological Contributions

Through the experimental work carried out in this study an insight into the combustion of biomass gas at elevated temperatures and pressures was provided. The concept that such a gaseous fuel can be implemented for use in HCCI engines was shown which could lead to potential for the development alternative power generation methods. It is well known that chemical kinetics play an extremely significant role in HCCI combustion. Related to the kinetics is the idea that without implementation of EGR combustion control can be maintained through manipulation of the fuel composition itself by varying the process and feedstock used for gas production.

6.3 Future Work Recommendations

In this work the experimental engine operates with only one active cylinder which causes pulsating flow. It is believed that charge mixing is of particular interest regarding some of the results found in this study and therefore an attempt to quantify mixing quality and the effects on combustion should be a next step in the HCCI biomass gas research. Injection timing variations could alter mixing quality and could be a first step. Location of injector and optimized intake runner design should also be considered.

One suggestion is to develop and implement a combustion chamber/head designed specifically for biomass gas operation. Such a design could aid in homogeneity of the mixture through inducing in-cylinder turbulence (from intake runner entry for example) minimizing the opportunity for charge stratification and combustion dependence on multiple cycle charge generation.

With respect to fuel composition; a specific gasifier setup (preferably commericial unit) should be utilized with a regionally specific and abundant feedstock (i.e. waste

sawdust from lumber industry), the composition of the gas then needs to be analyzed. Combustion characteristics (auto-ignition temperature, laminar flame velocity, etc.) of the fuel composition acquired should then be investigated in detail with the construction of a new setup such as a constant volume optical chamber of flame propagation duct. Such an investigation will contribute to literature and ultimately understanding for viability of such biomass gas derived fuels for practical use.

REFERENCES

[1] Mingfa Yao, Zhaolei Zheng, Haifeng Liu, “Progress and recent trends in homogeneous
charge compression ignition (HCCI) engines”, Progress in Energy and Combustion Science, 2009, 398-437.

[2] Willard W. Pulkrabek, “Engineering Fundamentals of the Internal Combustion Engine”, Prentice Hall, Upper Saddle River, NJ, 1997.

[3] Richard Stone, “Introduction to Internal Combustion Engines”, SAE International, Warrendale, PA, 1999.

[4] http://www.freepistonjetengine.741.com/HCCI.html. Accessed 26 January 2011.

[5] F. Zhao, T. Asmus, D. Assanis, J. Dec, J. Eng, P. Najt (Eds.), Homogenous Charge Compression Ignition (HCCI) Engines; Key Research and Development Issues, SAE International, Warrendale P.A., 2003.

[6] Chen, Z., and Mitsure, K., " How to Put the HCCI Engine to Practical Use; Control the Ignition Timing by Compression Ratio and Increase the Power Output by Supercharging", SAE Paper 2003-01-1971.

[7] Cairns, A., and Baxill, H., “The Effects of Combined Internal and External EGR on Gasoline Controlled Auto-Ignition”, SAE paper 2005-01-0133.

[8] Zhao, H. Peng, Z., Williams, J., and Ladommatos, N., "Understanding the Effects of Recycled Burnt Gases on the Controlled Autoignition (CAI) Combustion in Four-Stroke Gasoline Engines", SAE Paper 2001-01-3607.

[9] P. Hasler, Th. Nussbaumer, “Gas Cleaning for IC engine applications from fixed bed biomass gasification”, Biomass and Bioenergy, 1999, 385-395.

[10] Peter McKendry, “Energy Production from biomass (part 3): gasification technologies”, Bioresource Technology, 2002, 55-63.

[11] S.M. Walton, X. He, B.T. Zigler, M.S. Wooldridge, “An experimental investigation of the ignition properties of hydrogen and carbon monoxide mixtures for syngas turbine applications”, Proceedings of the Combustion Institute, 2007, 3147-3154.

[12] M. Iida, M. Hayashi, D.E. Foster, J.K. Martin, “Characteristics of Homogeneous Charge Compression Ignition (HCCI) Engine Operation for Variations in Compression Ratio, Speed, and Intake Temperature while using n-Butane as a Fuel”, ASME, 2003 , Vol. 125, 472-478.

[13] Rakesh Kumar Maurya, Avinash Kumar Agarwal, “Experimental investigation on the effect of intake air temperature and air-fuel ratio on cycle-to-cycle variations of HCCI combustion and performance parameters”, Applied Energy, 2011, 1153-1163.

[14] S. Swami Nathan, J.M. Mallikarjuna, A. Ramesh, “Effects of charge temperature and exhaust gas recirculation on combustion and emission characteristics of an acetylene fuelled HCCI engine”, Fuel, 2010, 515-521.

[15] Magnus Christensen, Bengt Johansson, Per Amnéus, Fabian Mauss, “Supercharged Homogeneous Charge Compression Ignition”, SAE Paper 980787, 1998.

[16] John E. Dec, Yi Yang, “Boosted HCCI for High Power without Engine Knock and with Ultra-Low NOx Emissions – using Conventional Gasoline”, SAE Paper 2010-01-1086, 2010.

[17] Koji Hiraya, Kazuya Hasegawa, Tomonori Urushihara, Akihiro Iiyama, Teruyuki Itoh, “A Study on Gasoline Fueled Compression Ignition Engine ~A Trial of Operation Region Expansion ~”, SAE Paper 2002-01-0416, 2002.

[18] Hatim Machrafi, Simeon Cavadias, Philippe Guibert, “An experimental and numerical investigation on the influence of external gas recirculation on the HCCI autoignition process in an engine: Thermal, diluting and chemical effects”, Combustion and Flame, 2008, 476-489.

[19] Magnus Sjöberg, John E. Dec, Wontae Hwang, “Thermodynamic and Chemical Effects of EGR and its Constituents on HCCI Autoignition”, SAE Paper 2007-01-0207, 2007.

[20] Tian Guohong, Wang Zhi, Wang Jianxin, Shuai Shijin, and An Xinliang, “HCCI Combustion Control by Injection Startegy with Negative Valve Overlap in a GDI Engine”, SAE Paper 2006-01-0415, 2006.

[21] Tomonori Urushihara, Koji Hiraya, Akihiko Kakuhou, Teruyuki Itoh, “Expansion of HCCI Operating Region by the Combination of Direct Fuel Injection, Negative Valve Overlap and Internal Fuel Reformation”, SAE Paper 2003-01-0749, 2003.

[22] Rahim Ebrahimi, Bernard Desmet, “An experimental investigation on engine speed and cyclic dispersion in an HCCI engine”, Fuel, 2010, 2149-2156.

[23] Vahid Hosseini, W. Stuart Neill, Wallace L. Chippior, “Influence of Engine Speed on HCCI Combustion Characteristics using Dual-Stage Autoignition Fuels”, SAE Paper 2009-01-1107, 2009.

[24] T.D. Pedersen, J. Schramm, “A Study on the Effects of Compression Ratio, Engine Speed and Equivalence Ratio on HCCI Combustion of DME”, SAE Paper 2007-01-1860, 2007.

[25] Allen Gray, Thomas W. Ryan, “Homogeneous Charge Compression Ignition (HCCI) of Diesel Fuel, SAE Paper 971676, 1997.

[26] N.L. Panwar, S.C. Kaushik, Surendra Kothari, “Role of renewable energy sources in environmental protection: A review”, Renewable and Sustainable Energy Reviews, 2011, 1513-1524.

[27] U. Wagner, S. Wiemer, A. Velji, U. Spicher, “An experimental study to assess the potential of homogeneous charge compression ignition diesel combustion with various fuels for light-duty engine”, International Journal of Engine Research, 2007, Vol. 8, Special Issue.

[28] Magnus Christensen, Anders Hultqvist, Bengt Johansson, “Demonstrating the Multi Fuel Capability of a Homogeneous Charge Compression Ignition Engine with Variable Compression Ratio”, SAE Paper 1999-01-3679, 1999.

[29] Haifeng Liu, Mingfa Yao, Bo Zhang, Zunqing Zheng, “Influence of Fuel and Operating Conditions on Combustion Characteristics of a Homogeneous Charge Compression Ignition Engine”, Energy & Fuels, 2009, 1422-1430.

[30] Gen Shibata, Tomonori Urushihara, “Auto-Ignition Characteristics of Hydrocarbons and Development of HCCI Fuel Index”, SAE Paper 2007-01-0220., 2007.

[31] J. Hiltner, R. Agama, F. Mauss, B. Johansson, M. Christensen, “Homogeneous Charge Compression Ignition Operation With Natural Gas: Fuel Composition Implications”, Journal of Engineering for Gas Turbines and Power, 2003, Vol. 125, 837-844.

[32] Hiroshi Kuzuyama, Masahiro Machida, Kazuhiro Akihama, Kazuhisa Inagaki, Matsuei Ueda, “A Study on Natural Gas Fueled Homogeneous Charge Compression Ignition Engine – Expanding the Operating Range and Combustion Mode Switching”, SAE Paper 2007-01-0176, 2007.

[33] Vahid Hosseini, M. David Checkel, “Effect of Reformer Gas on HCCI Combustion – Part I: High Octane Fuels”, SAE Paper 2007-01-0208, 2007.

[34] Vahid Hosseini, M. David Checkel, “Effect of Reformer Gas on HCCI Combustion – Part II: Low Octane Fuels”, SAE Paper 2007-01-0206, 2007.

[35] John Waldman, Dennis Nitz, Tanet Aroonsrisopon, David E. Foster, Minoru Iida, “Experimental Investigation into the Effects of Direct Fuel Injection During the Negative Valve Overlap Period in an Gasoline Fueled HCCI Engine”, SAE Paper 2007-01-0219, 2007.

[36] Peter McKendry, “Energy production from biomass (part 1): overview of biomass”, Bioresource Technology, 2002, 37-46.

[37] Peter McKendry, “Energy production from biomass (part 2): conversion technologies”, Bioresource Technology, 2002, 47-54.

[38] Pradeep Chaminda Munasinghe, Samir Kumar Khanal, “Biomass-derived syngas fermentation into biofuels: Opportunities and challenges”, Bioresource Technology, 2010, 5013-5022.

[39] Jacques Lédé, “Biomass Pyrolysis: Comments on Some Sources of Confusions in the Definitions of Temperatures and Heating Rates”, Energies, 2010, Vol. 3, 886-898.

[40] M.K. Karmakar, A.B. Datta, “Generation of hydrogen rich gas through fluidized bed gasification of biomass”, Bioresource Technology, 2011, 1907-1913.

[41] Wei Wu, Katsuya Kawamoto, Hidetoshi Kuramochi, “Hydrogen-rich synthesis gas production from waste wood via gasification and reforming technology for fuel cell application”, Journal of Material Cycles Waste Management, 2006, 70-77.

[42] A. Saravanakumar, T.M. Haridasan, Thomas B. Reed, R. Kasturi Bai, “Experimental investigations of long stick wood gasification in a bottom lit updraft fixed bed gasifier”, Fuel Processing Technology, 2007, 617-622.

[43] Weihong Yang, Anna Ponzio, Carlos Lucas, Wlodzimierz Blasiak, “Performance analysis of a fixed-bed biomass gasifier using high temperature air”, Fuel Processing Technology, 2006, 235-245.

[44] Siyi Luo, Bo Xiao, Xianjun Guo, Zhiquan Hu, Shiming Liu, Maoyun He, “Hydrogen-rich gas from catalytic steam gasification of biomass in a fixed bed reactor: Influence of particle size on gasification performance”, International Journal of Hydrogen Energy, 2009, 1260-1264.

[45] Chih-Jen Sung, Chung K. Law, “Fundamental Combustion Properties of H2/CO Mixtures: Ignition and Flame Propagation at Elevated Pressures”, Combustion Science and Technology, 2008, 1097-1116.

[46] Chung K. Law, “Combustion Physics”, Cambridge University Press, New York, NY, 2006.

[47] J. Chomiak, “Combustion: A Study in Theory, Fact and Application”, Gordon and Breach Science Publishers, Switzerland, 1990.

[48] J.B. Heywood, “Internal Combustion Engine Fundamentals”, McGraw-Hill, 1988.

[49] I. Wierzba, V. Kilchyk, “Flammability limits of hydrogen-carbon monoxide mixtures at moderately elevated temperatures”, International Journal of Hydrogen Energy, 2001, 639-643.

[50] Juan J. Hernandez, Clara Serrano, Javier Perez, “Prediction of the Autoignition Delay Time of Producer Gas from Biomass Gasification”, Energy & Fuels, 2006, 532-539.

[51] Gaurav Mittal, Chih-Jen Sung, Richard A. Yetter, “Autoignition of H2/CO at elevated Pressures in a rapid compression machine”, International Journal of Chemical Kinetics, 2006, Vol. 38,516-529.

[52] Francisco V. Tinaut, Andrés Melgar, Alfonso Horrillo, Ana Díez de la Rosa, “Method for predicting the performance of an internal combustion engine fuelled by producer gas and other low heating value gases”, Fuel Processing Technology, 2006, 135-142.

[53] G. Sridhar, P.J. Paul, H.S. Mukunda, “Biomass derived producer gas a reciprocating engine fuel – an experimental analysis”, Biomass and Bioenergy, 2001, 61-72.

[54] Dale Haggith, Andrzej Sobiesiak, Luke Miller, Grzegorz Pryzbyla, “Experimental Indicated Performance of a HCCI Engine Fuelled by Simulated Biomass Gas”, SAE Paper 2010-01-108, 2010.

[55] M. Muñoz, F. Moreno, J. Morea-Roy, J. Ruiz, J. Arauzo, “Low heating value gas on spark ignition engines”, Biomass and Bioenergy, 2000, 431-439.

[56] Hailin Li, Ghazi A. Karim, A. Sohrabi, “An Experimental and Numerical Investigation of Spark Ignition Engine Operation on H_2, CO, CH_4 and Their Mixtures”, Journal of Engineering for Gas Turbines and Power, 2010, Vol. 132.

[57] Ali Mohammadi, Masahiro Shioji, Takuji Ishiyama, Masato Kitazaki, “Utilization of Low-Calorific Gaseous Fuel in a Direct-Injection Diesel Engine”, Journal of Engineering for Gas Turbines and Power, 2006, Vol. 128, 915-920.

[58] A.S. Ramadhas, S. Jayaraj, C. Muraleedharan, “Dual fuel mode in diesel engines using renewable fuels: Rubber seed oil and coir-pith producer gas”, Renewable Energy, 2008, 2077-2083.

[59] S. Swami Nathan, J.M. Mallikarjuna, A. Ramesh, “An experimental study of the biogas-diesel HCCI mode of engine operation”, Energy Conversion and Management, 2010, 1347-1353.

[60] Toshio Shudo, Hiroyuki Yamada, “Hyrdrogen as an ignition-controlling agent for HCCI combustion engine by suppressing the low-temperature oxidation”, International Journal of Hydrogen Energy, 2007, 3066-3072.

[61] P. Zoldak, “Design of a Research Engine for Homogeneous Charge Compression Ignition (HCCI) Combustion”, Thesis, University of Windsor, 2005.

[62] Chunyi Xia, “The Behaviour of a Gaseous Transient Jet in a Direct Injection Turbulence Chamber”, Dissertation, University of Windsor, 2006.

APPENDIX A

A.1. Performance and Phasing Data Table – Fuel Composition 2

Fuel Composition 2

Φ	Coolant Temp	Intake Temp	RPM	IMEP (bar)		Pressure Rise (bar/deg)		Max Pressure (bar)		SOC (°CA)	HR Duration	ηi
	°C	°C		Value	Std. Dev.	Value	Std. Dev.	Value	Std. Dev.	CA10	CA10-90	%
0.346	83.5	160.8	933.8	2.51	0.07	5.31	0.60	69.37	1.91	0.5	5.2	31.4
0.346	84.1	160.9	1224.7	2.62	0.05	4.93	0.52	69.27	1.92	1.0	6.0	32.5
0.349	82.7	160.6	1522.0	2.32	0.10	2.18	0.54	59.27	3.70	2.5	9.6	28.1
0.407	81.0	142.2	940.9	3.03	0.08	5.72	0.82	72.89	2.84	1.7	5.4	32.6
0.402	82.3	142.4	1230.0	3.09	0.06	3.44	1.04	64.87	5.35	3.0	8.3	33.3
0.404	83.3	142.0	1521.0	2.99	0.05	4.33	0.73	70.38	3.40	2.4	6.1	31.9
0.398	82.0	149.7	933.6	2.87	0.07	5.80	0.88	72.26	2.77	1.2	5.3	31.7
0.398	82.6	153.4	1225.1	2.80	0.07	6.90	0.36	76.68	1.23	0.2	3.9	30.8
0.401	83.5	151.7	1523.9	2.72	0.06	6.38	0.39	77.56	1.53	0.1	4.0	29.7
0.400	82.3	155.9	934.5	2.69	0.08	8.79	0.32	79.70	0.85	-1.7	2.9	30.3
0.394	82.9	161.0	1228.0	2.64	0.07	8.09	0.28	79.22	0.87	-1.2	2.8	29.8
0.406	83.7	162.3	1523.0	2.58	0.06	7.89	0.31	81.48	0.77	-1.8	3.3	28.2
0.448	83.1	129.2	941.0	3.28	0.15	1.99	0.69	53.77	6.14	5.0	23.7	32.7
0.448	84.4	130.9	1228.5	3.12	0.37	1.78	0.47	50.95	6.00	5.8	20.1	30.7
0.458	84.4	130.3	1528.0	3.45	0.09	2.12	0.74	56.68	6.49	5.1	14.2	33.9
0.453	82.3	139.8	938.6	3.15	0.07	5.75	0.98	72.56	3.21	1.8	5.4	31.5
0.448	82.3	140.5	1228.0	3.17	0.06	4.97	0.87	70.73	3.71	2.3	6.4	31.7
0.451	82.4	139.8	1527.0	3.34	0.06	4.18	0.97	68.95	4.17	3.1	6.9	33.6
0.446	82.2	149.4	936.1	2.94	0.09	8.34	0.44	79.17	1.12	-0.3	3.4	30.3
0.458	82.0	150.5	1225.7	3.02	0.08	7.85	0.49	79.27	1.63	0.0	3.9	30.0
0.452	83.5	148.7	1524.3	2.96	0.07	8.10	0.41	82.35	1.30	-0.2	3.3	30.0
0.447	82.9	158.3	934.8	2.69	0.08	10.08	0.25	81.85	0.71	-2.8	2.3	28.0
0.452	84.3	160.2	1224.0	2.74	0.09	9.88	0.26	83.52	0.83	-2.7	2.1	27.9
0.455	84.0	160.6	1523.0	2.71	0.08	10.16	0.34	86.43	0.94	-3.5	2.7	27.7
0.501	82.8	128.6	936.9	3.41	0.10	8.34	0.68	80.76	2.36	1.1	4.1	31.3
0.510	83.1	129.2	1231.7	3.67	0.10	5.84	1.35	73.91	5.90	2.7	7.1	33.3
0.503	83.4	129.6	1530.5	3.61	0.08	7.23	0.86	80.82	3.37	2.1	4.9	33.6
0.477	82.8	138.7	935.6	3.05	0.08	8.72	0.55	81.16	1.50	0.2	3.3	29.6
0.509	82.4	140.7	1229.0	3.37	0.07	10.44	0.31	88.44	1.04	-1.5	3.5	31.1
0.508	83.6	141.0	1524.0	3.46	0.08	11.09	0.52	92.27	1.53	-1.6	3.2	32.6
0.513	81.4	147.6	931.8	3.03	0.09	11.48	0.34	87.81	1.00	-2.5	2.1	28.1
0.509	81.5	150.4	1222.1	3.05	0.10	10.84	0.33	88.75	1.06	-2.3	2.4	28.2
0.503	83.3	150.1	1525.1	3.19	0.10	11.49	0.47	92.27	1.52	-3.5	3.1	30.5

A.2. Performance and Phasing Data Table – Fuel Composition 3

Fuel Composition 3

Φ	Coolant Temp	Intake Temp	RPM	IMEP (bar)		Pressure Rise (bar/deg)		Max Pressure (bar)		SOC (°CA)	HR Duration (°CA)	ηi
	ºC	ºC		Value	Std. Dev.	Value	Std. Dev.	Value	Std. Dev.	CA10	CA10-90	%
0.351	83.4	141.5	934.8	2.56	0.07	4.75	0.70	68.03	2.42	1.4	5.7	31.1
0.346	83.8	141.5	1227.7	2.57	0.06	2.88	0.72	61.52	3.81	2.6	8.8	31.2
0.347	83.3	140.6	1519.6	2.57	0.05	3.47	0.62	65.49	2.79	2.4	7.2	31.6
0.347	82.9	150.9	934.0	2.46	0.07	6.46	0.48	72.73	1.36	-0.4	3.8	30.5
0.347	83.3	151.6	1224.2	2.48	0.05	5.03	0.47	69.37	1.65	0.9	5.4	30.4
0.352	82.5	150.3	1522.1	2.47	0.07	5.51	0.43	73.24	1.53	0.4	4.3	30.2
0.349	83.9	163.4	933.2	2.23	0.07	8.23	0.26	75.59	0.47	-2.9	2.7	28.2
0.354	83.8	162.0	1222.7	2.28	0.06	7.41	0.26	75.29	0.66	-1.9	3.1	28.1
0.354	84.5	161.8	1521.3	2.28	0.07	7.69	0.27	78.62	0.68	-2.7	2.9	28.4
0.404	83.2	131.1	936.2	2.84	0.08	6.20	0.63	74.29	1.78	1.1	4.6	30.5
0.395	83.7	131.1	1226.3	2.89	0.08	2.52	0.98	59.90	6.22	3.2	11.4	31.2
0.397	83.3	130.2	1524.8	2.92	0.05	4.57	0.68	71.21	2.75	2.3	5.6	32.0
0.393	83.0	140.8	938.4	2.68	0.07	7.89	0.49	78.28	1.25	-0.6	3.4	30.0
0.392	83.7	141.2	1225.3	2.75	0.07	5.84	0.54	73.56	1.82	1.0	4.7	30.5
0.393	83.7	139.7	1520.1	2.94	0.07	7.22	0.48	80.28	1.41	0.2	3.7	33.0
0.394	83.9	150.6	937.1	2.55	0.08	9.31	0.29	80.65	0.68	-2.6	2.6	29.2
0.401	84.2	151.2	1223.8	2.55	0.08	8.30	0.28	79.85	0.79	-1.5	2.8	28.1
0.396	84.2	150.5	1522.4	2.54	0.08	8.77	0.31	83.55	0.74	-2.3	2.9	28.8
0.391	84.0	161.4	936.1	2.37	0.09	9.76	0.23	79.97	0.50	-4.1	2.2	27.6
0.397	84.1	161.4	1229.9	2.36	0.08	9.06	0.17	80.61	0.63	-3.2	2.4	26.6
0.398	84.0	160.6	1518.0	2.43	0.08	9.37	0.31	83.74	0.88	-3.8	2.7	27.7
0.444	84.0	130.2	936.3	2.92	0.08	9.01	0.39	82.28	1.03	-0.4	3.1	29.5
0.454	83.6	130.7	1227.8	3.16	0.07	5.32	0.87	72.30	3.40	2.4	6.0	30.8
0.454	84.8	130.3	1524.4	3.08	0.08	9.54	0.47	87.96	1.27	-0.6	3.2	31.2
0.445	83.2	140.0	934.0	2.80	0.09	9.68	0.29	83.04	0.75	-1.7	2.7	28.4
0.455	83.2	140.7	1225.1	2.87	0.08	8.39	0.37	81.34	1.18	-0.4	3.2	28.2
0.450	84.0	139.8	1523.4	2.89	0.09	10.30	0.43	89.09	1.05	-2.0	2.9	29.6
0.455	83.7	153.8	932.6	2.66	0.09	10.58	0.28	83.55	0.78	-3.5	2.1	27.1
0.447	84.5	151.7	1223.5	2.64	0.09	9.85	0.23	84.41	0.78	-2.6	2.3	26.8
0.455	83.9	150.3	1522.6	2.81	0.10	11.02	0.49	89.67	1.53	-3.4	2.6	29.0

A.3. Performance and Phasing Data Table – Fuel Composition 4

Fuel Composition 4

Φ	Coolant Temp	Intake Temp	RPM	IMEP (bar)		Pressure Rise (bar/deg)		Max Pressure (bar)		SOC (°CA)	HR Duration (°CA)	ηi
	°C	°C		Value	Std. Dev.	Value	Std. Dev.	Value	Std. Dev.	CA10	CA10-90	%
0.354	83.4	164.5	938.8	2.76	0.06	6.18	0.62	73.28	1.87	0.8	4.6	32.9
0.350	83.7	162.1	1231.8	2.88	0.05	5.10	0.62	70.67	2.42	2.0	5.9	34.2
0.357	83.6	160.8	1524.9	2.69	0.04	4.07	0.49	68.35	2.20	2.2	5.7	30.7
0.351	83.3	170.5	937.5	2.60	0.05	6.56	0.51	73.43	1.55	-0.1	4.1	31.3
0.350	83.5	173.5	1223.0	2.61	0.05	7.52	0.26	77.51	0.82	-0.8	3.0	31.5
0.348	83.4	172.0	1520.6	2.45	0.04	5.79	0.33	74.68	1.07	-0.1	3.6	29.1
0.347	83.2	179.8	935.0	2.58	0.06	8.24	0.41	78.59	1.11	-1.6	3.2	32.4
0.350	83.6	181.2	1224.1	2.55	0.06	6.85	0.41	75.93	1.33	-0.6	4.1	31.5
0.354	83.9	184.6	1521.7	2.22	0.06	5.04	0.40	72.12	1.39	-0.4	4.9	26.3
0.405	83.3	151.9	943.0	3.30	0.06	3.17	1.14	63.12	6.00	3.6	9.9	34.8
0.381	83.6	151.8	1231.2	3.25	0.06	2.92	0.93	61.95	5.66	4.0	8.6	35.9
0.405	83.8	151.5	1524.0	3.14	0.04	4.88	0.74	71.78	3.16	2.6	6.0	32.7
0.398	83.3	161.6	936.6	3.14	0.06	5.51	1.08	71.73	3.75	1.8	5.9	34.2
0.395	83.3	161.4	1228.4	3.11	0.05	6.41	0.60	75.62	2.09	1.6	4.7	33.6
0.400	83.9	160.7	1525.3	2.95	0.05	7.04	0.41	79.52	1.38	0.6	3.8	31.5
0.409	84.3	169.4	938.1	2.89	0.06	9.24	0.35	80.58	1.00	-1.4	2.7	31.1
0.398	83.8	172.6	1225.8	2.79	0.06	9.74	0.24	84.03	0.89	-2.2	2.4	30.7
0.398	83.8	171.0	1524.6	2.72	0.05	8.51	0.33	82.85	0.80	-1.5	3.0	29.4
0.451	83.4	150.9	944.7	3.56	0.17	2.79	1.27	60.15	8.49	4.2	13.5	35.0
0.447	84.2	152.6	1229.2	3.44	0.06	3.91	1.14	67.20	5.25	3.6	8.0	34.0
0.449	84.2	151.6	1522.3	2.98	0.08	7.23	0.57	81.86	2.25	0.9	4.2	29.2
0.446	83.9	160.6	938.8	3.11	0.08	9.30	0.60	83.79	1.70	-0.1	3.4	31.6
0.448	84.1	161.4	1228.2	3.09	0.07	7.90	0.64	81.18	2.09	0.8	3.9	31.0
0.452	83.7	161.4	1524.3	2.74	0.08	9.13	0.59	86.89	1.58	-1.0	3.3	27.1
0.447	84.2	169.7	937.3	2.88	0.07	11.41	0.38	87.37	1.15	-2.8	2.7	29.7
0.447	84.9	173.6	1221.8	2.76	0.08	10.67	0.25	87.55	1.15	-2.6	2.4	28.2
0.447	84.5	172.5	1523.4	2.55	0.09	10.62	0.39	89.09	1.08	-3.3	2.5	25.8

APPENDIX B

B.1. Emissions Data Table – Fuel Composition 2

Fuel Composition 2

Φ	Coolant Temp	Intake Temp	RPM	CO_2 (%)		CO (%)		UHC (PPM)		NOx (PPM)	
	ºC	ºC		Value	Std. Dev.	Value	Std. Dev.	Value	Std. Dev.	Value	Std. Dev.
0.346	83.5	160.8	933.8	4.5	0.0	0.69	0.00	24	1	2	1
0.346	84.1	160.9	1224.7	4.6	0.0	0.69	0.01	22	1	1	0
0.349	82.7	160.6	1522.0	3.8	0.1	0.85	0.01	25	0	0	0
0.407	81.0	142.2	940.9	5.1	0.0	0.71	0.00	25	0	2	0
0.402	82.3	142.4	1230.0	4.8	0.0	0.74	0.00	23	0	0	0
0.404	83.3	142.0	1521.0	4.6	0.0	0.67	0.00	22	0	1	1
0.398	82.0	149.7	933.6	4.9	0.0	0.72	0.01	26	1	2	1
0.398	82.6	153.4	1225.1	4.8	0.0	0.64	0.00	23	0	2	0
0.401	83.5	151.7	1523.9	4.5	0.1	0.61	0.01	21	1	0	0
0.400	82.3	155.9	934.5	5.2	0.0	0.60	0.01	21	1	8	0
0.394	82.9	161.0	1228.0	4.9	0.0	0.59	0.01	20	0	4	1
0.406	83.7	162.3	1523.0	4.7	0.0	0.55	0.00	18	0	2	0
0.448	83.1	129.2	941.0	5.4	0.0	0.87	0.01	28	0	5	3
0.448	84.4	130.9	1228.5	5.0	0.1	1.00	0.02	33	0	2	2
0.458	84.4	130.3	1528.0	5.5	0.0	0.83	0.03	28	1	2	1
0.453	82.3	139.8	938.6	5.6	0.1	0.74	0.01	23	1	8	1
0.448	82.3	140.5	1228.0	5.4	0.0	0.71	0.01	22	0	5	1
0.451	82.4	139.8	1527.0	5.4	0.0	0.72	0.02	24	1	5	1
0.446	82.2	149.4	936.1	5.6	0.0	0.66	0.01	20	1	15	1
0.458	82.0	150.5	1225.7	5.5	0.0	0.65	0.01	19	0	11	1
0.452	83.5	148.7	1524.3	5.5	0.1	0.62	0.01	20	1	8	1
0.447	82.9	158.3	934.8	5.7	0.0	0.58	0.00	17	0	32	1
0.452	84.3	160.2	1224.0	5.6	0.0	0.57	0.00	20	1	21	1
0.455	84.0	160.6	1523.0	5.6	0.0	0.54	0.00	18	0	20	1
0.501	82.8	128.6	936.9	6.0	0.0	0.76	0.01	25	0	21	2
0.510	83.1	129.2	1231.7	6.1	0.0	0.74	0.01	25	1	17	1
0.503	83.4	129.6	1530.5	6.1	0.1	0.74	0.01	26	1	10	1
0.477	82.8	138.7	935.6	5.9	0.0	0.69	0.01	24	0	28	3
0.509	82.4	140.7	1229.0	6.0	0.0	0.60	0.01	21	1	47	3
0.508	83.6	141.0	1524.0	6.1	0.0	0.58	0.01	19	0	58	2
0.513	81.4	147.6	931.8	5.9	0.0	0.72	0.01	24	0	22	3
0.509	81.5	150.4	1222.1	6.0	0.0	0.61	0.59	24	0	58	3
0.503	83.3	150.1	1525.1	6.1	0.0	0.00	0.01	20	0	62	4

B.2. Emissions Data Table – Fuel Composition 3

Fuel Composition 3

Φ	Coolant Temp	Intake Temp	RPM	CO_2 (%)		CO (%)		UHC (PPM)		NOx (PPM)	
	ºC	ºC		Value	Std. Dev.	Value	Std. Dev.	Value	Std. Dev.	Value	Std. Dev.
0.351	83.4	141.5	934.8	3.7	0.0	0.51	0.00	20	0	0	0
0.346	83.8	141.5	1227.7	3.4	0.0	0.56	0.00	25	1	0	0
0.347	83.3	140.6	1519.6	3.4	0.0	0.53	0.01	25	1	0	1
0.347	82.9	150.9	934.0	3.7	0.0	0.47	0.01	22	1	0	1
0.347	83.3	151.6	1224.2	3.5	0.0	0.48	0.01	20	0	0	0
0.352	82.5	150.3	1522.1	3.6	0.0	0.45	0.00	22	1	0	0
0.349	83.9	163.4	933.2	3.8	0.0	0.41	0.00	19	0	1	0
0.354	83.8	162.0	1222.7	3.6	0.1	0.41	0.00	18	0	0	0
0.354	84.5	161.8	1521.3	3.6	0.0	0.38	0.00	18	1	1	0
0.404	83.2	131.1	936.2	3.9	0.0	0.48	0.00	22	0	0	1
0.395	83.7	131.1	1226.3	3.6	0.0	0.58	0.01	26	1	0	0
0.397	83.3	130.2	1524.8	3.8	0.0	0.49	0.01	21	1	0	1
0.393	83.0	140.8	938.4	4.0	0.0	0.45	0.01	20	0	2	0
0.392	83.7	141.2	1225.3	3.8	0.0	0.48	0.01	23	1	1	1
0.393	83.7	139.7	1520.1	3.9	0.0	0.46	0.01	18	1	1	1
0.394	83.9	150.6	937.1	4.1	0.0	0.41	0.00	18	0	3	0
0.401	84.2	151.2	1223.8	3.9	0.0	0.42	0.00	23	1	1	1
0.396	84.2	150.5	1522.4	3.9	0.0	0.40	0.00	18	0	1	1
0.391	84.0	161.4	936.1	4.1	0.0	0.39	0.00	16	1	5	0
0.397	84.1	161.4	1229.9	3.9	0.0	0.39	0.00	20	0	1	0
0.398	84.0	160.6	1518.0	3.9	0.0	0.37	0.00	17	0	2	0
0.444	84.0	130.2	936.3	4.4	0.1	0.44	0.00	20	0	7	1
0.454	83.6	130.7	1227.8	4.2	0.1	0.52	0.00	23	0	1	1
0.454	84.8	130.3	1524.4	4.5	0.0	0.44	0.01	19	0	5	1
0.445	83.2	140.0	934.0	4.3	0.0	0.43	0.00	20	0	7	1
0.455	83.2	140.7	1225.1	4.2	0.0	0.45	0.00	19	0	1	1
0.450	84.0	139.8	1523.4	4.5	0.0	0.43	0.00	18	1	6	1
0.455	83.7	153.8	932.6	4.4	0.0	0.39	0.00	21	1	17	0
0.447	84.5	151.7	1223.5	4.4	0.0	0.42	0.00	19	0	5	0
0.455	83.9	150.3	1522.6	4.6	0.0	0.43	0.08	20	0	12	1

B.3. Emissions Data Table – Fuel Composition 4

Fuel Composition 4

Φ	Coolant Temp	Intake Temp	RPM	CO_2 (%)		CO (%)		UHC (PPM)		NOx (PPM)	
	ºC	ºC		Value	Std. Dev.	Value	Std. Dev.	Value	Std. Dev.	Value	Std. Dev.
0.354	83.4	164.5	938.8	4.6	0.0	0.65	0.01	20	0	4	0
0.350	83.7	162.1	1231.8	4.6	0.0	0.63	0.00	17	0	2	0
0.357	83.6	160.8	1524.9	3.7	0.0	0.58	0.00	15	0	1	0
0.351	83.3	170.5	937.5	4.5	0.0	0.63	0.01	19	1	4	1
0.350	83.5	173.5	1223.0	4.7	0.0	0.57	0.00	15	1	6	1
0.348	83.4	172.0	1520.6	4.2	0.0	0.57	0.00	14	1	1	0
0.347	83.2	179.8	935.0	5.9	0.0	0.63	0.00	17	0	13	1
0.350	83.6	181.2	1224.1	5.5	0.0	0.68	0.01	20	1	4	1
0.354	83.9	184.6	1521.7	4.7	0.0	0.70	0.01	21	0	0	1
0.405	83.3	151.9	943.0	5.3	0.1	0.74	0.01	19	0	6	1
0.381	83.6	151.8	1231.2	5.0	0.0	0.73	0.01	19	1	3	0
0.405	83.8	151.5	1524.0	4.9	0.0	0.63	0.00	17	0	2	1
0.398	83.3	161.6	936.6	4.8	0.0	0.64	0.01	20	0	9	1
0.395	83.3	161.4	1228.4	4.8	0.0	0.60	0.01	17	0	8	1
0.400	83.9	160.7	1525.3	5.0	0.0	0.60	0.01	17	0	4	1
0.409	84.3	169.4	938.1	5.3	0.0	0.58	0.00	16	1	33	1
0.398	83.8	172.6	1225.8	5.4	0.0	0.56	0.00	14	0	31	1
0.398	83.8	171.0	1524.6	4.5	0.0	0.50	0.00	12	1	7	1
0.451	83.4	150.9	944.7	7.1	0.0	0.92	0.01	25	0	12	2
0.447	84.2	152.6	1229.2	6.6	0.0	0.84	0.01	24	0	10	1
0.449	84.2	151.6	1522.3	5.9	0.0	0.63	0.00	17	0	13	1
0.446	83.9	160.6	938.8	7.2	0.1	0.70	0.00	20	0	84	4
0.448	84.1	161.4	1228.2	6.7	0.0	0.74	0.01	22	1	30	2
0.452	83.7	161.4	1524.3	6.4	0.1	0.69	0.01	20	1	23	2
0.447	84.2	169.7	937.3	7.3	0.0	0.61	0.00	19	0	180	5
0.447	84.9	173.6	1221.8	6.9	0.0	0.63	0.00	20	0	82	1
0.447	84.5	172.5	1523.4	6.4	0.0	0.60	0.00	18	0	40	1

VITA AUCTORIS

Dale Edward Haggith was born in January of 1984 in Leamington, Ontario. Throughout Dale's development as a child he worked with his father who was a mechanic by trade learning valuable practical skills for his future. In 1998 Dale graduated from Mill Street Public School in Leamington where he received the scholastic award for achieving the highest academic marks of his class. From 1998-2003 Dale attended and graduated from Leamington District Secondary School after which he decided to attend St. Clair College of Applied Arts and Technology with the strategy to pursue not only a practical knowledge of engineering but later a theoretical understanding. Dale was enrolled in St. Clair College's Mechanical Engineering Automotive Product Design program and graduated with honours in spring 2006. In 2005-2007 Dale worked at Gates Rubber Company as a part time junior product engineer while attending classes full time. It was at Gates where he was involved in product development and testing/validation gaining industry experience for future endeavours. In fall 2006 he transferred to the University of Windsor's Mechanical Engineering Automotive Option Honours program. Dale graduated with his Bachelors of Applied Science in Mechanical Engineering in 2008. During his time spent at the University of Windsor regarding his undergraduate degree he became involved in applied combustion research. January of 2009 Dale decided to return to the University of Windsor as a full time M.A.S.c student to working on internal combustion engine and alternative fuels research.